A High Precision Two Dimensional Stage Using Friction Drive

by

Razman Zambri

B.S.E., Mechanical Engineering (1995)
University of Michigan at Ann Arbor.

Submitted to the Department of Mechanical Engineering
in Partial Fulfilment of the Requirements for the
Degree of Master of Science in Mechanical Engineering

at the

Massachusetts Institute Of Technology

September, 1997

Author _____

Department of Mechanical Engineering
August 22, 1997

Certified by _____

Professor Kamal Youcef Toumi
Associate Professor of Mechanical Engineering
Thesis Supervisor

Accepted by _____

Professor A. Sonin
Chairman, Department Committee on Graduate Students

A High Precision Two Dimensional Stage
Using Friction Drive

by

Razman Zambri

Submitted to the Department of Mechanical Engineering
in partial fulfillment of the requirements
for the
Degree of Master of Science in Mechanical Engineering

September 1997

Abstract

A precision two dimensional stage was designed to achieve subnanometer resolution using a piezoelectric based actuator. The design incorporates a PTFE based sliding bearing on Silicon Carbide ceramic bearing way for high stiffness, low sliding friction and high motion smoothness. A new configuration of piezo actuator was designed and, by concept, is capable of driving the stage in any direction on a 2D workspace. The design also include a study of different method of stage suspension and evaluation of sensors for the system.

The motion of the stage heavily depends upon the contact interface between the stage and the actuator. Therefore a study of friction was carried out and dynamic friction models was surveyed. A bond graph analysis was also done on the friction model to study the energetic relations between elements in friction. The friction model studied was found to be non-causal, and a modified causal model was derived. The two models along with an intermediate model, were simulated. All these model captured the presliding, hyteresis and exhibit stick-slip motion phenomenon.

Thesis Supervisor: Professor Kamal Youcef-Toumi.
Title: Associate Professor of Mechanical Engineering

Acknowledgements

The success of this research is largely owed to Professor Kamal Youcef-Toumi. His invaluable advice and guidance greatly helped me to go the design and analysis of work presented in this thesis. He is willing to spend the extra hours (even late nights on Sundays) to meet with me and his other students and help us with our research problems.

I appreciate grants from the Malaysian Government, the Mechanical Engineering Department and Daewoo Korea that help finance my education and my research at MIT.

I am very deeply indebted to my parents (Mr. Zambri and Mrs. Rahmah) and my family (Nizar, Syazali and Suzana) for their constant love, encouragement and support in my long stint away from home. A special thank you to Miss Rafizah for her love, support, patience and encouragement during the period I am at MIT.

I am ever so grateful to Bernardo Aumond, Larry Barrett, Steven Villareal, Karl Iagnemma, Mike Timmons and many others for being such great friends, which makes tough days at MIT fun to go through, and make every tomorrow, a day to look forward to. I also appreciate great times with my lab mates, Florian Schmidt, and Masaki Mori, the Juicy Chicken IM basketball team, for their friendship on and off the court. I appreciate friendship of Malaysians at MIT for making MIT "a home away from home." I wish them all the best in their future endeavours.

My experience at MIT has been a great one. The experience of learning from the greatest mentors on the planet and being around a crowd of very intelligent and resourceful colleague, is indeed very interesting, enlighten but humbling. My MIT experience makes me realize how much knowledge is there to be learnt, how much I benefited from my interactions with my colleague I saw enthusiasm in learning and self-improvising traits in my colleagues and other people around me. And what amazes me is that, despite the enormous expectations and work load were imposed upon us, we still manage to meet those expectations and yet able to have fun.

Table of Content

List of Figures

Chapter 1
Introduction

History has shown that precision machines are essential elements of an industrial society. Modern industries are critically dependent on precision machines ranging from those for the manufacture of integrated circuits, to machines for the manufacture of optical components. In the manufacture of DRAM chips for example, the industry is moving toward requiring subnanometer level positioning resolution over 200-300 mm range [22]. The next generation Pentium processors, for instances, demands more and more fantastic performances for machines that makes them. This in turn drives the need for actuators and sensors to achieve this super high accuracy, along with unbelievable resolution requirements. To add more interest to the problem, the society today is not only concerned with high performance machines, but also economics and cost play a very significant role to stay ahead in a very highly competitive world. Machine tools have to be made better and cheaper. Thus the major thrust of this thesis is to lay the foundations of the design and develop a precision two dimensional stage using cheaper actuation modes.

1.1 Background

There are several concepts that will be often used in this thesis. Therefore it would be advantageous to introduce them early on. In this thesis, the notion of subnanometer and nanometer resolution ranges are common. Figure 1 [22] provides the reader with a valuable tool to visualize and to compare of the precision levels generally addressed in this thesis.

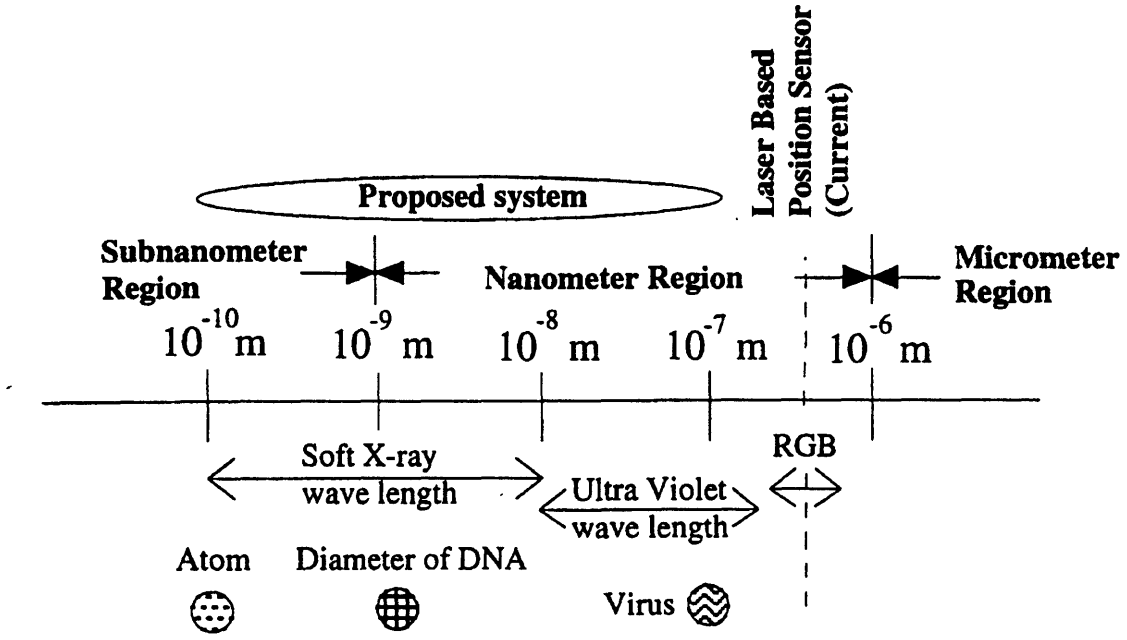

Figure 1 Comparison of precision levels

Other basic definitions commonly used are *accuracy, precision* and *resolution.* These are three basic definitions with respect to how well a machine can position its axes [29]. These terms can be represented diagramatically as shown in Figure 2

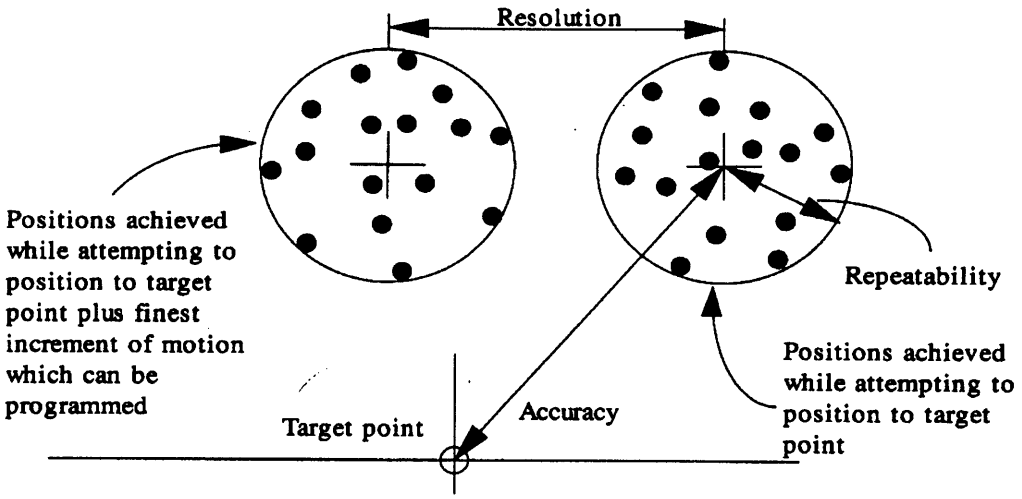

Figure 2 Description of accuracy, precision and resolution

Accuracy is the ability to tell the truth [29]. Accuracy is the maximum translational or rotational error between any two points in the machine's work volume. Linear, planar and volumetric accuracy can all be similarly defined for a machine. *Precision (repeatability)* is the ability to tell the same story over and over again [29]. Repeatability is the error between a number of successive attempts to move the machine to the same position. *Resolution* is how detailed your story is [29]. Resolution is the larger of the smallest programmable step or the smallest mechanical step the machine can make during point-to-point motion.

Error motion is deviation from the intended or ideal path of motion. In this thesis, smoothness error is often referred to. Smoothness errors, can be used to described straightness errors that are dependent on the surface finish of parts in contact.

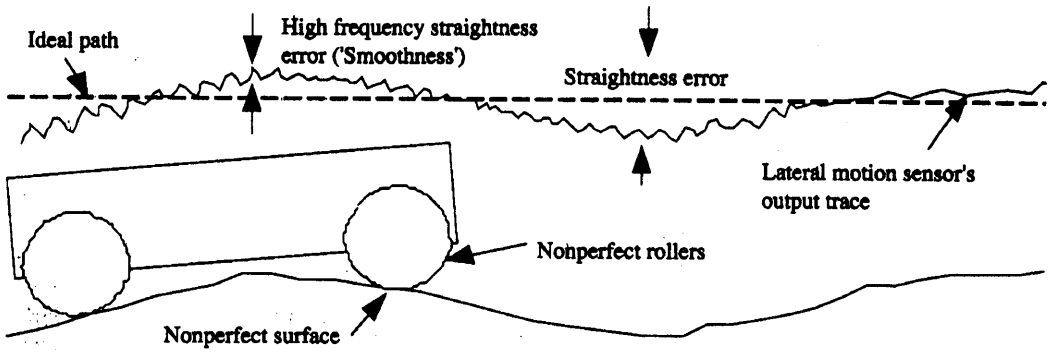

Figure 3 Straightness errors caused by surface forms and finish errors

1.2 Previous Work

This thesis was based on previous work done by H. Choi [1], in which he has proved that linear motions of 1nm resolution or better is achievable using piezoelectric transducer. The linear actuator presented possesses excellent potential as a nano-actuator that will drive tomorrow's high performance devices. Extremely high speed motion capability was achieved without sacrificing either the sub-nanometer positioning accuracy, high bandwidth, high static stiffness, or high torque to weight ratio. These performance advantages over other nano-actuators stem from effective design that couples superior material property of piezoelectric material with a simple structure, and allows direct friction contact between the motor and the linear guide.

However, several problems were reported in [8]. Consistency in positioning accuracy were very poor as friction, the main driving mechanism, were not understood. Payloads bays are not accessible in this current prototype. The current design is also specific for single axis motion. Hence the focus of this thesis is to improve on these limitations.

1.3 Thesis Outline

The actuator redesign considers two dimensional workspace, accessible payload bays and as mechanically sound as possible. A study into physics of friction is also the

other focus of the thesis as an effort to refine and hopefully develop a friction model for the revised system, specifically and also a generalized friction model for control systems.

In this thesis, the design of the precision stage prototype is explained in Chapter 2. Several stage designs were investigated and requirements were refined. Detailed discussion of design of parts and components selection, as well as important design issues are addressed in this chapter.

In Chapter 3, a study of friction physics is conducted. Understanding of the nature and causes of friction non-linearity is described. Survey of friction model friction model is done and the most recent and accurate model are described. Bond graph representation of this model is then performed.

In Chapter 4, a simulation of actuator tip motion was done. Friction simulations was also performed to verify that these models exhibit characteristic friction phenomenon.

Lastly in Chapter 5, conclusion and recommendations of future work follow.

Chapter 2
Precision Stage Design

In following previous effort by Choi [8], a more elaborate experimental prototype was proposed. The goal is to transform the linear slider design configuration into a more "useable" form i.e. having the slider readily accessible to place payloads. It is also desirable to add another dimension to the workspace.

The focus of this chapter is to address the issues considered pertaining to the design and development of the new prototype. First, various stage designs were studied for idea, and performance specifications. A concept for a linear carriage is then detailed, where the carriage is accessible for payload placement. The chapter looks into the discussion of the details of each components design and selection. This chapter also describes various consideration and issues encounter in several design iteration of the device. Extension of the design to a two dimensional prototype is also described.

2.1 Review of Precision Stage Systems

Many researchers have studied the control in planar motion. Some of the most common precision stages uses magnetically levitated and actuated stages as in [13][32][33]. Air bearings based stage systems are also described, actuated by magnets-stator-armature system [12] and by application of electric fields [24]. A clever design

utilizing kinematic coupling mechanism for two dimensional stage described in [31]. A piezo driven, flexure supported stage is designed and described in [34].

Unfortunately, these stage designs are incapable of high resolution motions (in the order of nanometers), long range (more that micron range) and two dimensional motion all in the same device. Almost all of the stages described earlier either have low resolution (in the order of microns) or have very small workspace (microns range). However, the stage in [13] has been reported to achieve 0.1nm steps, unfortunately motion range is only limited to 100 μm in two dimensions.

Longer range actuators usually incorporate a fine motion stage, usually with two dimensional travel range of microns, on top of two coarse motion stages actuated by linear motors for each of the X and Y axis. This configurations usually will be able to get down to nanometric resolution (with a relatively poor settling time), unfortunately involves a highly coupled stage dynamics and makes controls of such systems very difficult and complicated.

2.2 Functional Requirements

The position precision level frontier is constantly being challenged by industries such as the semiconductor industry. The key trends in semiconductor design are clear: features size are getting smaller, circuits are getting larger, and wafers are getting larger [4]. These trends has profound influence to set of functional requirements that should be achieved by a machine.

One set of requirements are classified as *performance requirements.* Performance of the proposed prototype is the set of parametric specifications which specifies resolution, motion smoothness, travel range and speed.

Item	Specifications	Remarks
Resolution.	0.1 - 10 nm	This is the primary goal of the project. In lithography applications, for instance, the resolution requirement has shrunk tremendously in accordance to advancements in VLSI design.
Travel Range	200 mm (8 in)	This requirement depends on the application it used for. For lithography, wafer sizes has grown to be 300mm in diameter, for instance. However, infinite range is desirable, with only the stage design becomes the limiting factor.
Speed	200 mm/s [22]	Speed has direct effect to the economics of the industry. The faster the machine, the higher the throughput of the machine.
Acceleration	0.2 G - 1 G [22]	This would have an effect to actuator sizing, stage size and power requirements.
Smoothness	1 nm	Smoothness is defined to be the error in the direction normal to motion plane.

Table 1 Specifications Requirements

Another set of requirements are *components* that should be used for the prototype.

Item	Remarks
Actuator	Piezoelectric actuator has been identified as a feasible driver for linear actuation [8]. Therefore, it is a goal of this project to pursue the technology as a cheap alternative to magnetic driven stages.
Sensors- Range	same as the system range - 200 mm (8 in.)
Resolution	same or better than system resolution - 10 - 0.1 nm.
	Additional Remarks: For a 2D system, it is desirable have a non-contact sensor.
Material	Two consideration: a. Thermal stability - the system should use material with low thermal expansion coefficient. b. The interface with the actuator should use a friction material layer for optimized drive force.

Table 2 Components Requirements

Other pertinent issues related to the stage design are:

1. **Ergonomics** - accessibility to placing payloads on the stage, access to make fine adjustments on critical components.
2. **Modular Design** - The design of the prototype should take into considerations to easiness to assemble components and replacing them. The design should be also adaptable to 2D motion.

2.3 Component Design

The functional requirements as described in Section 2.2 yields the system in Figure 4 as a possible prototype.

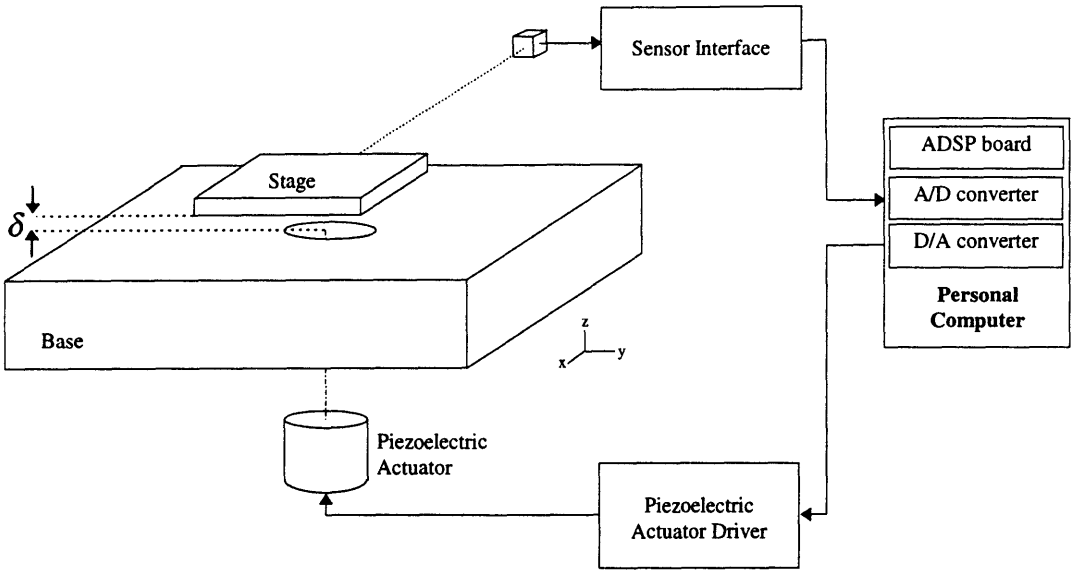

Figure 4 Schematic view of prototype for the proposed stage

From the schematic shown above, we have identified the major functions that need to be performed for a working prototype. The stage needs to be *levitated* to allow motion in the X-Y plane. Once this is achieved, the stage needs to be driven, by means of *piezoelectric actuation*. In order to accurately position the stage, appropriate *sensors* needs to be installed in the system. The *design of the base* is also important, as the base will house the actuation device, levitation mechanism and possibly the sensors. Since the device is going to operate in the nanoscale range, it is also important to consider thermal and vibration issues of the system.

Although piezoelectric actuation was proved to be a feasible option for linear motion in [8], the actuator to be used in this project uses a new configuration of piezoelectric transducer and therefore needs to be tested and verified. Therefore, decision was made to employ a single axis motion stage using sliding bearings as the first stage prototype. However, in the design process, two dimensional stage design is always kept in mind, making the first prototype readily adaptable to a two dimensional stage. Figure 5 shows the exploded view of the final prototype.

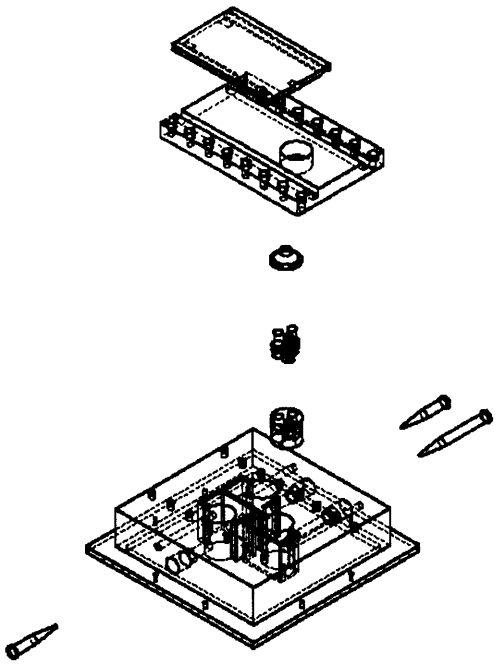

Figure 5 Stage Assembly

In the following sections, the components of the system is described. Other options that were considered are also presented.

2.3.1 Piezoelectric actuation

A piezoelectric material changes shape when a voltage is applied across it or gives out a voltage when it is subjected to a deforming force. Typically these changes in shapes are so small, that it is often used in stacks to provide appreciable effects. Depending on its mass and stiffness, the bandwidth of the piezoelectric actuator is in the order of several kilohertz, and usually has better resolution than of those other actuators. A typical piezoelectric actuator would only dissipate milliwatts of power which will not disturb the thermal equilibrium of a precision machine. Given these desirable properties of piezoceramic, many research activity has been conducted to study the usage of piezoelectric actuator in precision motion control. Piezoelectric actuators have found widespread applications in high precision positioning devices including VCR auto tracking head, fast tool servos (FTSs), spindle error compensation, Scanning Probe

Microscope (SPM) and ultrasonic motors [8][29]. They has also been used as fine motion stage actuator which has about 100 μm linear travel range [23][25].

The basic idea of our proposed actuator prototype is to generate elliptical motion using a combination of at least two piezoelectric actuator as shown in Figure 6 and Figure 7. These figure shows, in succession, that the tip goes through some trajectory of elliptical shape. In Figure 6 and Figure 7, the first sketch ("Ref") shows the zero position in the actuator. Using the same general concept and adding a third piezo, one can generate an ecliptic tip trajectory in any vertical plane. This tip motion is then utilized to "push" the levitated stage. In practical, this mode of drive relies heavily on contact between the tip and the bottom of the stage. Therefore, careful considerations are to be taken in choosing the friction materials and surface finish on these components. Extensive study and modeling of friction is therefore necessary. Choi [8] has shown that although the mechanism is based on friction, high resolution is achievable.

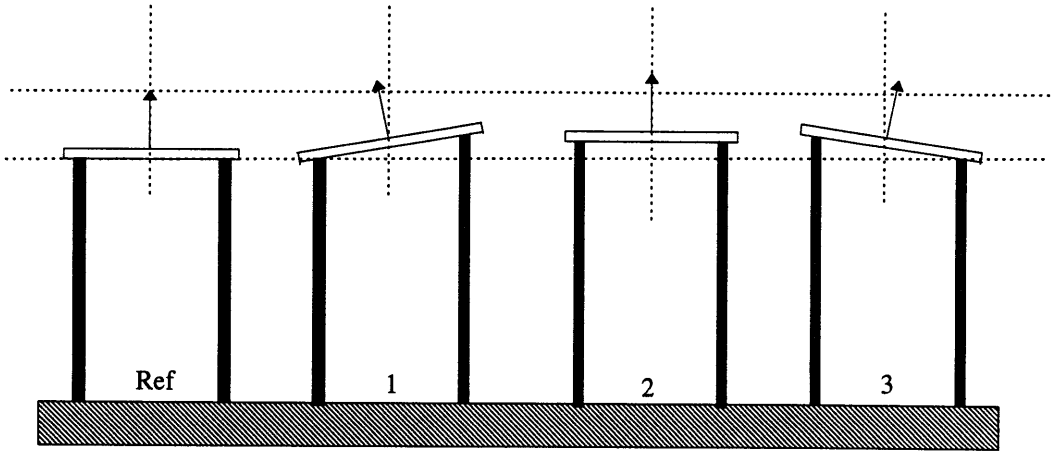

Figure 6 Piezoelectric actuation concept with elongated piezos

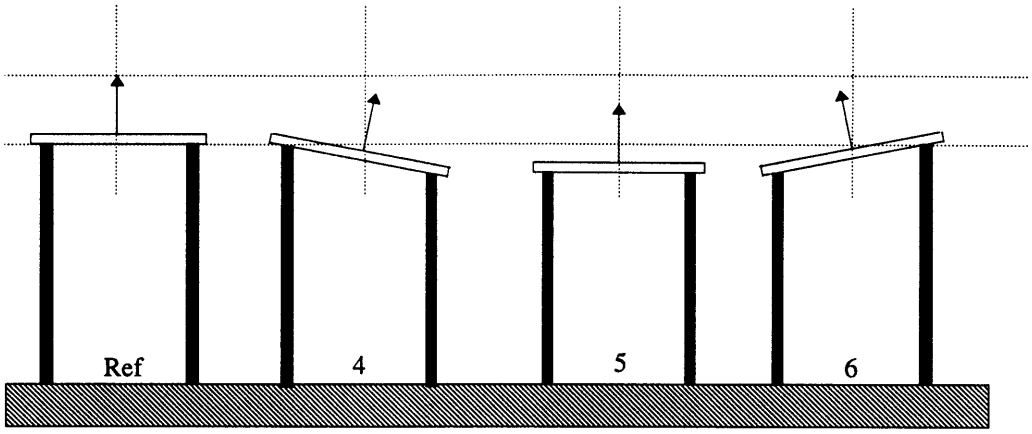

Figure 7 Piezoelectric actuation concept with contracting piezos

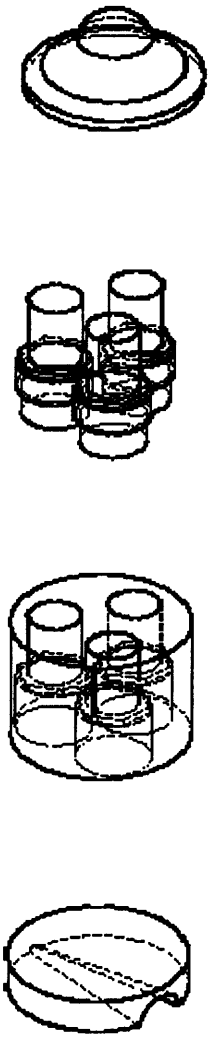

Figure 8 Actuator Assembly

The actuator prototype is based on the described concept is designed. Three piezoelectric actuator will be used to allow for two dimensional motion. An actuator assembly as shown in Figure 8 is designed. Loading on the actuator will primarily be in the lateral directions. Therefore, lateral stiffness is provided by the piezo housing. This design also allows piezo replacements, in case one of the actuators becomes defective. The tip is made out of aluminum because aluminum is light and very machinable; and will be coated with friction material for optimized friction behaviour.

2.3.2 Stage Suspension

Stage suspension is a critical issue in the design of the prototype. The stage is where the payload would be placed. However it is also necessary to keep the inertia of the stage to be small. This is to keep acceleration force requirements as small as possible and in turn would minimize slippage of the drive system. Therefore it is desirable to have any necessary components for suspension to be attached to the base instead of the stage. Resolution, smoothness and stiffness of the stage is a direct consequence from the design of the suspension mechanism. Stage suspension can be achieve by using bearing or by levitating the stage.

Resolution , as described earlier, is the smallest achievable step of a machine. Smoothness is the variation of motion in the direction normal to the motion plane. These parameters are intimately related to the surface finish and friction between the stage and the slide-way. Stiffness is sensitivity of the stage assembly to load variation. High stiffness is desirable, however there is a trade off between stiffness, and resolution and smoothness [29]. In addition to the above mentioned parameters, the following are also important factors influencing the suspension mechanism: repeatability, range of motion and cost.

For the first prototype, sliding contact bearings was use as a mechanism for stage suspension. Considerations and issues in this choice is discussed in the following sections. Other bearing options were also described.

Sliding Contact Bearings

Sliding contact is the oldest, simplest, least expensive bearing technology, and they still have a wide range of application. Sliding bearing has been used in Nanosurf 2, a long range surface profilometer developed at National Physical Laboratory [29]. A thin film, 2-3μm thick, of PTFE (polytetraflouroethylene) is deposited onto a convex bearing pads and the bearing rail is lapped to have a surface finish in the nanometer range. Using this bearing design, Nanosurf 2 has been reported to achieve 1nm or better resolution and 0.05 nm smoothness of motion normal to the direction of motion.

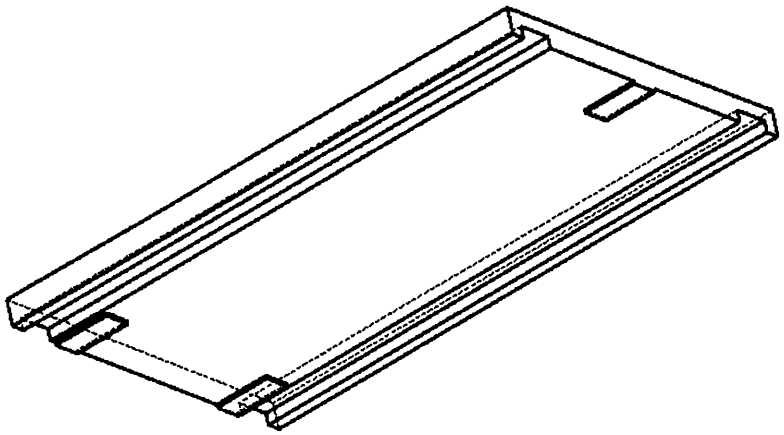

Figure 9 Stage Design

Material combination at the sliding interface has a profound effect to bearing performance. In our application, the bottom of the stage needs to be essentially layered with high friction coefficient material because it is a friction drive stage. At the same time, the sliding pads, needs to be virtually friction free. The stage is made of Aluminum because its is readily machinable, light weight, cheap and can serve as a thermal sink for heat generated during sliding process. Bearing pads "islands" are placed in such a way so that is not over constraining kinematically (See Figure 9). This also allows the friction material be deposited on the "sea" and not sliding on the bearing way. According to [29], the general rule of thumb for dimensioning the pad is that its dimensions are of 2:1 ratio. The choice of material for the bearing pad- bearing way are based on Nanosurf 2 experience. A thin film (1 mm - 2 μm) PFTE has been chosen to be deposited on to these

bearing pads. It is important to keep this layer thin, so that heat generated from sliding can easily be conducted away onto the metal stage [30] to minimize wear. PFTE has also been engineered to have static coefficient of friction within 10-20% of dynamic coefficient of friction to minimize stick-slip and wear. Ceramic material (Silicon Carbide) is chosen as the bearing slide surface. It has been documented [29] that ceramics works well with polymer based material such as PFTE. Ceramics are brittle and has negative skew surface finish making friction and wear very low and often negligible. Although ceramics are generally harder to machine, however it is easier to grind or lap because residual stresses are not easily built up in brittle materials. Smoothness of motion, due to the averaging effects of surface finish are in the order of $\sqrt{R_a^3}$ where R_a is the measure of surface finish. Therefore surface finish of ceramic is specified to be 1 μm R_a.

In designing high precision machines, how the *bearing way is mounted* to the base is also important. Proper bolt size and spacing is essential to ensure that the region of bearing way material under the bolts' cone of influence can provide for adequate tensile and lateral stiffness at the bolted joint. The mating surfaces of the base and the bearing way, is finished to a relatively high surface finish (1 μm). This reduces surface imperfection and allows the joint to mate better. Torque level of the bolt should not be exceedingly high, to minimize warping, compression and Poisson compression of the bearing way. Uniform distribution of stiffness would also allow for a flatter bearing way, which will reduce errors in motion smoothness. A spreadsheet calculating the necessary bolt spacing for optimum stiffness are included in the appendix.

Preloading of the stage is needed to impose and maintain stiffness between the slide interface. High stiffness is desirable as high stiffness systems are insensitive to error motion. On the other hand, high preloading causes higher friction coefficient between the sliding surfaces. Therefore, trade off need to be found. In this application, applied loading will be small (or none), therefore a light preloading in the order of 10% of the applied load is adequate. In fact, light preloading is necessary so that friction between the bearing

pads and the slide-way is minimal. Preloading force is achieved using attraction of permanent magnets and ferromagnetic material built into the stage.

Another task built into the design is the *alignment* of stage about axis of motion. Error motions may cause the stage to be driven at a certain distance from its axis generating moments and undesirable yaw motions. We can also use the same permanent magnets used to preload the stage as a alignment mechanism. Ratio of lateral and normal stiffness can be maximized using "teeth" as shown in Figure 10. A study [36] has determined that the ratio of stiffness is maximum when the tooth width l/p is approximately equal to 0.4 of the gap, *e*. The study also stated the requirement of this teeth material to be homogenous and isotropic. This is so that its hysteresis cycle reduces to its first magnetization curve.

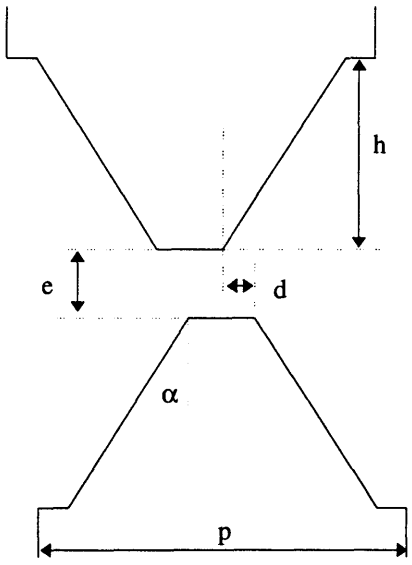

Figure 10 Definition of the geometrical parameters of tooth shape

Resolution in sliding bearing systems is limited by friction. Friction, as will be discussed in chapter 3, is very non-linear at low velocities. One of the friction phenomenon dominant at low velocities which is an obstacle for precision motions is called stiction. However, stiction is less pronounced is PTFE based bearings that has been worn in. Therefore, wear in period of several thousand cycles is necessary. This would

allow static friction coefficient to drop to 0.03 - 0.1 and dynamic friction coefficient may decrease to 0.02 - 0.1 [29] . This value, however varies with preload, surface finish etc. Straight line accuracy and repeatability of similar bearing systems typically are in the order of 5-10μm and 0.1-1.0μm respectively, when surfaces are ground and heavily preloaded. Submicron accuracy and repeatability may be possible with hand finished surfaces and lightly preloaded systems. Nanosurf 2, achieved accuracy and repeatability in the order of nanometer (10^{-9} m) and angstroms (10^{-10} m) respectively.

2.3.3 Base and Assembly

Another critical component of the stage assembly is the base. The base houses the actuator and the bearing way. Figure 5 shows how these components are assembled together. The current design allows us to make fine adjustments to the actuator's height and hold them in place reliably. It was also design to accommodate the implementation of a two dimensional stage.

During installation, it is necessary to be able to make fine adjustments for the actuator. As was described earlier, the height issue is critical as the ecliptic cycle of the driving tip is in the order of 1-10 μm. To ensure contact, therefore it is critical to adjust the gap, between the "zero" position of the tip and the bottom of the stage, to within this tolerance. Installing set screws from the bottom of the base was the initial choice, however for ergonomics reasons, assembly in Figure 11 is chosen instead. It allows making the necessary height adjustments from the sides of the base.

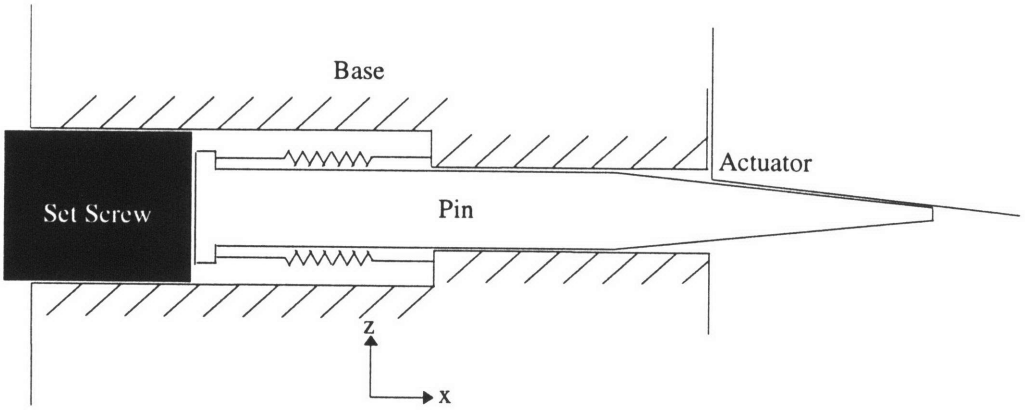

Figure 11 Height adjustment assembly

The actuator is then fixed using a set of clamps. The slots are specified to go through all the depth of the base for ease of machining. The shape of the slots are so that the clamps are not over-stiff. From experience in design of the Scanning Tunnelling Microscope (STM) [22], the material of the base is chosen to be INVAR SUS416, because of its low thermal expansion properties and is designed as asymmetrically as possible for thermal stability.

As a suggestion, a shim stock can be used during installation of the stage. Height adjustments can be made with the help of the shim which will maintain a specified gap (0.0005 in to 0.030 in) between the actuator tip and the bottom of the stage. Once proper height adjustment is made, the clamps should be tightened and the shim should be removed.

2.3.4 Sensing System

Sensor feedback is indispensable not only for closed loop feedback control, but also for open loop performance analysis. The quantities that are of interest in position and velocity. From experience of Choi [8] and for simplicity for the current stage of the project, long range high speed movement and nanometer precision measurements, are achieved by using two types of sensors.

For position sensing during the high speed movement, an LVDT[1] (Linear Voltage Differential Transducer) was used. The full range of the LVDT is 1 inch, corresponding to $\pm$ 10V DC voltage output from the LVDT housing. Since we use a 12 bit A/D converter to read the LVDT position signal, this LVDT setup has a quantized resolution of 6.2 μm [8]. And with the full scale static linearity of 0.25% of full range and the 3 dB bandwidth of 500 Hz [17], it proved adequate for course resolution position sensing [8].

Issue mentioned by Choi [8] for velocity sensing is revisited. The importance of reliable real-time velocity for servo-systems, especially for a high speed and performance system such as this, needs no further emphasis. The raw position signal may be differentiated to approximate the velocity, instead of using a separate velocity sensor. This, however, is not the best choice since differentiation of quantized position signal induced noise that worsens as the sampling rate increases. A causal digital filter, otherwise known as an observer, may be implemented to estimate the velocity from the position signal. Implementation of observers however requires more computing power especially for fast systems, such as this, and always associated with an inherent time delay. Another alternative would be installing a separate velocity sensor which require involves a careful design compromise weighing performance requirement against project constraints that include budget and size. For full state feedback, the indicated issue becomes critical.

For high precision movement, we aimed at nanometer or better resolution to support the nanometer resolution claim. Again from experience [8], a parallel plate capacitive probe[2] with a static linearity of $\pm$0.2% of full range and better than 5kHz band width [19] met the accuracy and robustness requirement with some modification: the probe had 25μm range and 25 nm resolution initially--inadequate for the proposed resolution experiment. However same technique used in [8], could also be used to

[1] Model 100 DC-D manufactured by Lucas Control Systems Products, 1000 Lucas Way, Hampton VA 23666, (804) 766-4494.

[2] Probe model ASP-1 with probe signal amplifier model AS-1021-SAI, both manufactured by Mechanical Technology, Inc., 968 Albany-Shaker Road, Latham NY 12110, (518) 785-2211

achieve the desired resolution. The raw signal from the AS-1021-SAI amplifier unit connected to the capacitive probe was first filtered through a low pass RC filter with a cutoff frequency of 24 Hz to attenuate high frequency noise, and then amplified 25 times through a non-inverting op-amp, yielding 1 nm resolution before it is converted by a 12-bit A/D [8].

Future candidate for sensing system is an interferometry based laser sensing systems. This type of systems provides a non contact position measurement which would allow for two dimensional position sensing. A Displacement Measurement Interferometer System[3] can detect up to 0.6 nm linear displacement resolution and 0.1 microradian angular displacements. It is also capable of tracking a plane mirror target at a moving velocities up to 500 mm/s and has an operation range of ± 1.328m. A typical system configurations is as in Figure 12. This system meets the requirements of the proposed system and is an ideal sensor candidate for the two dimensional stage design.

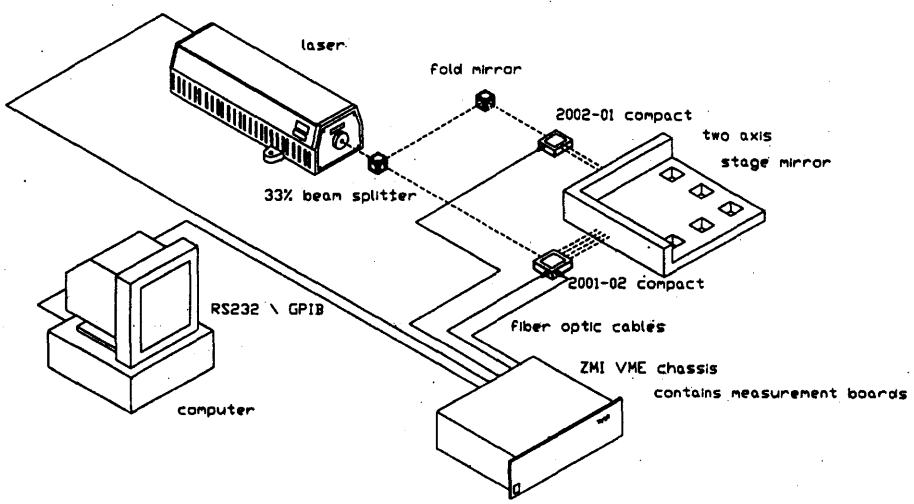

Figure 12 Typical Interferometer System

[3] Model ZM-1000 manufactured by Zygo Corp., Laurel Brook Road, PO Box 448, Middlefield CT 06445, (860) 347-8506.

2.4 Other Components

In designing the stage, there are many other components that were also considered. For our project however, most components are already predetermined from the goals of the project itself, e.g. the actuator. Sensor selection was heavily influenced by the resolution requirement, and that there is not a large selection of sensors that would fulfil such stringent requirement. This is not the case, however for bearing design. There is many types of other configuration, other that discussed earlier, using different mediums as mode of levitation, with its advantages and disadvantages. The following sections discusses the candidates for levitation mechanism considered in the project.

2.4.1 Air Bearing

There are many type of air bearing design and configuration; but the most common is externally pressurized air bearings. Externally pressurized refers to the use of high-pressure air that is forced into a gap between the two moving surfaces usually through an orifice or a slot. These gaps very small, typically in the order of 1-10μm.[29]. Only the difference is that air comes from the bottom, if used in our application.

Design of porous carbon air bearings[4] would supply air pressure equally across the whole bearing surface. One can think of a porous media as an air bearings with infinitely many orifices. Construction of such air bearing is shown in Figure 13. Porous carbon bearing's ability to create a uniform distribution of air over the entire surface, makes it very stable and not susceptible to "pneumatic hammer instability" [10]. This uniform air distribution also gives the porous pad superior tilt stiffness, which allows the pad to self-align to the guide surface.[7]. Lateral stiffness is adequate in most applications. Tests have shown that a 25.4mm (1") diameter air bearing has a stiffness of 24.5 N/μm (140,000 lb./in) and load carrying capacity of 90 N (20 lb.) operating at 413 KPa (60 psi.) air supply and 5μm (200 micro-inch) gap [20]. Bearing pads made from porous carbon has an added advantage in that graphite in carbon is a natural lubricant [7]. This feature, in addition to low flying height, make contact between the guide and the carbon pad safe

in case of accidental touchdowns during motion. The bearing way scores and scratches, which is often more expensive and difficult to repair, can therefore be avoided. Scores and scratches on the porous material itself, have little effect on lift and stiffness. Test has shown that, even after a deep groove made on the porous carbon bearing, it will still have more than 50% of its original lift [10]. The porous air bearings is currently being used by G&L Metrology in their CMMs (Coordinate Measuring Machines) and by Boeing Corp. for their large gantry type CMMs [10].

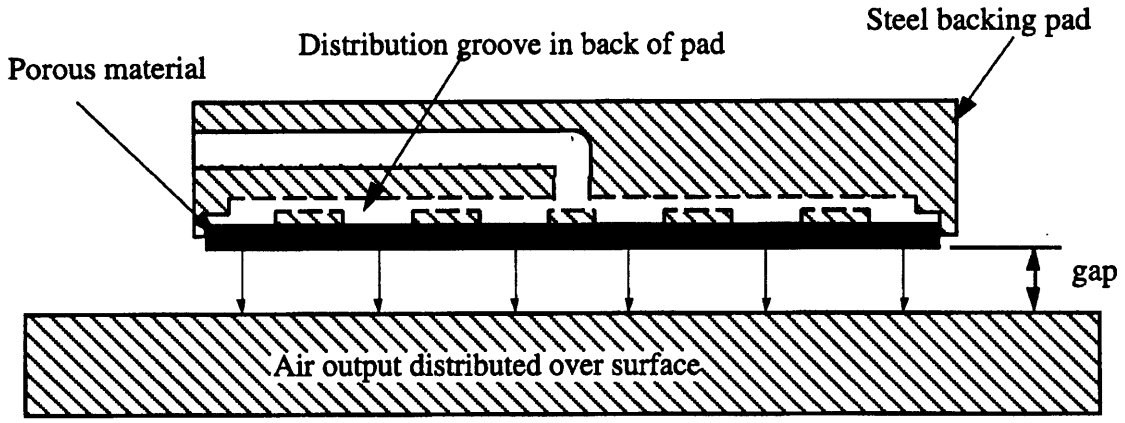

Figure 13 Cross section view of a porous air bearing

Externally-pressurized air bearings do offer many advantages over conventional contact based bearings. They exhibit zero stiction and very low, predictable operating friction. Since there is virtually no friction, resolution of systems employing air bearings is limited by the actuator it is driven by. Air bearings is perhaps the most accurate bearings of all bearings [29]. There is no wear in sliding surface and negligible heat generation as there is no contact. The effect of film averaging and squeeze film damping averages out high frequency motion errors and transmittance of machine vibrations [7].

On the other hand, they exhibit poor dynamic performance, expensive precision manufacturing and requires an external source of pressurized air. Load carrying capacity

[4] New Way Machine Components, Inc., 4001-I Market Street, Aston PA 19014

and stiffness of an air bearing system is also somewhat limited compared to bearing systems [7]. Design of actuator and control system is not trivial because air bearings is not well damped. Air bearings also requires that maximum peak-to-peak surface roughness of air bearing component not be greater that one-forth of the bearing gap [29].

Despite the desirable performances of porous carbon bearings, it is not a design choice for this phase of the project, because it requires a 1" thickness which is negated by the requirements of preload and alignment magnets. In addition to that, the focus at this point of the project is to develop a stage prototype to test the functionality of the integral component of the stage, the piezo actuator, before decision to further invest in the development of the stage is actually made.

2.4.2 Passive Magnetic Levitation

Passive magnetic suspension with permanent magnets offer numerous advantages. These passive systems do not need external power, reliable and last very long. Most of the applications of passive magnetic bearings are on rotary systems as described in [9][33].

One possible concept, is to utilize the repulsion of same magnetic poles to produce repulsive levitation. In this configuration, permanent magnets will be laid on the base, such that it creates a uniform magnetic field across the workspace. "Enough" magnets is the placed under the stage, with the same poles facing down to create repulsion forces. Stiffness of a passive magnetic levitation systems can be optimized by stacking the magnets in rotating magnetization direction (RMD) [37]. The RMD study was done for a rotary levitation system. However, there are two main obstacle to perfecting this mode of levitation. Firstly, according to Earnshaw's theorem, stability cannot be obtained with only permanent magnets. For repulsive levitation, Z axis is stable, but the X and Y axes are not. If we let lateral stabilization be achieve via contact with the actuators, then the actuator dynamics is not decoupled from magnetic lateral instabilities, which would make controls a bit more difficult. For instance, in [33], an

additional stabilizer were used, freeing actuator from stabilizing task. However lateral vibration with 2μm amplitude at steady state is observed. Creating a uniform magnetic field across a 200mm x 200mm workspace will be a daunting task. It will require very powerful magnets to generate such fields.

2.4.3 Ball – Spring

Another mechanism that was thought of to provide levitation is as shown in Figure 14. The ball is place on a fixture with three rollers to allow free rotation in any direction. The initial idea is to use three of such suspension devices on the base to provide a stable support while not over-constraining the stage. Springs are used to provide a more deterministic stiffness. This type is mechanism is simple to construct and cheap.

However, it is not suitable for precision applications. As with many contact bearings, it has very poor smoothness of motion. The highest precision steel balls are made to 44μm. variation for 127 μm diameter balls and 25μm. variation for 50.8 mm diameter balls [28]. For other type of ball material, variation varies with 50 μm for 25.4mm diameter ceramic and polymer based balls. Such high variation induced a big smoothness error motion. Hertz contact analysis [29] shows that contact stress of the ball and the stage is very localized and in the order of 1 GPa if small (5mm diameter) balls are used . Therefore balls an order of magnitude (50mm diameter) to reduces the stress levels so that they do not permanently damage the bottom of the stage. The corresponding contact stiffness between the ball and the stage is in the order of 30 N/μm (for steel and ceramics) and much lower for polymer based balls. Although, theoretically we can put a stiffer spring, however the lower stiffness will dominate. Therefore the levitation stiffness of this mechanism can only get as high as 30 N/μm. This levitation scheme is also very sensitive to load distribution. As stage moves in its two dimensional workspace, position of center of gravity of the stage will be shifting and therefore result in varying deflection of the ball- spring system causing the stage to tilt.

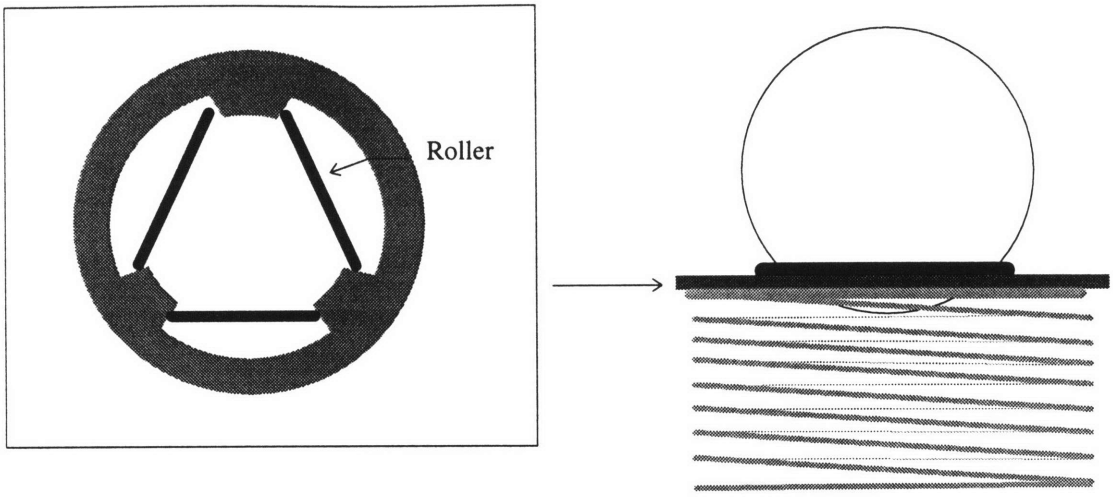

Figure 14 Ball - Spring Levitating Mechanism

2.5 Two Dimensional Stage Adaptation

From this prototype, extension to two dimension stage design is simple. The bearing support need to extended to cover the workspace, using the current bearing design. The only difference is that there will be no alignment magnets or magnetic preloading. Gravity preload is thought of as an alternative. Another option is to use porous air bearings or active magnetic suspension. The former case, it will be just as similar to the proposed 2D slider, however usage of active magnetic suspension adds significant amount of complexity to the problem, but of course will yield better result.

Maintaining alignment of motion is achieved via using a set of 3 actuators. The base is already capable of accommodating two more actuators. Controls of stage will be more difficult due to the cross-coupling of the X-Y motion and synchronizing the actuators. For instance, to get a linear motion all three actuators will have to be precisely synchronized to give the desired linear motion, while reducing tilt, yaw and pitching.

2.6 Summary

In this chapter, a design of a precision stage is outlined. Stage requirements were established and using precision design methodology, a prototype is proposed. The prototype incorporates a PTFE based sliding bearing on Silicon Carbide ceramic bearing

way for high stiffness, low sliding friction and high motion smoothness. Details of dimension, bolt spacing and assembly method is also described.

A new configuration of piezo actuator was designed and, by concept, is capable of driving the stage in any direction on a 2D workspace. The design of the prototype also include a study of different method of stage suspension and evaluation of sensors for the system. In the end, several other component candidates that were studied but not used in the design are also described.

The actuator being designed relies heavily on the contact between the tip of actuator and bottom of the base. Therefore a study of interaction of these surfaces is necessary to improve predictability the driving process. A study on friction phenomenon and its model is conducted in Chapter 3.

Chapter 3

Friction Modeling

The precision stage designed relies heavily on contact between the actuator and the stage. To achieve the desired nanometric resolution, a comprehensive understanding of friction is required. In this chapter, friction and friction models are reviewed. The physics of friction, contact topography between engineering surfaces and friction models developed by researchers are being presented in the next sections. The friction model is then being rewritten in bond graph notation to clearly see the energetic interaction between the different subsystems involved.

3.1 Physics of Friction

Friction is present in the motion of bodies in contact. It plays a role in even the simplest actions of living, such as walking, grasping and stacking. Although it is a desirable property, it is generally an impediment for servo control, especially that of requiring high precision and resolution servo mechanism, such as the stage we are proposing. These types of machines require small motions and low relative velocities at which friction non-linearities become more evident.

For a controls engineer, it is the friction dynamics which is of greatest interest. Friction affects the system dynamics in all regimes of operation. The motivation for study of contact friction is to develop or apply friction models that would predict friction phenomenon such as stick- slip, presliding and hyteresis. These models would aid in studying the controllability and stability from the systems perspective. A compensation technique would then be readily applied to the system to achieve the performance specifications with great reliability, repeatability and precision.

3.1.1 Topology of Contact

In order to understand the physics of the friction phenomenon, it is necessary to consider the surface topography. In Figure 15, a conformal contact is shown. Kinematically, such conformal contact is identified as area of contact: the apparent area of such contact is determined by the size of the part. On the other hand, surfaces that does not enjoy matching radii of curvature meet at a non-conformal contact, as shown in Figure 16. Ideally the non-conformal contact is kinematically characterized by a point or line contact. These is a common type of contact in engineering problems and often referred to as Hertzian contact. In these types of contacts, peak stresses can be 100 times greater than that of conformal contact stresses [1] [2].

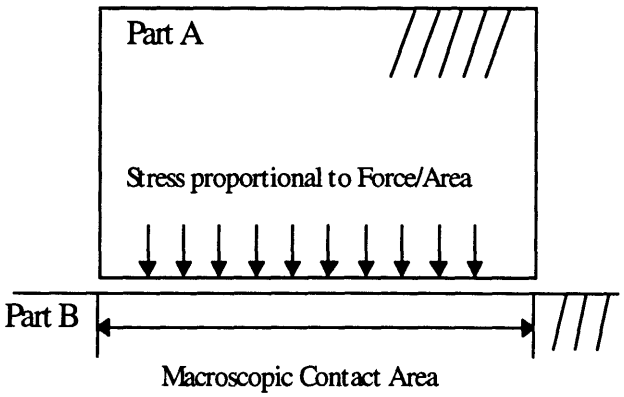

Figure 15 Conformal contact

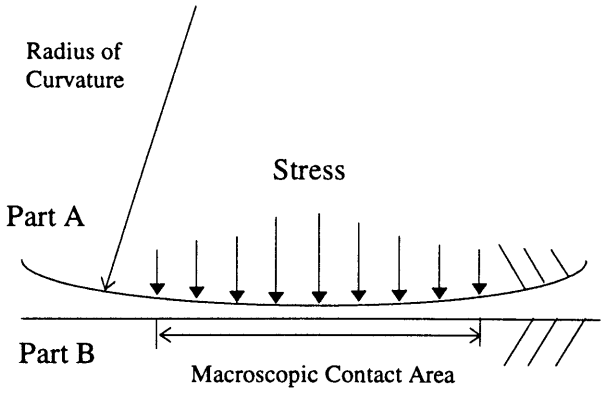

Figure 16 Non-conformal contact

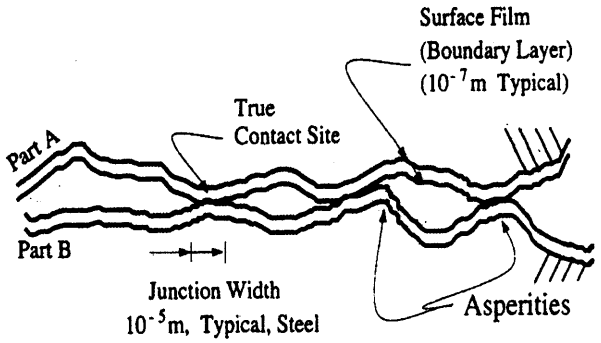

Figure 17 Contact between engineering surface

Even apparent smooth surfaces are microscopically rough. The peaks of the surfaces, called asperities, and true contact occurs at points where asperities come together (see Figure 17). Contact stresses at these asperities could be as high as three times the yield strength (this is possible because the stresses are compressive) [1][2]. The shear strength of these asperity junctions are constant, which makes the friction force proportional to load normal to the sliding surfaces. The proportionality constant, called the friction coefficient, are as a result of oxide films that will form on engineering surfaces, producing a boundary layer on contacting surfaces. The oxide film are solid, but has a lower shear strength, and most shearing will occur in this boundary layer. These films are very thin - they vary from a few atomic thickness (in the order of several angstroms) to a fraction of a micron [1][2].

3.1.2 Friction Dynamic Regimes

The simplest explanation of friction subdivides friction into static and kinetic (sliding) friction. In these definition of friction, the friction forces is simply the normal load multiplied by either a static or kinetic coefficient of friction. Static friction refers to friction behavior without any transients. Therefore rate of changes in relative velocities would result in an instantaneous change in friction force. The term Coulomb friction refers to dry friction.[3] This simple representation of friction is not capable of explaining most of the non-linear friction phenomenon. Therefore, it is logical to pursue a more comprehensive understanding of friction.

The relationship of friction and velocity are sub-divided into four regimes of lubrication for a system with lubricant. Different friction phenomenon of interest to a control engineer are observed in these different regimes because different forces are dominant in different regions. The curve shown in Figure 18 is known as the Stribeck curve. This curve depicts the four regimes (one of which are zero velocity regime). Note that the constitutive law falls in the first and the third quadrant [1][11][18].

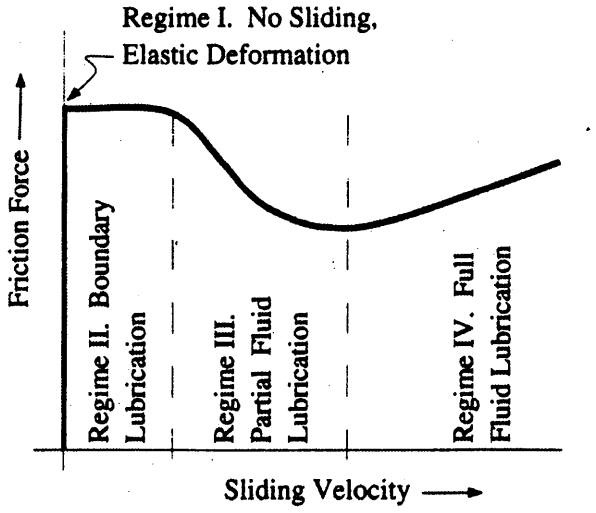

Figure 18 Generalized Stribeck Curve [1]

The four regimes as defined in [1][2] are as follows:

1. *The first regime and presliding displacement.* As shown in Figure 17, contact between two engineering surface occurs at asperity junctions. From the control standpoint, these asperities deform elastically to cause the presliding phenomenon. Presliding are infinitesimal displacements that occur at zero relative velocity, to be discussed further in Section 3.1.3. The asperities and boundary layers also deform plastically to give rise to rising static friction. Rising static friction is known to have an important influence to another interesting friction phenomenon called the stick-slip or stiction [1][2], to be discussed in Section 3.1.3.

2. *The second regime: Boundary Lubrication.* Sliding velocity in this regime is very low. The boundary lubrication is dominant in this regime as the velocity is inadequate to cause a fluid lubrication on the contacting surfaces. There is solid to solid contact, shearing occurs in the boundary lubricant. This is a process of shear in solid, therefore friction force is higher than that of regimes three and four. Some boundary lubricants do reduce the static friction level to below Coulomb friction level thus entirely eliminating stick- slip [1][2].

3. *The third regime: partial fluid lubrication.* The velocity in this regime is high enough to draw fluid lubricants into the contact zone. The greater viscosity or motion velocity, the thicker the fluid film will be. However, for fluid films thickness less than asperities height, solid to solid contact still occurs, there will be partial fluid lubrication. Controls issue of interest is the dynamics of partial fluid lubrication with varying velocity. Researchers have observed in many circumstances that there is a time lag between change in velocity or load conditions and the change in friction force to its new steady state level. The lag is in the order of milliseconds and may have substantial effect of stick- slip and hyteresis cycle of friction. This time or phase lag is called friction memory [1][2].

4. *The fourth regime: full fluid lubrication.* As fluid lubricant layer becomes thicker, solid to solid contact is totally eliminated, thus giving rise to full fluid lubrication. Hydrodynamic and elasto-hydrodynamic lubrication are two form of full fluid lubrication. In this regime, wear is reduced in orders of magnitude and friction is deterministic and linear. General predictive models for steady state film thickness are available for predicting friction. For controls, the main interest is in studying the transients of state transition to full fluid lubrication regime [1][2].

3.1.3 Friction Phenomenon

Friction involves has several non-linearities that are of interest for a control engineer. Most of these phenomenon are observed at very low velocity or even zero velocity. The Dahl effect, for example, involves very small displacements between rubbing parts with zero relative velocity. Stick- slip occurs at low relative velocity that could possibly cause limit cycles for precision machines.

Presliding and the Dahl Effect

To most, during static friction, there are no displacements involved. However, a more through study [1][2], have shown that presliding, a very small displacement between contacting surfaces, occurs in the first regime of the generalized Stribeck curve. In this regime, the surfaces meet at asperity junctions. The asperities deform elastically to give way for these small displacements.

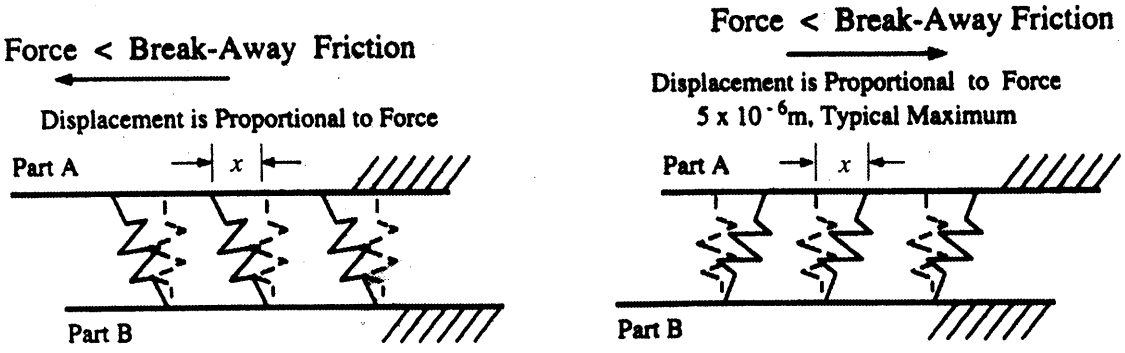

Figure 19 Idealized static contact. Asperities behave like springs.

Armstrong [1][2], has idealized the asperities junctions behavior like a spring. Figure 19 shows the idealized model, where F_t is the tangential force, k_t is the tangential stiffness and x is the displacement from the equilibrium position. The tangential stiffness, k_t, is a function of asperity geometry, material elasticity and applied normal force. When the tangential force is greater than the break away force, then the junction breaks and true sliding begins. Breakaway is observed to occur in the order of 2-5 microns in steel junction.

Presliding is of interest to the controls engineers in extremely high precision applications, our project being one of those that require such high precision. Presliding can be significant for submicron precision machines, as the magnitude of presliding deflection magnitude is in the order of micron. Presliding also has been important in establishing that there are no discontinuities in friction as a function of time and velocity.

Stick-slip

When bodies in contact move at a velocity just above the breakaway relative velocity, a phenomenon called the stick- slip occurs. Stick- slip, like the name implies, is a stepping motion of the two surfaces. The friction force, during this motion, oscillates about the kinetic friction level. Figure 21 and Figure 22 shows displacement versus time and force versus time of the stick- slip phenomenon.

Rabinowicz [26] observed two temporal phenomena in the stick- slip process. They are:

1. A connection between the time a junction spends in the stuck condition, dwell time and the level of static friction (rising static friction);

2. A delay between a change in velocity and the corresponding change the friction (frictional lag). A more detailed description in Section 3.1.3.

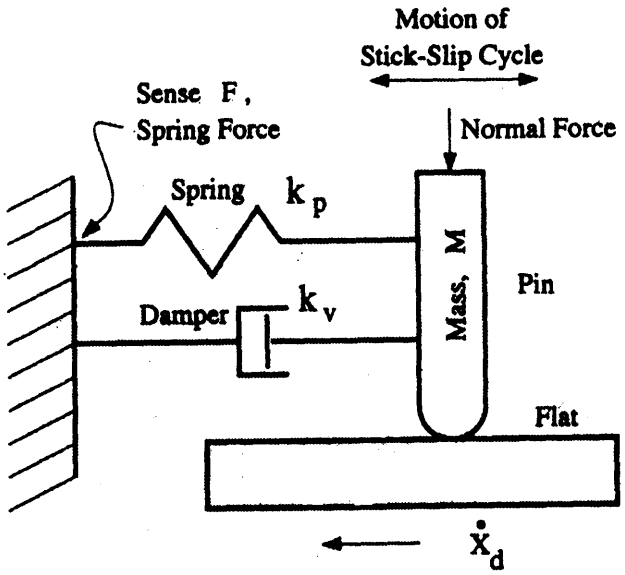

Figure 20 Pin on flat friction machine [1]

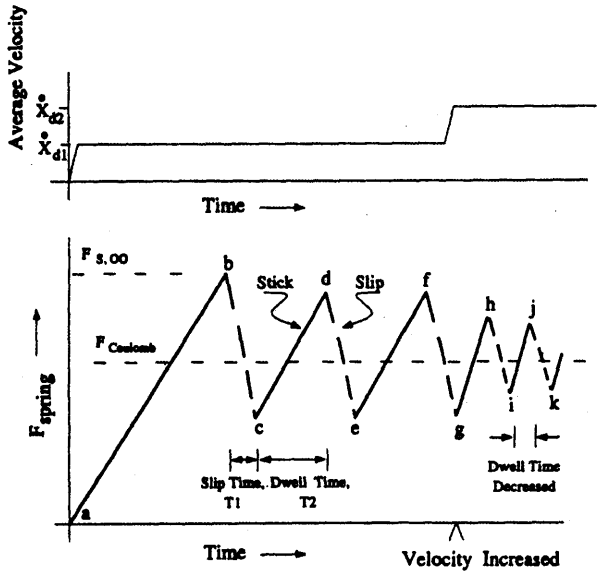

Figure 21 Spring force profile during stick- slip motion at two velocities. [1]

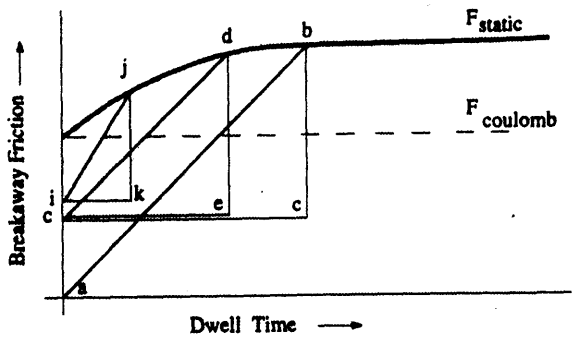

Figure 22 Static friction as a function of dwell time. [1]

To illustrate the role of rising static friction, consider the mass-spring-damper system shown in Figure 20. This mechanism, under moderate values of damping, k_v and some conditions for spring stiffness, k_p, will exhibit stick- slip behavior. With reference to Figure 21 and Figure 22, during stick period a-b, the force builds up. At point b, the force reaches the ultimate static friction, breakaway occurs and slippage begins. At point c, the relative velocity between the mass and the flat becomes zero and the force start to build up again. As velocity is kept within this neighborhood ($\dot{x} \sim \dot{x}_{d1}$), the system enters a stable limit cycle of points c-d-e. Point d is lower than point b because the system has only be resting for a shorter dwell time c-d. As the mass moves with the flat with constant velocity, the spring deflection is less since velocity a-b and c-d is constant but dwell time is less for c-d. Therefore the spring force build up during c-d is less than during a-b. For increasing velocity, the limit cycle size diminishes, as seen in cycles g-h-i and i-j-k. The static friction level is a function of dwell time and as velocity increases, dwell time decreases and the static friction level also decreases to the kinetic friction level. This is also the reason why the limit cycle is smaller at higher velocity. Some empirical models describing the static friction and dwell time and rising static friction are cited in [1][2]. One of them, by Kato *et al.*, as cited in [1], is given by:

$$F_s(t) = F_{s,\infty} - (F_{s,\infty} - F_c)e^{-\gamma t^m}$$

where $F_{s,\infty}$ is the steady state kinetic friction; F_c is the coulomb friction at the moment of arrival in the stick condition; γ and m are empirical parameters. Values of γ and m has

been examined to be 1.66 and 0.65 respectively for conformal contact [1]. A small value of γ indicates a long rise time thus resist stick slip.

These models would be useful, from controls standpoint, for analyses such as of how slow a machine could be driven.

Frictional Memory

From the generalized Stribeck curve, one might presume that a change in velocity is accompanied by an instantaneous change in friction force. However, Hess and Soom as cited in [1][2] observed that there is a 3 to 9 ms time delay in the corresponding changes. This delay is called the frictional lag or frictional memory. Figure 23 show a section on the Stribeck curve which shows friction force levels and its corresponding velocities. Changes in these velocities is not followed by an instantaneous change in friction force as shown in Figure 24. Hess and Soom, also observed that the lag increasing with increasing lubricant viscocity and increasing with increasing contact load, but independent of the oscillatory frequency. In the same experiment, hyteresis is evident in a friction coefficient versus velocity plot and derived a pure lag model of frictional memory.

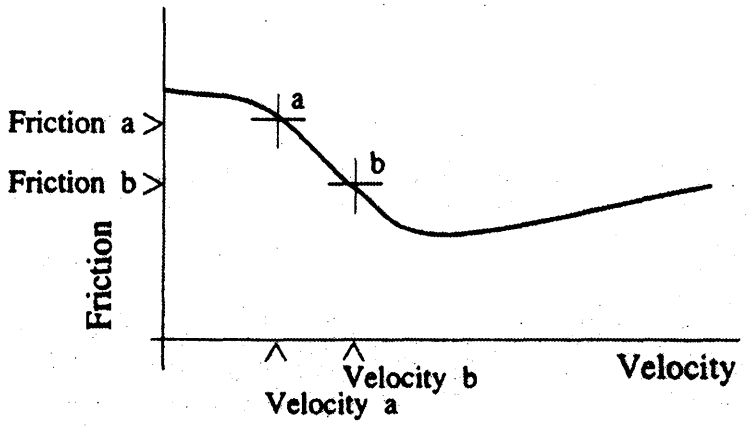

Figure 23 Stribeck friction versus velocity curve

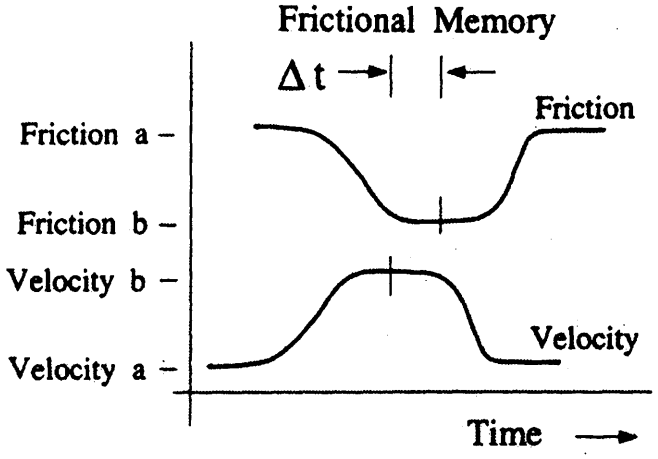

Figure 24 Friction and velocity versus time, showing friction memory

Stribeck Effect

Stribeck effect, the phenomenon of decreasing friction force with increasing velocity, is observed at very low velocity. This is also know as negative viscous friction is as a result of fluid lubrication [1][2]. Stribeck effect is closely linked to the stick- slip phenomenon, in fact stick- slip could not be explained without Stribeck effect, as explained in a literature by Tustin cited in [1]. Researchers, as reviewed in [1][2] also observed that motion in velocities in the Stribeck region is relatively unstable and would result in limit cycles.

3.2 Friction Models

Most of the available friction model are described by static maps between velocity and friction force. These type mapping have failed to capture the dynamics of friction, such as the hyteresis, stick- slip, stiction, friction memory etc. Failure to capture frictional dynamics can lead to tracking errors, limit cycles and undesirable stick- slip motion. Therefore, a good friction model is necessary to analyze stability, predict limit cycles, determine controller gains, perform simulations, etc.

Most of model-based friction compensation schemes, use classical friction models, such as Coulomb and viscous friction. This models do not yield satisfactory

results for applications with high precision positioning and low velocity tracking, because of many of the friction phenomena occurs at velocity close to zero. Classical models explains neither hysteretic behavior nor variations in break- away force. It also usually involve a hard non-linearity at $velocity = 0^{+}$, where friction force instantaneously jumps from static level to Coulomb friction level. This is unrealistic and not observed in practice [18].

Canudas, Olsson, Astrom and Lischinsky's in [5] considered the following to be key properties of friction models.

- Steady state characteristic including Coulomb friction, viscous friction and Stribeck effect
- Ability to predict stick slip motion.
- Hysteresis for friction as a function of relative velocity and as a function of relative displacement
- Spring like stiction behavior

In the following sections, we describe the newer dynamic friction models that is considered to be the most accurate friction models presented at the moment.

3.2.1 New Friction Model for Control System

In [6], a new friction model was proposed. This dynamic friction model combines stiction behavior, i.e. the Dahl effect, with arbitrary steady state friction characteristics which can also include Stribeck effect.

The model is based on averaged behavior of the bristle deflection, denoted by z and given by:

$$\frac{dz}{dt} = v - \frac{|v|}{g(v)} z \qquad (3.1)$$

$$F = \alpha_o z + \alpha_1 \frac{dz}{dt} + \alpha_2 v \qquad (3.2)$$

where

v = relative velocities between the two surfaces,

z = average bristle deflection,

F = total friction force.

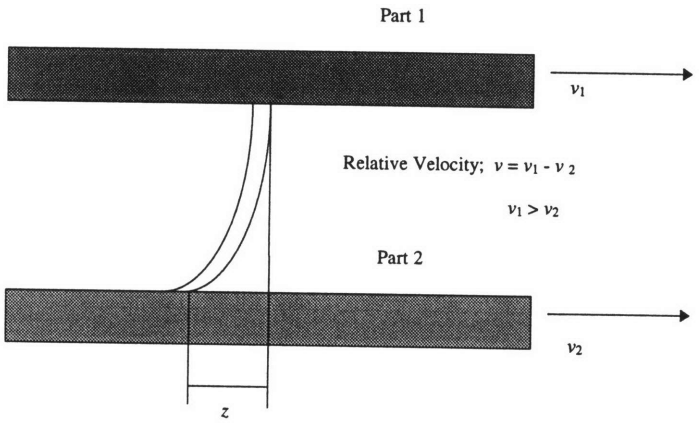

Figure 25 Definition of z

The function $g(v)$ is positive and depends on many factors, such as material properties, lubrication, temperature. A parameterization of $g(v)$ that has been proposed in [6] to describe the Stribeck effect is:

$$\alpha_o g(v) = F_C + (F_S - F_C) e^{-(v/v_s)^2} \qquad (3.3)$$

where

F_C = Coulomb friction level,

F_S = level of stiction force,

v_s = Stribeck velocity; see [1]

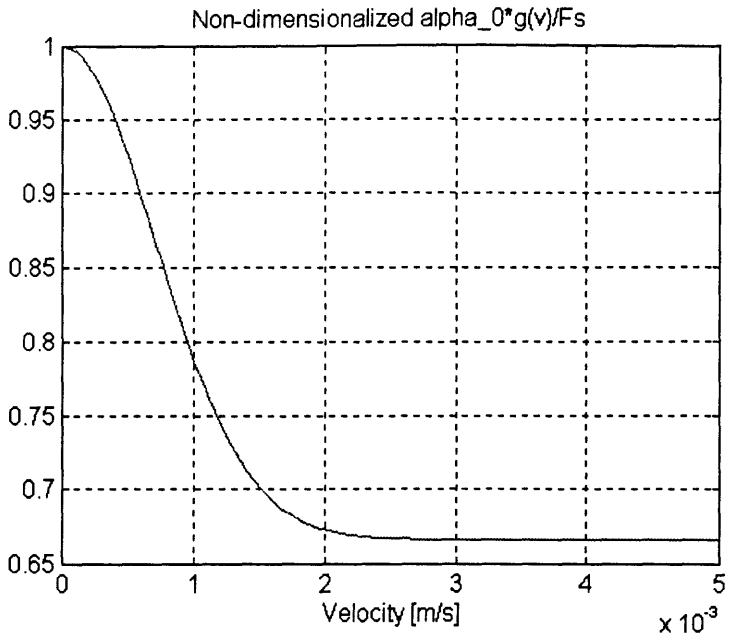

Figure 26 Graph of non-dimensionalized $\alpha_0 g(v)$ as a function of velocity

Simulations of this model for different frictional behavior are also reported in [6]. This model has been simulated to exhibit pre-sliding displacement as was shown by Courtney-Pratt and Eisner. It also captures the hysteretic behavior of real friction, with the loop becoming wider with higher rates of velocity changes. Rising static friction (varying break- away force) is also predicted and reported to agree qualitatively with the experimental results by prior investigators. Lastly, stick- slip motion is also captured by this model. However, there is a highly irregular behavior of the friction force around the region where the mass stops.

3.2.2 Other Models

Other than the model presented, there are many other models introduced of the years attempting to address frictional non-linearities. Canudas *et al.* [5] , proposed a model that maps the static relation between friction force and relative velocity. The mapping include Coulomb friction, viscous friction and the Stribeck effect. This model

also predicts stick-slip motion and hysteresis, however simulations are quite different from actual data.

P.Dahl, as cited in [1], introduced a dynamic friction model, describing spring like behavior during stiction. It predicts frictional lag and is very well understood, however does not exhibit the Stribeck Effect. An attempt to incorporate this into Dahl model was done, where a second order Dahl Model was introduced using linear space invariant descriptions. The Stribeck effect is only exhibited in transient, however, and is not present in steady state descriptions. Armstrong- Helouvry [2] proposed a seven parameter model. This model is a piece-wise model for stiction and sliding friction.

3.3 Bond Graph Analysis of Friction Model

The central idea in the study of dynamics of a real system is the idea of a system model. The equations (3.1) through (3.3) gives the model of friction in mathematical form. However, it would be interesting to relate these equations to the physical phenomenon they represent and reconstruct them in another form of system model, i.e. the physical model.

One possible way to represent the friction models using physical elements is to use the bond graph notation. Bond graph notation, introduced by H.M. Paynter in 1960 at MIT, is a graphical notation that describe concisely the energy and information flow between elements in models of engineering systems. It also reflects the system structure and the causal energetic interaction between subsystems [38]. Bond graph notation is also convenient for control engineers as the system equations derived will already be in state space form. Karnopp [15] describes the bond graph method more rigorously.

Using the bond graph approach, a system model is represented as series of energy source elements, energy storage (capacitive and inductive) elements, energy dissipation (resistive) elements and energetic junctions linked by power bonds. In this thesis, we attempt to reduced the mathematical equations (3.1), (3.2) and (3.3) to some bond graph

representation. In doing so, we tried to find the elements and their constitutive relations that will allow the rederivation of the equations.

As a background, is advantageous to understand how friction model described in Section 3.2.1 was based on. The contact interface shown in Figure 17 is thought of as bristles and he model was based on the aggregated behavior of these bristles [6][11]. The bristle and its bond graph notation are shown schematically in Figure 27.

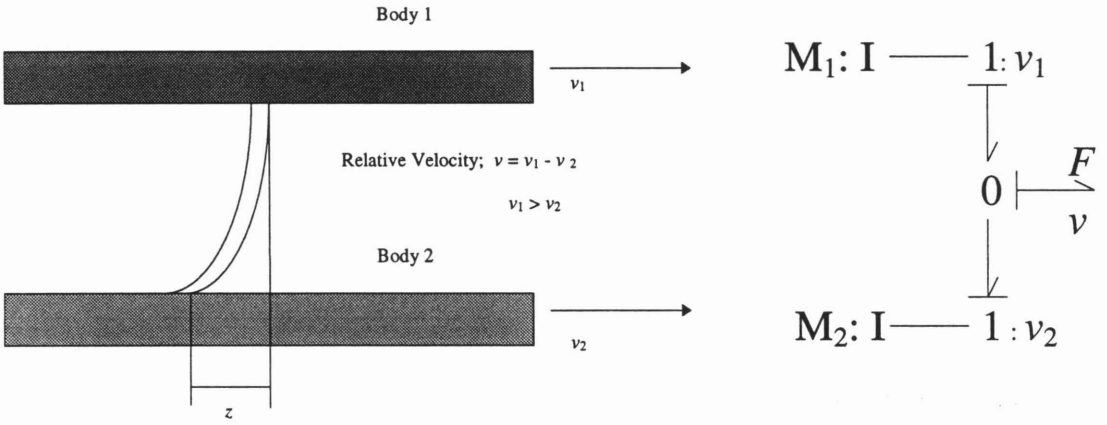

Figure 27 Idealized bristle model and its corresponding bond graph notation

Observation of equation (3.2) reveals that the total friction force is contributed by three terms:

$\alpha_0 z$ resulting from the compliance of the bristle,

$\alpha_1 \frac{dz}{dt}$ resulting from damping in the bristle,

$\alpha_2 v$ resulting from viscous friction between surfaces 1 and 2

The model is also reported to exhibit hysteretic behavior. Karnopp showed that a generalized mechanical hysteresis can be modelled by using a capacitive element and a resistive element [16] as shown in Figure 28.

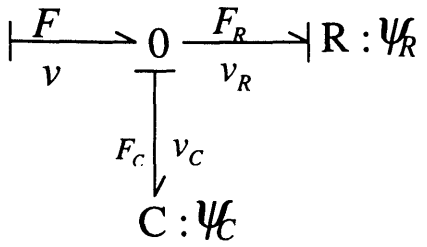

Figure 28 Generalized mechanical hysteresis

The goal here is to find the constitutive relations of the C and R element. However before proceeding to write those relations, it is also important to have a an intuition of what the internal variable z means. The authors of [6] defined z as an internal state which corresponds to the deflection of the bristle. The bristle can be thought of as a cantilever beam, with a deflection z and has a rate of deflection $\dot{z}$ (see Figure 27). To verify this, consider the following:

Suppose $g(v) = \dfrac{F_C}{\alpha_0}$

Then equation (3.1) becomes $\dot{z} = v - \dfrac{|v|}{F_C / \alpha_0} z$ or

$$\dot{z} = v - |v| \frac{\alpha_o z}{F_C}$$

The ratio $\alpha_0 z / F_C$ is the ratio of "bristle spring" force over Coulomb friction level. When part 1 is in motion relative to part 2, the bristle begins to deflect, until the force due to the deflection of bristle equals the Coulomb friction level. When this happens the ratio $\alpha_0 z / F_C = 1$, and $\dot{z} = 0$, which means the bristles stops bending. From this discussion one can intuitively verify the definition of z.

Similarly, one can consider the following non-linear differential equation in z:

$$\dot{z} + \frac{|v|\alpha_0}{F_C} z = v$$

at steady state, $\dot{z} = 0$ and the steady state value of z, z_{ss} is given by:

$$z_{ss} = \frac{F_C}{\alpha_0}\frac{v}{|v|} \text{ or in absolute value, } z_{ss} = \frac{F_C}{\alpha_0}$$

which agrees with statement made above.

One can consider that the term $\alpha_0 g(v)$, which has units of force, as a form of force. Following along the lines of the previous discussion, we can conclude that z_{ss} varies as a function of velocity, specifically in compliance with g(v).

The equation (3.1) imposes an **0** junction with flow energetic flow and causality as shown in Figure 28 because equation (3.1) is sum of velocities. Equation (3.1) is a first order differential equation, implying that a combination of two **R** elements are not possible. To construct a first order dynamics, a energy storage element (**C** or **I**) in integral causality is needed. A **C-C** combination is also unacceptable, because Karnopp [16] has shown that hysteresis is captured only with an **R-C**. This leaves us with a **R-C** or a **C-R** element combinations as shown in Figure 29. In both cases, in order to be consistent with equation (3.1), $v_c = \dot{z}$ and $v_R = [|v| / g(v)]z$.

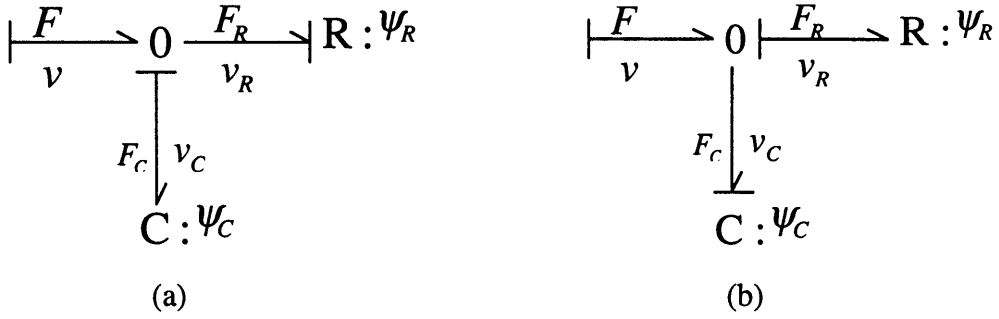

Figure 29 Possible **R-C** combinations

Using the argument mention before, the combination in Figure 29b cannot be used because the **C** element is in derivative and does not contribute to the system state. Therefore equations derived from Figure 29b would be algebraic and not a differential equation. In Figure 29a, if we suppose $\psi_C = \alpha_0$ and $F_R = \psi_R v_R$, then,

$$F_R = F_C = \alpha_0 z$$

$$v_R = \frac{F_R}{\psi_R} = \frac{\alpha_0 z}{\psi_R} = \frac{|v|}{g(v)} z$$

Therefore, $\psi_R = \frac{\alpha_0 g(v)}{|v|}$

As a self check, if we derive the equations using these constitutive laws:

$$\frac{dF_C}{dt} = \alpha_0 v_C = \alpha_0 \dot{z} = \alpha_0 (v - v_R)$$

$$\alpha_0 \dot{z} = \alpha_0 v - \alpha_0 \frac{F_R}{\psi_R}$$

$$\alpha_0 \dot{z} = \alpha_0 v - \alpha_0 \frac{|v|}{\alpha_0 g(v)} F_R$$

$$\alpha_0 \dot{z} = \alpha_0 v - \alpha_0 \frac{|v|}{\alpha_0 g(v)} \alpha_0 z$$

$$\dot{z} = v - \frac{|v|}{g(v)} z$$

which agrees with equation (3.1). The causality of the bond graph in Figure 29a reveals that the effort is dictated by the **C** element. Therefore the force is

$$F = F_C = \alpha_0 z$$

The bond graph of the friction (interconnecting Figure 27 and Figure 28) for bristle compliance and viscous friction terms can be redrawn as shown in Figure 30. Note

that the viscous friction term, with parameter α_2, is added to represent the viscous friction between the two surfaces.

The following equations are the equations for the friction force and the dynamics for the system in Figure 30,

$$F = \alpha_0 z + \alpha_2 v \qquad (3.4)$$

$$\dot{z} = v - \frac{|v|}{g(v)} z \qquad (3.5)$$

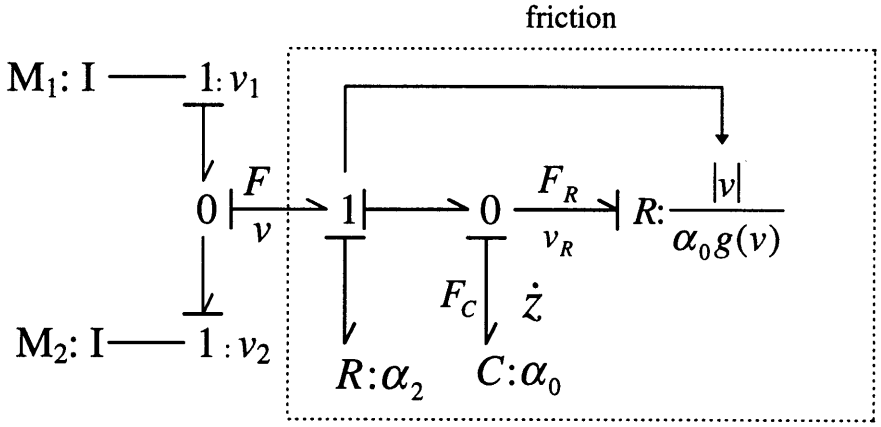

Figure 30 Bond graph notation of Eq. (3.4) and (3.5)

From this analysis, using velocity constraint, one can deduce that only friction force terms such as in equation (3.4) may be obtained. Causality requirements of a **0** junction also state that the force can only be imposed by one element, as shown in Figure 29a. This means, even if Figure 29b is possible, the force term according to this configuration will be $\alpha_1 \dot{z}$. By causality only one of the friction force terms can result from velocity constraint equation (3.1). This is inconsistent with the model proposed where the friction force of equation (3.2) may be obtained using the velocity constraint of equation (3.1).

The friction force resulting from damping of the bristle is missing from equation (3.4). The term $\alpha_1\dot{z}$ has units of force and see the same flow variable ($\dot{z}$) as the term $\alpha_0 z$. This implies a **1**-junction, i.e. constant flow junction. To take the previous analysis one step further, a **1**-junction is appended. Figure 30 then becomes as shown in Figure 31.

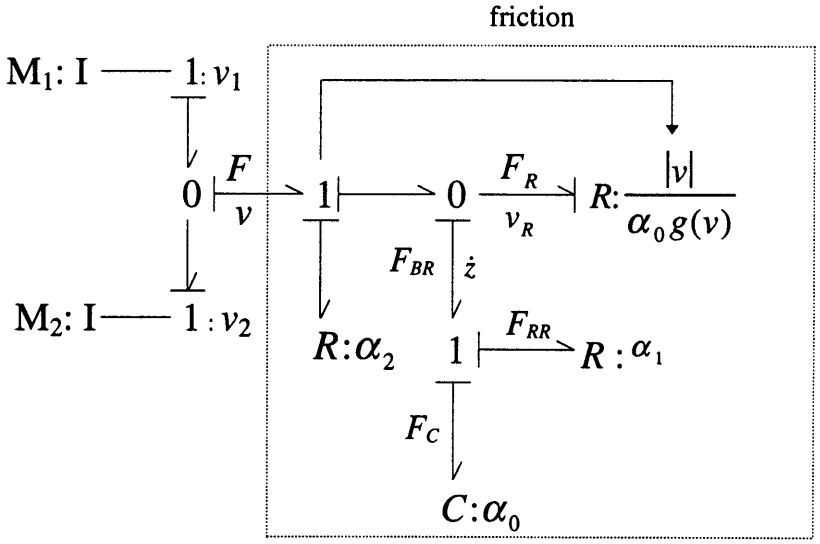

Figure 31 Bond graph notation of Eq. (3.9) and (3.10)

The model's order does not change, because we did not introduce any new energy storage elements. Derivation of state equations from Figure 31, leads to the following:

$$\frac{dF_C}{dt} = \alpha_0\dot{z} = \alpha_0(v - v_R) = \alpha_0\left(v - \frac{|v|}{\alpha_o g(v)}F_R\right)$$

Factoring α_0 out and realizing that $F_R = F_{BR} = F_C + F_{RR}$, we get

$$\dot{z} = v - \frac{|v|}{\alpha_0 g(v)}\left(F_C + F_{RR}\right)$$

$$= v - \frac{|v|}{\alpha_0 g(v)}\left(\alpha_0 z + \alpha_1\dot{z}\right)$$

Collecting and rearranging terms,

$$\dot{z} = \frac{1}{1+\frac{\alpha_1|v|}{\alpha_0 g(v)}} v + \frac{|v|}{\left(1+\frac{\alpha_1|v|}{\alpha_0 g(v)}\right) g(v)} z \text{ or} \qquad (3.6)$$

$$= \frac{1}{1+\frac{\alpha_1|v|}{\alpha_0 g(v)}} \left(v - \frac{|v|}{g(v)} z \right) \qquad (3.7)$$

The total friction force for system in Figure 31 is given by:

$$F = \alpha_o z + \alpha_1 \frac{dz}{dt} + \alpha_2 v \qquad (3.8)$$

Equation (3.8) agrees with the proposed model. However, with the inclusion of another **R** element, with parameter α_1 changes the equation (3.1) by the addition of a non-constant coefficient as shown in equation (3.7). This bond graph analysis showed that a causal friction model would have additional terms to its velocity constraint as in equation (3.7).

The preceding analysis has showed that there is a non-linear **R** element which does not contribute to the total friction force. To help understand what the bond graph in Figure 31 physically means, consider the mass-spring damper system in Figure 32. The elements **C**, **R1** and **R2** impose force when velocity is applied to them and contribute to the total friction force. The element, **R3**, on the other hand defines the difference between the relative velocity and bristle deflection when subjected to a force. The g(v) term, which defines the Stribeck Curve, is only included in the constitutive law of element **R3**. Therefore, we could associate **R3** to the slippage dynamics at the interface where the bristle contacts surface 2, which determines deflection but not contributing to the friction force.

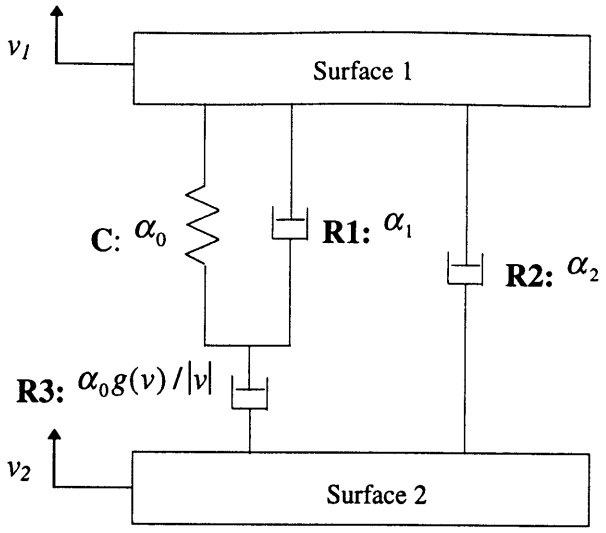

Figure 32 Mass-Spring-Damper equivalent of Figure 31

3.4 Summary

The motivation to conduct an extensive study on friction arises from the need to carefully model the contact between the tip of the proposed actuator and the stage designed in Chapter 2. In this chapter, the physics of friction was studied. Friction phenomenon were understood and friction models were sought after. After the comprehensive survey of friction and of friction models, the friction model presented by Canudas *et al.* was determined to be most current and captures the pertinent friction dynamics. However, since we are also interested in the physical meaning of the friction model, bond graph analysis was performed.

The bond graph analysis was able to show that the friction model presented in [6] is non- causal. The energetic interaction between physical elements if the model is not consistent with the velocity constraint proposed in [6]. Realizing the discrepancy, further analysis was done and a modified constraint was derived. To verify that this modified model also capture the friction phenomenon, simulations are to be performed in Chapter 4.

Chapter 4
Simulations

As a tool to verify its ability of the actuator described in Chapter 2 to generate elliptical motions simulations are performed. The simulations are conducted using two piezo transducers to show that elliptical motion can be generated by elongating the piezo transducer lengths. These simulations are performed and presented in this chapter.

The second part of this chapter, compares friction models proposed in Chapter 3. The objectives of performing the simulations are to compare presliding, hysteretic and stick-slip behaviours of the model proposed by Canudas *et al.* and the model variations. It is also desired to show that the modified models also exhibit characteristics mentioned above.

4.1 Two Dimensional Actuator Kinematic Simulation

In this section, an actuator such as in Figure 6 and Figure 7 is simulated to verify that such elliptical motion is possible. Before we perform the simulation, kinematics of such assembly is derived. Consider Figure 33. **T1** is the vector from point 1 to the midpoint of 1-2 and **T2** is a vector normal to **T1** to the top of the actuator tip. Quantities $\pm\Delta 1$, $\pm\Delta 2$ are displacements induced by the piezo transducer. The horizontal distance between point 1 and 2 is 46mm and is considered to be constant. This assumption is

warranted as $\pm\Delta 1$ and $\pm\Delta 2$ are both in the order of microns (10μm to be exact). Taking the equilibrium of point 1 as the origin, **T1** and **T2** are given by:

$$T1=\frac{1}{2}\left[D,(\Delta 2-\Delta 1)\right] \tag{4.1}$$

$$T2=\left[-(\Delta 2-\Delta 1),h\right] \tag{4.2}$$

and tip position is given by

$$[x,y]=[0,\Delta 1]+T1+T2 \tag{4.3}$$

where h=20mm, D=46mm and $\Delta 1,\Delta 2=\pm 10\mu m$

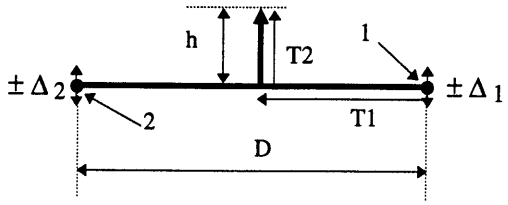

Figure 33 Vector representation of actuator in Figure 6

$\Delta 1$ and $\Delta 2$ are elongations of the piezo transducers at point 1 and 2, respectively. In this simulation they are modeled as sinusoidals and treated as input signals to equations (4.1) and (4.2). These two input signals are out of phase by φ. $\Delta 2$ lags $\Delta 1$ by the amount φ. Equations (4.1), (4.2) and (4.3) are simulated and the tip positions are represented by x and y as shown in Figure 34.

The simulations verifies that elliptical motions are indeed possible from the proposed actuator. Furthermore, the orientation and shapes of the ecliptic trajectory are as a function of phase lag φ. This is an interesting result that can be manipulated for control purposes during implementation of the actuator.

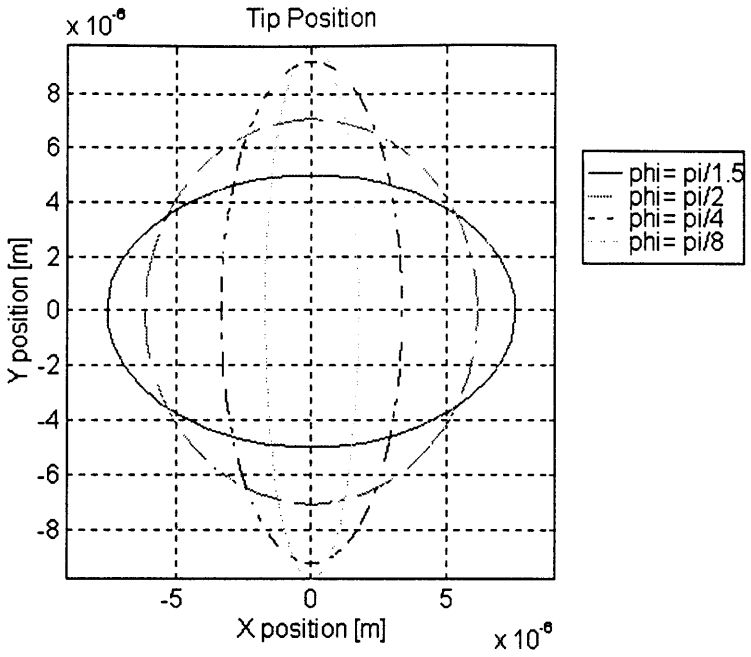

Figure 34 Simulations showing elliptical actuator tip motion

4.2 Friction Simulations

In Chapter 3, we have described a new friction model by Canudas *et al.* [6]. We have developed two modified models. These models are consistent with bond graph notation and are considered causal. The following is a summary of the equations of the different models. Variables used in the model, are defined in Chapter 3.

The first model is proposed by *Canudas et al.* in [6] and its equations were introduced as equations (3.1),(3.2) and (3.3). Equation (3.3) and (4.6) are parameterized equations that regulates different friction force level and induces the Stribeck effect is accepted for all three models.

$$\dot{z} = v - \frac{|v|}{\alpha_0 g(v)} z \tag{4.4}$$

$$F = \alpha_o + \alpha_1 \frac{dz}{dt} + \alpha_2 v \tag{4.5}$$

$$\alpha_o g(v) = F_C + (F_S - F_C) e^{-(v/v_s)^2} \tag{4.6}$$

The second model (Equations 4.7 and 4.8) referred to as "*No Bristle Damping*" model in this thesis, was derived to be consistent with (4.4) and its bond graph notation is shown in Figure 30. To maintain causality, the total friction force given by equation (4.8). The purpose of simulating this model is to demonstrate the effect of eliminating the damping term from the total friction force.

$$\dot{z} = v - \frac{|v|}{\alpha_0 g(v)} z \tag{4.7}$$

$$F = \alpha_0 z + \alpha_2 v \tag{4.8}$$

The third model, is referred to as "*Modified Dynamics*" model (Equations. 4.9 and 4.10). In this model, the total friction force is consistent with [6]. However, the dynamics is derived from Figure 31 and happens to be slightly modified from the proposed dynamics (Eq. 4.4).

$$\dot{z} = \frac{1}{1 + \frac{\alpha_1 |v|}{\alpha_0 g(v)}} \left(v - \frac{|v|}{g(v)} z \right) \tag{4.9}$$

$$F = \alpha_o + \alpha_1 \frac{dz}{dt} + \alpha_2 v \tag{4.10}$$

Chapter 3 and [5] described key properties of a friction model as a guideline to comparing the models. In general, friction models should capture the most important friction phenomenon, namely presliding, hyteresis and stick-slip motion. In accordance to these set of guidelines, simulations are conducted to demonstrate the capabilities of each friction model to capture each of the friction phenomenon listed. All simulations were performed for unitary mass system with friction. Parameters used in all simulations, similar to the ones used in [6], are listed in Table 3.

Parameter	Value	Unit
α_0	10^5	[N/m]
α_1	$\sqrt{10^5}$	[Ns/m]
α_2	0.4	[Ns/m]
F_C	1	[N]
F_S	1.5	[N]
v_S	0.001	[m/s]

Table 3 Parameters values used in all simulations

4.2.1 Presliding Displacement

Friction behaves like a spring if the applied force is less than the break-away force. If a force is applied to the two masses in contact, there will be a displacement [6]. A simulation was performed to compare how the three models differ in capturing this phenomenon.

The system of equations for this simulations are as follows:

$\dot{v} = u - F$; where F is replaced by equations (4.5), (4.8) and (4.10) for respective models and u is the input force,

$\dot{x} = v$

$\dot{z}$ is equals to equations (4.4), (4.7) and (4.9) according to the respective models.

The input force u is increased linearly to 1.425 N which is 95% of F_S from t=0 to t=1sec. Then the force is decreased linearly to -1.425 N until t=3 sec. and ramped up to 0 N until t=4 sec. Results of the simulations are shown in Figure 35, Figure 36 and Figure 37.

These simulations clearly shows that presliding is captured. This is because a small displacements are observed even then the applied force has yet to exceed static force level.

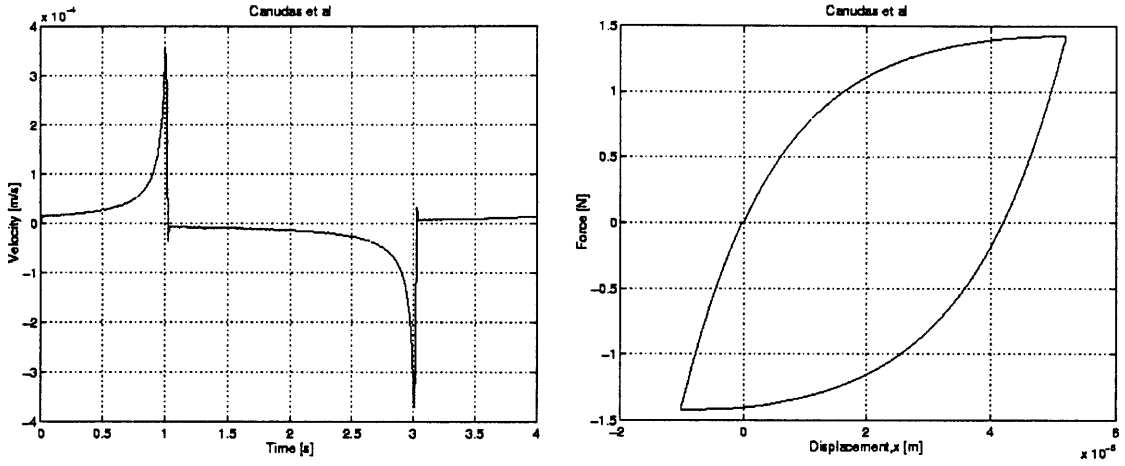

Figure 35 Presliding displacement for Canudas *et al.* model

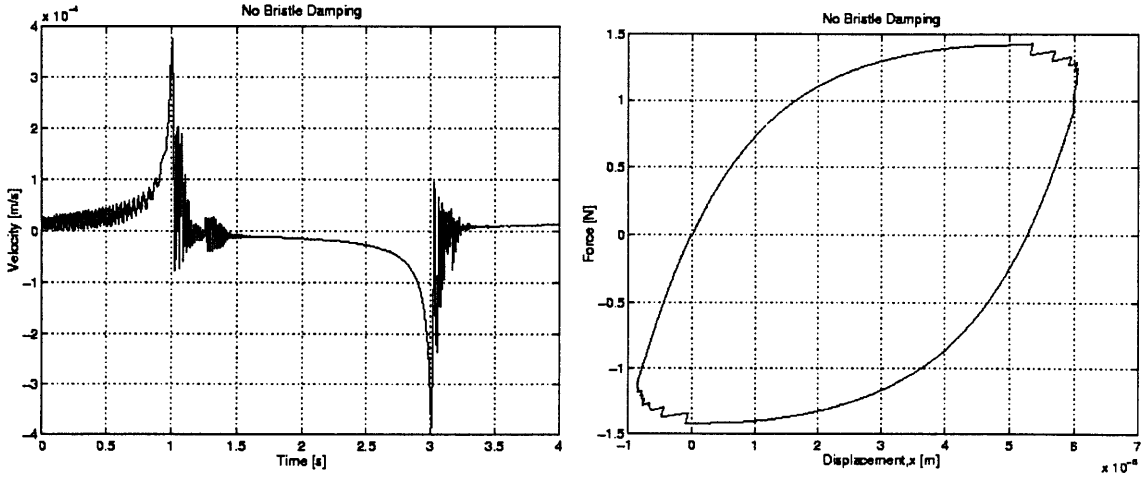

Figure 36 Presliding displacement for "No Bristle Damping" model

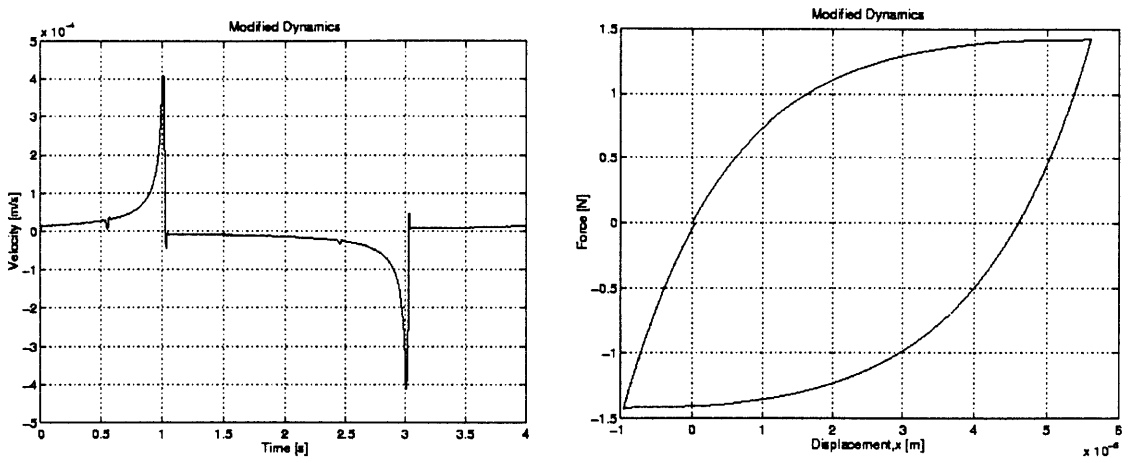

Figure 37 Presliding displacement for "Modified Dynamics" model

4.2.2 Hysteresis

Hysteresis behavior has been observed by many researchers as cited in [1]. A simulation was conducted to investigate and to compare the hysteresis phenomenon by the three models. The simulation imposes an acceleration profile to achieve sinusoidal velocity profile around an equilibrium. The system of equations for this simulation are as follows:

$\dot{v} = u$ where $u = 1.0^{-3} \cdot \omega \cdot \sin(\omega t)$, with initial conditions, $u_0 = 1.5^{-3}$

$\dot{x} = v$

$\dot{z}$ is equals to equations (4.4), (4.7) and (4.9) according to the respective models.

The results of the simulations are shown in Figure 38. For all three models, the simulations clearly shows hysteresis. The width of the hyteresis loop is observed to increase with frequency.

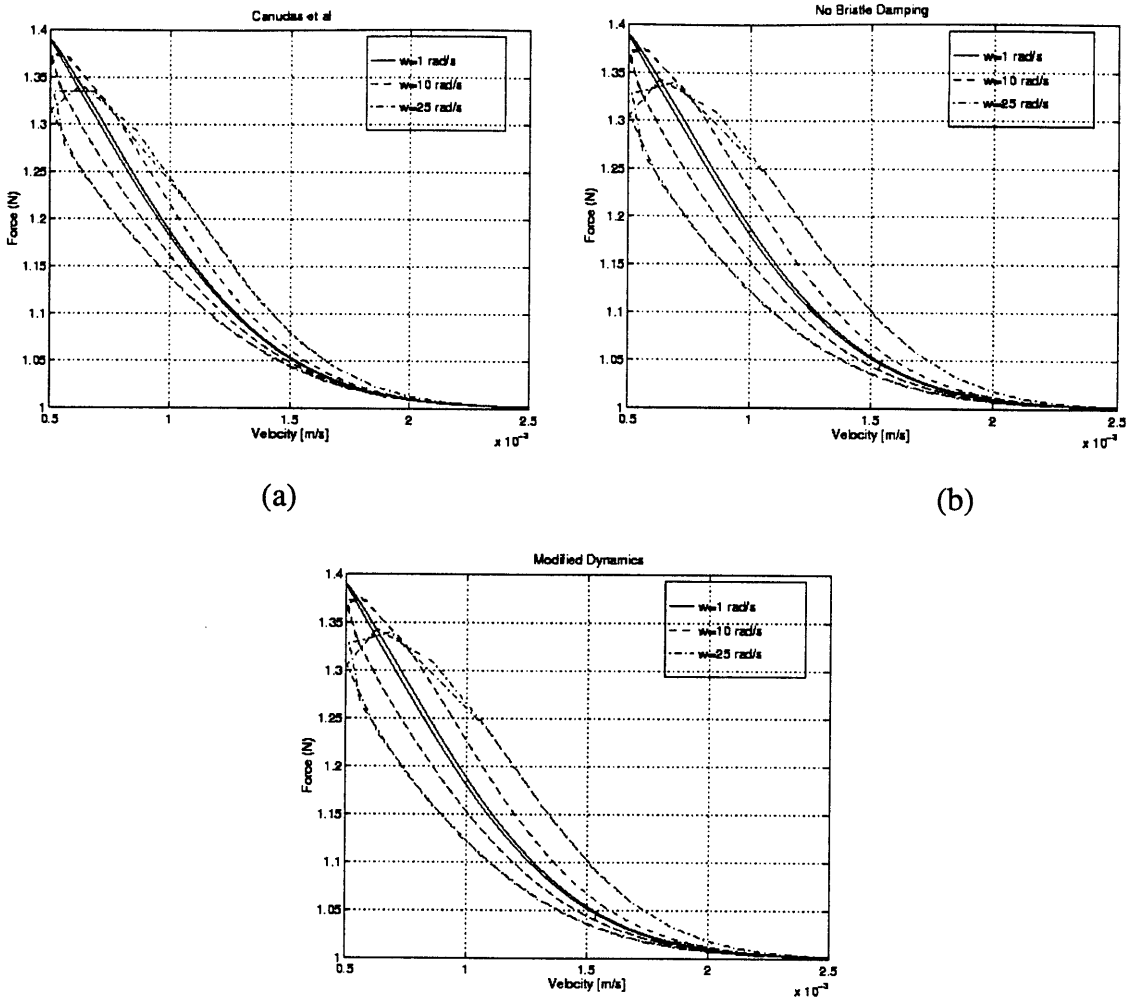

Figure 38 Hysteresis in friction force with varying velocity for (a) Canudas *et al.* model, (b) "No Bristle Damping" model, (c) "Modified Dynamics" model.

4.2.3 Stick Slip Motion

Stick - slip is a typical behavior for systems with friction. It is caused by the fact that friction is larger at rest than during motion. A simple experiment, with a set up such as in Figure 39, can be done to show stick- slip motion. A unit mass is attached to a spring with stiffness k=2 N/m. The end of the spring is pulled with constant velocity, i.e. dy/dt = 0.1 m/s.

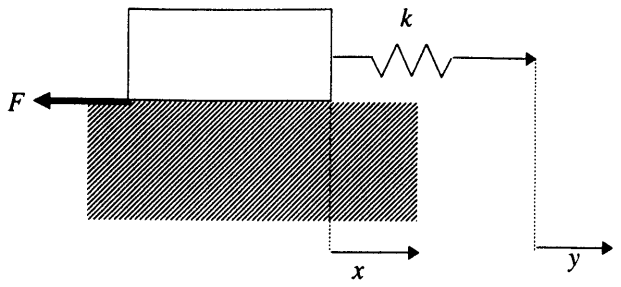

Figure 39 Experimental Setup for stick-slip motion

The equations of motion of the system in Figure 39 are given by:

$\dot{v} = k(y - x) - F$; where F is given by eq (4.5), (4.8) or (4.10)

$\dot{x} = v$

$\dot{y} = 0.1$

$\dot{z}$ is equals to equations (4.4), (4.7) and (4.9) according to the respective models.

The figures on the next pages show results of the stick-slip simulation. The results of all simulations exhibit stick-slip motion. However, the "No Bristle Damping" model and "Modified Dynamics" model exhibit high frequency force oscillations in the stick-slip region.

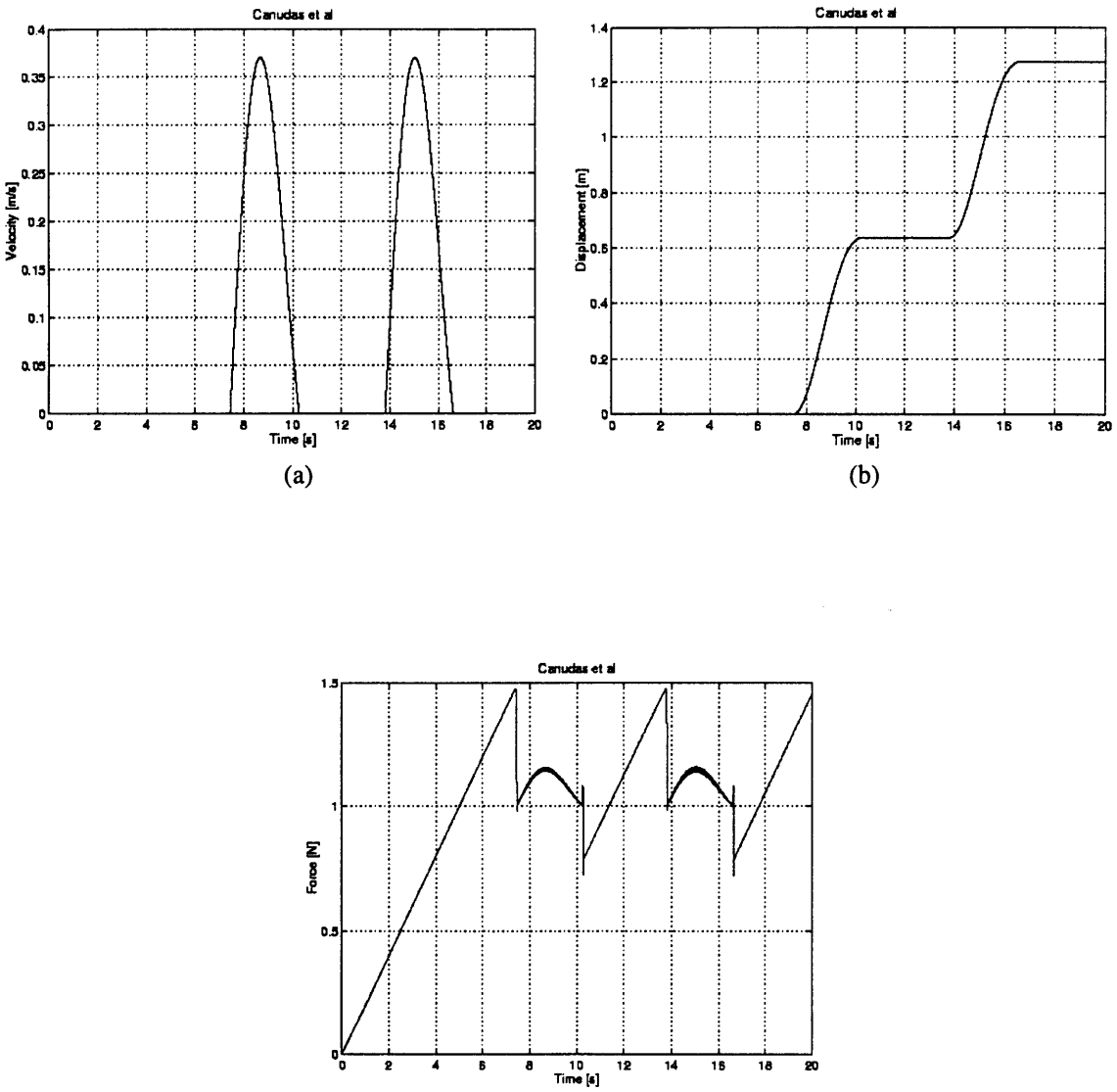

Figure 40 Simulation of stick-slip motion for Canudas *et al.*

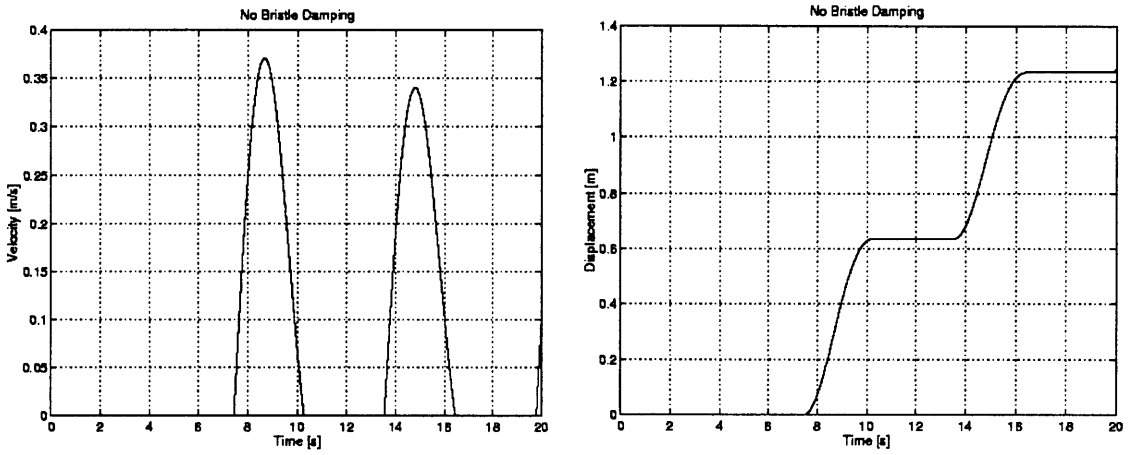

(a) (b)

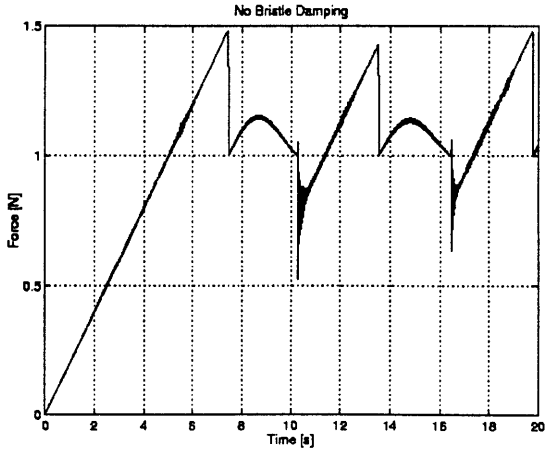

(c)

Figure 41 Simulation of stick-slip motion for "No Bristle Damping" model

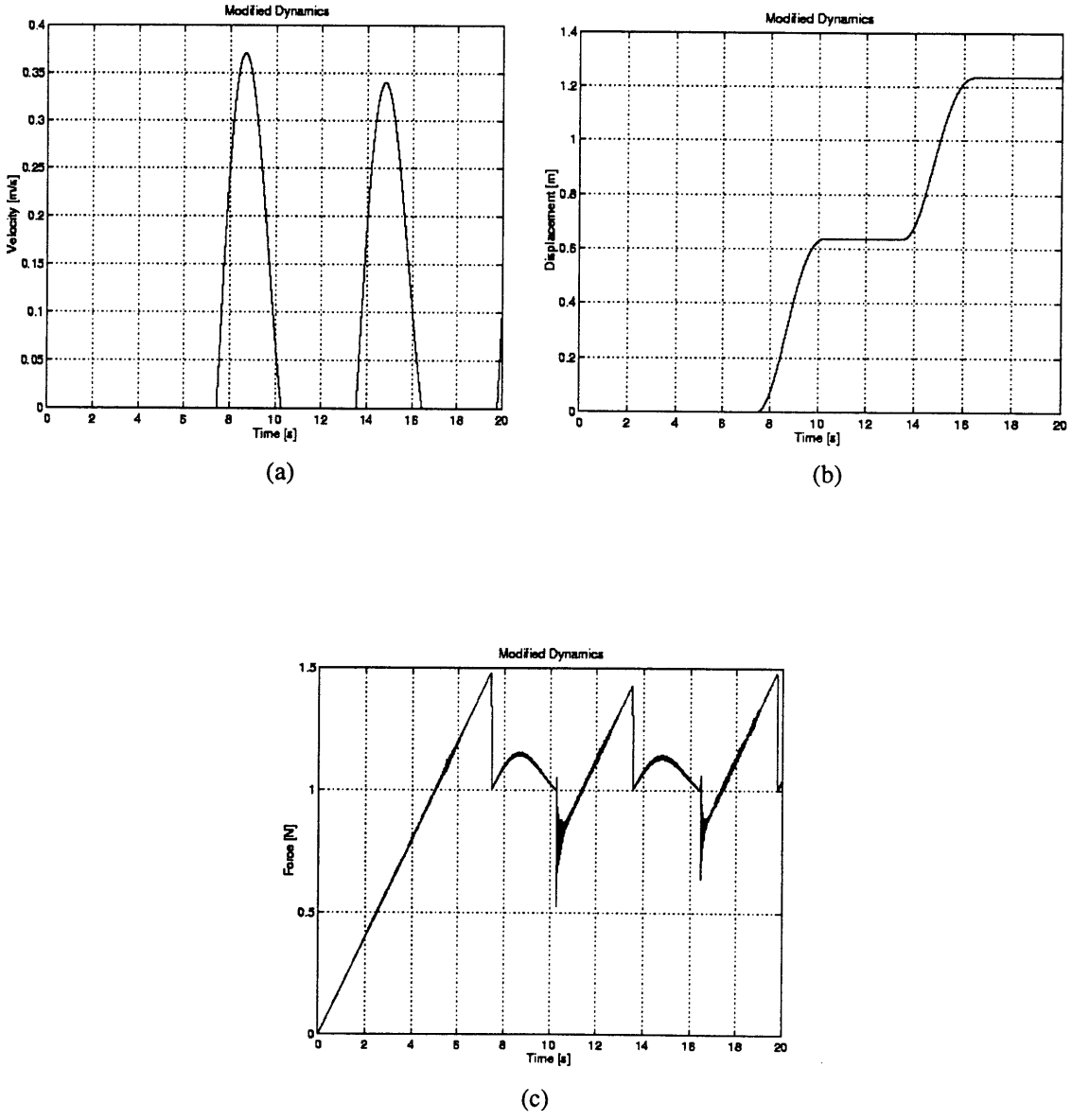

Figure 42 Simulation of stick-slip motion for "Modified Dynamics" model

4.3 Summary

The results obtained from the simulations of the piezo actuator proved that indeed, ecliptic trajectory proposed to drive the precision stage can be produced using two or more piezo actuators. Even more interesting, is that the shape of the trajectory can be controlled by regulating the phase lag between driving signals of the actuators. If the ecliptic trajectory can be controlled, perhaps an optimized shape can be found to improve the friction interaction between the actuator tip and the bottom of the stage.

The friction simulations demonstrated that the "Modified Dynamics" model captures the important characteristics of friction non-linearity as was discussed in Chapter 3. This is an interesting result, as it warrants "Modified Dynamics" as a possible candidate for a more accurate (and causal) friction model.

Conclusion and Future Work

A high precision two dimensional actuator using friction as described in this thesis possesses a tremendous potential as a device for very high precision positioning system. Most high precision stages today, uses magnetic levitation and actuation which is far much costly that piezoelectric actuators based stages, such as the one we are proposing.

Application of precision design methodology makes the design process of the precision stage very deterministic, such that most design parameters are precomputed to minimize trial and error cycle. The current design, as described in this thesis allows for infinite range and has very high stiffness for smoothness in the direction normal to the direction of motion. The proposed stage prototype is also very modular, such that a two dimensional application is easily adaptable. The proposed prototype is design to match up with the capabilities of current high precision stages.

The reliance of the stage to friction drive creates the motivation to conduct a comprehensive study on friction. As an effort to understand the friction phenomenon, and a causal friction model based on work of [6] is derived. Friction simulations showed that this model exhibit the important friction phenomenon - presliding, hyteresis and stick-slip

motion. This results establishes that the causal friction model as a candidate for an accurate friction model for controls applications.

Although a detailed design was outlined and a friction model was developed, there are still many issue that need to be addressed to completely develop the two dimensional stage.

1. *Stage Development*: Piezoelectric actuator needs to be verified. The electronics of the actuator needs to be designed and dynamics of the actuator needs to the developed. Then testing of the actuator is imminent to verify the functionality of the actuator. Secondly, contact dynamics between the actuator and the stage has to be analyzed and closed loop operation is appropriate next. The next phases, would include extending the workspace into two dimension, actuator synchronization for different modes of motion etc.
2. *Friction Modeling*: The model developed has a potential to be an accurate causal model for friction. It is, therefore, appropriate to continue the study and development of this model so that the model is further understood and behavior of the model is better predicted.

A. Hertz Contact Analysis

The Hertz contact analysis was done to size the balls to be used in the design of ball spring levitating mechanism. This is done to calculate the local stresses at the point of contact between the ball and the bottom of the stage. It is important so that the bottom of the stage is not deformed and dented by the stresses induced by the contact. A more detailed description can be found in [29]

Contact pressure q is given by $q = \frac{3F}{3\pi cd}$

where F is the applied load, c and d are the major and minor semiaxes of the elliptical contact area.

The variables d and d are given by:

$$c = \alpha\left(\frac{3FR_e}{2E_e}\right)^{1/3} \text{ and } d = \beta\left(\frac{3FR_e}{2E_e}\right)^{1/3}$$

The corresponding deflection is given by:

$$\delta = \lambda\left(\frac{3FR_e}{2E_e}\right)^{1/3}$$

The parameters R_e and E_e are the equivalent radius and equivalent modulus of elasticity of contacting surfaces. They are given by:

$$R_e = \frac{1}{\frac{1}{R_{1\text{major}}} + \frac{1}{R_{1\text{minor}}} + \frac{1}{R_{2\text{major}}} + \frac{1}{R_{2\text{minor}}}}$$

$$E_e = \frac{1}{\frac{1-\eta_1^2}{E_1} + \frac{1-\eta_1^2}{E_2}}$$

and R_1, R_2 are radiuses of the contacting surfaces. In our application, R_1 is ∞ (for flat surface) and R_2 is the radius of the ball. E_1, E_2 are moduli of elasticity of the two surfaces and η_1, η_2 are the Poisson ratio of the materials of the surfaces.

α, β and λ can be obtained from a table on page 232 in [29] . The values in the table are as a function of a cos θ function. The function cos θ is given by:

$$\cos\theta = R_e\left[\frac{1}{R_{2\text{major}}} - \frac{1}{R_{2\text{minor}}}\right]$$

as major and minor radii R_1 are infinite.

The following are spreadsheets performing the described calculations for a aluminum stage and three different ball materials.

HCONTACT.XLS
To determine the HERTZIAN contact stress Al Stage and Aluminum Oxide Ball.

Material Property

	Stage	Ball
Density[kg/m^3]	2795	
Elastic modulus	7.20E+10	2.86E+11
Poisson's ratio	0.33	0.01
Yield Strength [Pa]	4.80E+08	
Max contact stress	4.80E+08	
Applied load F [N]	42.18	

Stage Dimensions

Aluminum Alloy 7075 T6			
x	2.54E-01	m	
y	2.54E-01	m	
z	1.50E-02	m	
Weight [N]	26.534	2.705	kg
Preload[N]	100		

Diameter	4.00E-04	2.00E-03	5.00E-03	1.00E-02	2.00E-02	5.00E-02	1.00E-01
Ball Radius [m]	2.00E-04	1.00E-03	2.50E-03	5.00E-03	1.00E-02	2.50E-02	5.00E-02
Contact Pressure [Pa]	9.28E+09	3.17E+09	1.72E+09	1.09E+09	6.84E+08	3.71E+08	2.34E+08
Deflection [micrometer]	10.790	6.310	4.649	3.690	2.929	2.158	1.713
Stiffness [N/micrometer]	5.9	10.0	13.6	17.1	21.6	29.3	36.9
	NO	NO	NO	NO	NO	OK	OK
Contact Area Geometry:							
c	4.66E-05	7.97E-05	1.08E-04	1.36E-04	1.72E-04	2.33E-04	2.94E-04
d	4.65E-05	7.96E-05	1.08E-04	1.36E-04	1.71E-04	2.33E-04	2.93E-04
c/d	1.00E+00	1.00E+00	1.00E+00	1.00E+00	1.00E+00	1.00E+00	1.00E+00
Equivalent Parameters							
Rtwomin	2.000E-04	1.000E-03	2.500E-03	5.000E-03	1.000E-02	2.500E-02	5.000E-02
Equivelent modulus Ee	6.300E+10	6.300E+10	6.300E+10	6.300E+10	6.300E+10	6.300E+10	6.300E+10
Equivelent radius Re	1.000E-04	5.000E-04	1.250E-03	2.500E-03	5.000E-03	1.250E-02	2.500E-02
Hertz Contact Exact Solution Parameters							
costheta	0.0000	0.0000	0.0000	0.0000	0.0000	0.0000	0.0000
theta - [rad]	1.5708	1.5708	1.5708	1.5708	1.5708	1.5708	1.5708
alpha	1.0030	1.0030	1.0030	1.0030	1.0030	1.0030	1.0030
beta	1.0014	1.0014	1.0014	1.0014	1.0014	1.0014	1.0014
lambda	0.7490	0.7490	0.7490	0.7490	0.7490	0.7490	0.7490

.

HCONTACT.XLS

To determine the HERTZIAN contact stress Al Stage and Polymer Based Ball.

Material Property

	Stage	Ball
Density[kg/m^3]	2795	
Elastic modulus	7.20E+10	1.30E+07
Poisson's ratio	0.33	5.00E-01
Yield Strength [Pa]	4.80E+08	
Max contact stress	4.80E+08	
Applied load F [N]	42.18	

Stage Dimensions

Aluminum Alloy 7075 T6			
x	2.54E-01	m	
y	2.54E-01	m	
z	1.50E-02	m	
Weight [N]	26.534	2.705	kg
Preload[N]	100		

Diameter	4.00E-04	2.00E-03	5.00E-03	1.00E-02	2.00E-02	5.00E-02	1.00E-01
Ball Radius [m]	2.00E-04	1.00E-03	2.50E-03	5.00E-03	1.00E-02	2.50E-02	5.00E-02
Contact Pressure [Pa]	3.93E+07	1.34E+07	7.29E+06	4.59E+06	2.89E+06	1.57E+06	9.89E+05
Deflection [micrometer]	2550.919	1491.795	1099.167	872.411	692.435	510.192	404.941
Stiffness [N/micrometer]	0.0	0.0	0.1	0.1	0.1	0.1	0.2
	OK	OK	OK	OK	OK	OK	OK
Contact Area Geometry:							
c	7.17E-04	1.23E-03	1.66E-03	2.10E-03	2.64E-03	3.58E-03	4.52E-03
d	7.16E-04	1.22E-03	1.66E-03	2.09E-03	2.64E-03	3.58E-03	4.51E-03
c/d	1.00E+00	1.00E+00	1.00E+00	1.00E+00	1.00E+00	1.00E+00	1.00E+00
Equivalent Parameters							
Rtwomin	2.000E-04	1.000E-03	2.500E-03	5.000E-03	1.000E-02	2.500E-02	5.000E-02
Equivelent modulus Ee	1.733E+07	1.733E+07	1.733E+07	1.733E+07	1.733E+07	1.733E+07	1.733E+07
Equivelent radius Re	1.000E-04	5.000E-04	1.250E-03	2.500E-03	5.000E-03	1.250E-02	2.500E-02
Hertz Contact Exact Solution Parameters							
costheta	0.0000	0.0000	0.0000	0.0000	0.0000	0.0000	0.0000
theta - [rad]	1.5708	1.5708	1.5708	1.5708	1.5708	1.5708	1.5708
alpha	1.0030	1.0030	1.0030	1.0030	1.0030	1.0030	1.0030
beta	1.0014	1.0014	1.0014	1.0014	1.0014	1.0014	1.0014
lambda	0.7490	0.7490	0.7490	0.7490	0.7490	0.7490	0.7490

HCONTACT.XLS
To determine the HERTZIAN contact stress Al Stage and Steel Ball.

Material Property

	Stage	Ball
Density[kg/m^3]	2795	
Elastic modulus	7.20E+10	2.00E+11
Poisson's ratio	0.33	0.3
Yield Strength [Pa]	4.80E+08	
Max contact stress	4.80E+08	
Applied load F [N]	42.18	

Stage Dimensions

Aluminum Alloy 7075 T6		
x	2.54E-01 m	
y	2.54E-01 m	
z	1.50E-02 m	
Weight [N]	26.534	2.705 kg
Preload[N]	100	

Diameter	4.00E-04	2.00E-03	5.00E-03	1.00E-02	2.00E-02	5.00E-02	1.00E-01
Ball Radius [m]	2.00E-04	1.00E-03	2.50E-03	5.00E-03	1.00E-02	2.50E-02	5.00E-02
Contact Pressure [Pa]	8.89E+09	3.04E+09	1.65E+09	1.04E+09	6.55E+08	3.56E+08	2.24E+08
Deflection [micrometer]	11.262	6.586	4.853	3.852	3.057	2.252	1.788
Stiffness [N/micrometer]	5.6	9.6	13.0	16.4	20.7	28.1	35.4
	NO	NO	NO	NO	NO	OK	OK
Contact Area Geometry:							
c	4.76E-05	8.14E-05	1.11E-04	1.39E-04	1.75E-04	2.38E-04	3.00E-04
d	4.76E-05	8.13E-05	1.10E-04	1.39E-04	1.75E-04	2.38E-04	3.00E-04
c/d	1.00E+00	1.00E+00	1.00E+00	1.00E+00	1.00E+00	1.00E+00	1.00E+00
Equivalent Parameters							
Rtwomin	2.000E-04	1.000E-03	2.500E-03	5.000E-03	1.000E-02	2.500E-02	5.000E-02
Equivelent modulus Ee	5.908E+10	5.908E+10	5.908E+10	5.908E+10	5.908E+10	5.908E+10	5.908E+10
Equivelent radius Re	1.000E-04	5.000E-04	1.250E-03	2.500E-03	5.000E-03	1.250E-02	2.500E-02
Hertz Contact Exact Solution Parameters							
costheta	0.0000	0.0000	0.0000	0.0000	0.0000	0.0000	0.0000
theta - [rad]	1.5708	1.5708	1.5708	1.5708	1.5708	1.5708	1.5708
alpha	1.0030	1.0030	1.0030	1.0030	1.0030	1.0030	1.0030
beta	1.0014	1.0014	1.0014	1.0014	1.0014	1.0014	1.0014
lambda	0.7490	0.7490	0.7490	0.7490	0.7490	0.7490	0.7490

B. Bearing Way Design

The bearing way design is done to ensure the bearing way can provide appropriate support for the sliding stage. And since the bed is specified to a certain flatness, there proper attachment of the bearing way then will minimize error motions. A more detailed description of the analysis can be found in [29]

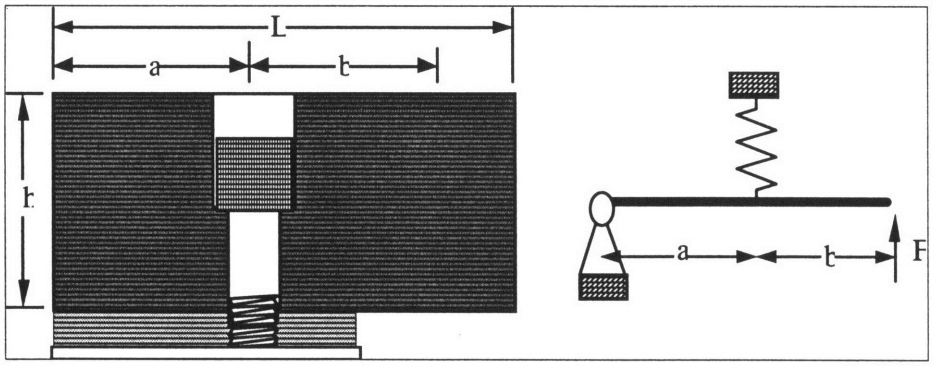

The system behaves like a beam attached to a pivot point so the equivalent stiffness at the point of force application is:

$$K_{eqbolt\,system} = \frac{Ka^2}{(a+b)^2}$$

$$K_{eqbolt\,system} = CD_B$$

where C is the bolt stiffness and D_B is the bolt diameter.

The bending and shear deflection is given by:

$$\delta_{bend} = F\frac{(a+b)b^2}{3EI} \text{ and } \delta_{shear} = \frac{Fbh^2(a+b)(1+\eta)}{5aEI} \text{ respectively.}$$

Bolt spacing is a function of bolt diameter and given by:

$$l = D_b(M-1)$$

This equation represents M bolt diameters minus the section occupied by the bolt.

Therefore the total stiffness for N segments of the bearing way is given by:

$$K = \frac{N}{\frac{1}{K_{bend\&shear}} + \frac{1}{K_{join} + \frac{1}{\frac{1}{K_{flange\,comp}} + \frac{1}{K_{flange\,shear}} + \frac{1}{K_{bed\,shear}} + \frac{1}{K_{bolt}}}}}$$

The spreadsheet performing these calculations follows. The stiffness is calculated as a function of bolt spacing.

To design bolted "boxway" bearing rails

Kjoint/Kboltflange (kjkb)	**10**
Kjoint (N/μm)	4.56E+09
K for length of rail (mm) (Lor)	**280**
Rail Modulus of elasticity (Erail)	**2.07E+11**
Bed Modulus of elasticity (Ebed)	**2.07E+11**
Bolt modulus of elasticity (Ebolt)	**2.07E+11**
Rail width (rw) (mm)	**80.000**
a (mm)	**10.000**
b (mm)	**70.000**
h (mm)	**25.400**
J = (a/(a+b))^2	0.016
Aterm	1.26E+09
Bolt diameter (mm) (Db)	**10**

t	Kfc	Kfs	Kts	Kb	Total	x2
1	3.075	3.486	3.486	0.449	0.293	0.586
1.5	2.714	5.230	3.486	0.349	0.250	0.500

2	2.530	6.973	3.486	0.286	0.217	0.433

Flange thickness	t = 2Db	t = 1.5Db	t = Db
K flange comp/E*Dbolt	2.530	2.714	3.075
K flange shear/E*Dbolt	6.973	5.230	3.486
K thread shear/E*Dbolt	3.486	3.486	3.486
K bolt/E*Dbolt	0.286	0.349	0.449
Bolt joint K at bolt: Cb/Db	4.78E+10	5.58E+10	6.62E+10

Bolt spacing/ Bolt diameter	t=2Db	t=1.5Db	t=Db
2	153	156	159
3	180	186	192
4	181	190	198
5	175	185	195
6	166	177	189
7	157	169	182
8	149	161	174
9	141	153	166
10	133	145	159

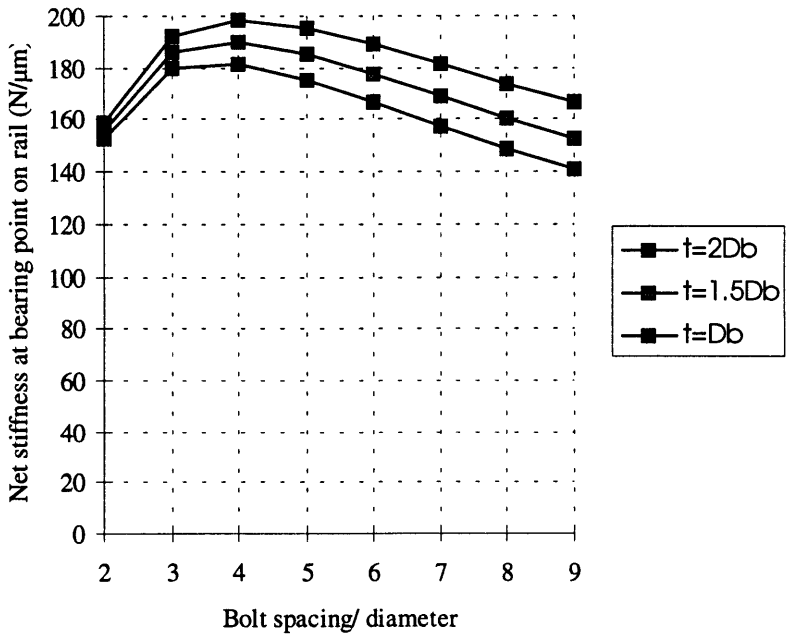

C. Matlab Simulation Source Codes

This appendix contains listings of matlab script files of simulations performed in this thesis.

C.1 Actuator tip simulation

```
% Tip.m
%     Matlab script file to simulate the
%     motion of piezo actuator tip given
%     actuator input
%

clear;

lgt=46e-3;                    % Model Parameter
tiphgt=20e-3;



% Simulations for phi=pi/1.5
n=1;
phi=pi/1.5;
for t=0:.05:2;
      y1(n) = 10e-6*sin(pi*t);
      y2(n) = 10e-6*sin(pi*t - phi);

      origin(n,:) = [lgt/2 (-tiphgt+y1(n))];

      vect1(n,:) = [-lgt  y2(n)-y1(n)];
      vect1(n,:)=0.5*sqrt(lgt^2+(y2(n)-y1(n))^2)*vect1(n,:)/norm(vect1(n,:));

      vect2(n,:) = [y2(n)-y1(n) lgt];
      vect2(n,:) = tiphgt*vect2(n,:)/norm(vect2(n,:));

      tippos1(n,:)=origin(n,:)+vect1(n,:)+vect2(n,:);
    n=n+1;
end
```

```
% Simulations for phi=pi/2
phi= pi/2;
n=1;
for t=0:.05:2;
      y1(n) = 10e-6*sin(pi*t);
      y2(n) = 10e-6*sin(pi*t - phi);

      origin(n,:) = [lgt/2 (-tiphgt+y1(n))];

      vect1(n,:) = [-lgt  y2(n)-y1(n)];
      vect1(n,:)= 0.5*sqrt(lgt^2+(y2(n)-y1(n))^2)*vect1(n,:)/norm(vect1(n,:));

      vect2(n,:) = [y2(n)-y1(n) lgt];
      vect2(n,:) = tiphgt*vect2(n,:)/norm(vect2(n,:));

      tippos2(n,:)=origin(n,:)+vect1(n,:)+vect2(n,:);
    n=n+1;
end


% Simulations for phi=pi/4
n=1;
phi=pi/4;
for t=0:.05:2;
      y1(n) = 10e-6*sin(pi*t);
      y2(n) = 10e-6*sin(pi*t - phi);

      origin(n,:) = [lgt/2 (-tiphgt+y1(n))];

      vect1(n,:) = [-lgt  y2(n)-y1(n)];
      vect1(n,:)=0.5*sqrt(lgt^2+(y2(n)-y1(n))^2)*vect1(n,:)/norm(vect1(n,:));

      vect2(n,:) = [y2(n)-y1(n) lgt];
      vect2(n,:) = tiphgt*vect2(n,:)/norm(vect2(n,:));

      tippos3(n,:)=origin(n,:)+vect1(n,:)+vect2(n,:);
    n=n+1;
end




% Simulations for phi=pi/8
n=1;
phi=pi/8;
for t=0:.05:2;
      y1(n) = 10e-6*sin(pi*t);
      y2(n) = 10e-6*sin(pi*t - phi);

      origin(n,:) = [lgt/2 (-tiphgt+y1(n))];

      vect1(n,:) = [-lgt  y2(n)-y1(n)];
      vect1(n,:)= 0.5*sqrt(lgt^2+(y2(n)-y1(n))^2)*vect1(n,:)/norm(vect1(n,:));

      vect2(n,:) = [y2(n)-y1(n) lgt];
      vect2(n,:) = tiphgt*vect2(n,:)/norm(vect2(n,:));

      tippos4(n,:)=origin(n,:)+vect1(n,:)+vect2(n,:);
    n=n+1;
end
```

```
% Plotting Data
whitebg('white')
plot(tippos1(:,1),tippos1(:,2),'-',tippos2(:,1),tippos2(:,2),'--',
       tippos3(:,1),tippos3(:,2),'-.',tippos4(:,1),tippos4(:,2),':')
legend('phi= pi/1.5','phi= pi/2','phi= pi/4','phi= pi/8',-1)
ylabel('Y position [m]')
xlabel('X position [m]')
axis('equal')
grid
hold off
```

C.2 Canudas et al. Friction Simulations Scripts

The following are the simulation script files used to simulate the Canudas et al. friction model.

Function	Filename
Presliding Simulation Script	2friction.m
Presliding Model	2fcmodel.m
Hysteresis Simulation Scripts	2hys.m
Hysteresis Model	2hymodel.m
Stick-slip Simulation Scripts	2stkslp.m
Stick- slip Model	2ssmodel.m

Presliding Simulation Script - 1friction.m

```
%     1friction.m
%     Script of simulation of Presliding
%     for Canudas et al. friction model
%

clear,clg,clf
global Fc Fs vs alpha_0 alpha_1 alpha_2 flag t1 t2 t3 t4 omega


Fc = 1.0;                       % Model parameters
Fs = 1.5;
vs = .001;
alpha_0 = 1e5;
alpha_1 = sqrt(1e5);
alpha_2 = .4;
omega=1;


t0 = 0;                         % Simulation Parameters
tfinal =4;
x0=[0 0 0]';
tol=1e-6;
```

```
[t,x] = ode45('fcmodel',t0,tfinal,x0,tol);      %ODE45


% Computing input

[count,width]=size(t);
for n = 1:count,
      g=(Fc + ( Fs - Fc )*exp(-(x(n,1)/vs)^2))/alpha_0;
      zdot(n)=x(n,1)-(abs(x(n,1))/g)*x(n,3);

      t1=1;, t2=1;, t3=3;,t4=3;
      if (t(n)>=0 & t(n)<=t1),u(n)=1.425*t(n)/t1;,end;
      if (t(n)>t1 & t(n)<=t2),u(n)=1.425;,end;
      if (t(n)>t2 & t(n)<=t3),u(n)=-(2*1.425*(t(n)-t2)/(t3-t2))+1.425;,end;

      if (t(n)>t3 & t(n)<=t4),u(n)=-1.425;,end;
      if (t(n)>t4),u(n)=1.425*(t(n)-t4)/t1 -1.425;,end;
end

force=[alpha_2 alpha_1 alpha_0]*[x(:,1),zdot',x(:,3)]';
force=force';



% Plotting Data

whitebg('w'),figure(1)
plot(t,x(:,1)),grid,title('Canudas et al')
ylabel('Velocity [m/s]'), xlabel('Time [s]')

whitebg('w'),figure(2),plot(t,x(:,2),'-',t,x(:,3),'--')
grid,title('Canudas et al'),ylabel('Displacement [m]')
xlabel('Time [s]'),legend(' x','z')

whitebg('w'),figure(3),plot(x(:,2),force),grid
title('Canudas et al'),ylabel('Force [N]')
xlabel('Displacement,x [m]')

whitebg('w'),figure(4),plot(t,force,t,u)
grid,title('Force & u')
```

Presliding Friction Model - fcmodel.m

```
function xdot=fcmodel(t,x)

%     Function file used with 1friction.m
%     Used to simulate Presliding for
%     Canudas et al. model
%
%     State variables
%          |v
%     x =  |x
%          |z
%

global Fc Fs vs alpha_0 alpha_1 alpha_2 flag  t1 t2 t3 t4 omega

% Define Input
       t1=1;, t2=1;, t3=3;,t4=3;
      if (t>=0 & t<=t1),u=1.425*t/t1;,end;
```

```
      if (t>t1 & t<=t2),u=1.425;,end;
      if (t>t2 & t<=t3),u=-2*1.425*(t-t2)/(t3-t2)+1.425;,end;
      if (t>t3 & t<=t4),u=-1.425;,end;
      if (t>t4),u=1.425*(t-t4)/t1-1.425;,end;

% Computer g(v)
g=(Fc + (Fs-Fc)*exp(-(x(1)/vs)^2))/alpha_0;


% Differential Equations
xdot = [-alpha_0*x(3)-alpha_1*(x(1)-(abs(x(1))/g)*x(3))-alpha_2*x(1)+u;
      x(1);
      x(1)-(abs(x(1))/g)*x(3)];
```

Hysteresis Simulation Script - 1hys.m

```
%     1hys.m
%     Script of simulation of hysteresis
%     for Canudas et al. friction model
%

clear,clg,clf
global Fc Fs vs alpha_0 alpha_1 alpha_2 flag t1 t2 t3 t4 omega

Fc = 1.0;                              % Model parameters
Fs = 1.5;
vs = .001;
alpha_0 = 1e5;
alpha_1 = sqrt(1e5);
alpha_2 = .4;
omega=25;


t0 = 0;                                % Simulation Parameters
tfinal =.51;
x0=[1.5e-3 0 0]';
tol=1e-9;

[t,x] = ode45('hymodel',t0,tfinal,x0,tol);      %ODE45

% Computing input
[count,width]=size(t);
for n = 1:count,
      g=(Fc + ( Fs - Fc )*exp(-(x(n,1)/vs)^2))/alpha_0;
      zdot(n)=x(n,1)-(abs(x(n,1))/g)*x(n,3);

      u(n)=(2)+(.1)*sin(pi*omega*t(n));
end

force=[alpha_2 alpha_1 alpha_0]*[x(:,1),zdot',x(:,3)]';
force=force';


% Plotting Data
whitebg('w'),figure(1),plot(t,x(:,1))
grid,title('Canudas et al')
ylabel('Velocity [m/s]'), xlabel('Time [s]')

whitebg('w'),figure(2),plot(t,x(:,2),'-',t,x(:,3),'--')
grid,title('Canudas et al')
ylabel('Displacement [m]'), xlabel('Time [s]')
```

```
legend(' x','z')

whitebg('w'),figure(3),plot(x(:,1),force)
grid,title('Canudas et al')
ylabel('Force [N]'),xlabel('Velocity [m]')
```

Hysteresis Model - 1hymodel.m

```
function xdot=hymodel(t,x)

%     Function file used with 1hys.m
%     Used to simulate hysteresis for
%     Canudals et al. model
%
%     State variables
%          |v
%     x = |x
%          |z


global Fc Fs vs alpha_0 alpha_1 alpha_2 flag  t1 t2 t3 t4 omega

% Define Input
      u=(1e-3)*omega*cos(omega*t);

% Computer g(v)
g=(Fc + (Fs-Fc)*exp(-(x(1)/vs)^2))/alpha_0;


% Differential Equations
xdot = [u;
      x(1);
      x(1)-(abs(x(1))/g)*x(3)];
```

Stick-slip Simulation Script - 1stkslp.m

```
%     1stkslp.m
%     Script of simulation of stick-slip motion
%     for Canudas et al. friction model
%


clear,clg,clf
global Fc Fs vs alpha_0 alpha_1 alpha_2 flag K

Fc = 1.0;                      % Model parameters
Fs = 1.5;
vs = .001;
alpha_0 = 1e5;
alpha_1 = sqrt(1e5);
alpha_2 = .4;
K=2;

t0 = 0;                                % Simulation Parameters
tfinal = 20;
x0=[0 0 0 0]';
tol=1e-6;

[t,x] = ode45('ssmodel',t0,tfinal,x0,tol);      %ODE45


% Computing input
```

```
[count,width]=size(t);
for n = 1:count,
      g=(Fc+(Fs-Fc)*exp(-(x(n,1)/vs)^2))/alpha_0;
      zdot(n)=x(n,1)-(abs(x(n,1))/g)*x(n,3);
end

force=[alpha_2 alpha_1 alpha_0]*[x(:,1),zdot',x(:,3)]';
force=force';



% Plotting Data
whitebg('w'),figure(1),plot(t,x(:,1)),grid,title('Velocity')
whitebg('w'),figure(2),plot(t,x(:,2)),grid,title('Position')
whitebg('w'),figure(3),plot(t,x(:,4)),grid,title('Position')
whitebg('w'),figure(4),plot(t,force),grid,title('Force')
```

Stick-slip Model - 1ssmodel.m

```
function xdot=ssmodel(t,x)

%     Function file used with 1stkslp.m
%     Used to simulate stick-slip motion for
%     Canudals et al. model
%
%     State variables
%          |v
%     x =  |x
%          |z
%          |y

global Fc Fs vs alpha_0 alpha_1 alpha_2 K


% Computer g(v)
g=(Fc+(Fs-Fc)*exp(-(x(1)/vs)^2))/alpha_0;


% Differential Equations
xdot = [K*(x(4)-x(2))-alpha_0*x(3)-alpha_1*(x(1)-(abs(x(1))/g)*x(3))-
       alpha_2*x(1);
        x(1);
        x(1)-(abs(x(1))/g)*x(3);
        0.1];
```

C.3 "No Bristle Deflection" Friction Simulations Scripts

The following are the simulation script files used to simulate the "No Bristle Damping" friction model.

Function	filename
Presliding Simulation Script	2friction.m
Presliding Model	2fcmodel.m
Hysteresis Simulation Scripts	2hys.m
Hysteresis Model	2hymodel.m
Stickslip Simulation Scripts	2stkslp.m
Stickslip Model	2ssmodel.m

Presliding Simulation Script - 2friction.m

```
%     2friction.m
%     Script of simulation of Presliding
%     for "No Bristle Damping" friction model
%

clear,clg,clf
global Fc Fs vs alpha_0 alpha_1 alpha_2 flag t1 t2 t3 t4 omega

Fc = 1.0;                       % Model parameters
Fs = 1.5;
vs = .001;
alpha_0 = 1e5;
alpha_1 = sqrt(1e5);
alpha_2 = .4;
omega=1;

t0 = 0;                                 % Model parameters
tfinal =4;
x0=[0 0 0]';
tol=1e-6;

[t,x] = ode45('fcmodel',t0,tfinal,x0,tol);      %ODE45

% Computing input
[count,width]=size(t);
for n = 1:count,
      g=(Fc + ( Fs - Fc )*exp(-(x(n,1)/vs)^2))/alpha_0;
      zdot(n)=x(n,1)-(abs(x(n,1))/g)*x(n,3);


      t1=1;, t2=1;, t3=3;,t4=3;
      if (t(n)>=0 & t(n)<=t1),u(n)=1.425*t(n)/t1;,end;
      if (t(n)>t1 & t(n)<=t2),u(n)=1.425;,end;
      if (t(n)>t2 & t(n)<=t3),u(n)=-(2*1.425*(t(n)-t2)/(t3-t2))+1.425;,end;
      if (t(n)>t3 & t(n)<=t4),u(n)=-1.425;,end;
      if (t(n)>t4),u(n)=1.425*(t(n)-t4)/t1 -1.425;,end;
end
```

```
force=[alpha_2 0 alpha_0]*[x(:,1),zdot',x(:,3)]';
force=force';

% Plotting Data
whitebg('w'),figure(1),plot(t,x(:,1))
grid,title('No Bristle Damping')
ylabel('Velocity [m/s]'), xlabel('Time [s]')

whitebg('w'),figure(2),plot(t,x(:,2),'-',t,x(:,3),'--')
grid,title('No Bristle Damping')
ylabel('Displacement [m]'), xlabel('Time [s]')
legend(' x','z')

whitebg('w'),figure(3),plot(x(:,2),force)
grid,title('No Bristle Damping')
ylabel('Force [N]'), xlabel('Displacement,x [m]')

whitebg('w'),figure(4),plot(t,force,t,u)
grid,title('Force & u')
```

Presliding Model - 2fcmodel.m

```
function xdot=fcmodel(t,x)


%     Function file used with 2friction.m
%     Used to simulate Presliding for
%     "No Bristle Damping" model
%
%     State variables
%          |v
%     x = |x
%          |z
%

global Fc Fs vs alpha_0 alpha_1 alpha_2 flag  t1 t2 t3 t4 omega

% Define Input
      t1=1;, t2=1;, t3=3;,t4=3;
      if (t>=0 & t<=t1),u=1.425*t/t1;,end;
      if (t>t1 & t<=t2),u=1.425;,end;
      if (t>t2 & t<=t3),u=-2*1.425*(t-t2)/(t3-t2)+1.425;,end;
      if (t>t3 & t<=t4),u=-1.425;,end;
      if (t>t4),u=1.425*(t-t4)/t1-1.425;,end;

% Computer g(v)
g=(Fc + (Fs-Fc)*exp(-(x(1)/vs)^2))/alpha_0;

% Differential Equations
xdot = [-alpha_0*x(3)-alpha_2*x(1)+u;
      x(1);
      x(1)-(abs(x(1))/g)*x(3)];
```

Hysteresis Simulation Scripts - 2hys.m

```
%     2hys.m
%     Script of simulation of hysteresis
%     for No Bristle Damping friction model
%

clear,clg,clf
global Fc Fs vs alpha_0 alpha_1 alpha_2 flag t1 t2 t3 t4 omega
```

```
Fc = 1.0;                                          % Model Parameter
Fs = 1.5;
vs = .001;
alpha_0 = 1e5;
alpha_1 = 0;
alpha_2 = .4;
omega=25;

t0 = 0;                                            % Simulation Parameter
tfinal =.51;
x0=[1.5e-3 0 0]';
tol=1e-9;

[t,x] = ode45('hymodel',t0,tfinal,x0,tol);      %ODE45

% Computing input
[count,width]=size(t);
for n = 1:count,
      g=(Fc + ( Fs - Fc )*exp(-(x(n,1)/vs)^2))/alpha_0;
      zdot(n)=x(n,1)-(abs(x(n,1))/g)*x(n,3);

      u(n)=(2)+(.1)*sin(pi*omega*t(n));

end


force=[alpha_2 alpha_1 alpha_0]*[x(:,1),zdot',x(:,3)]';
force=force';

% Plotting Data
whitebg('w'),figure(1),plot(t,x(:,1))
grid,title('No Bristle Damping')
ylabel('Velocity [m/s]'), xlabel('Time [s]')

whitebg('w'),figure(2),plot(t,x(:,2),'-',t,x(:,3),'--')
grid,title('No Bristle Damping')
ylabel('Displacement [m]'), xlabel('Time [s]')
legend(' x','z')

whitebg('w'),figure(3),plot(x(:,1),force)
grid,title('No Bristle Damping')
ylabel('Force [N]'), xlabel('Velocity [m/s]')
```

Hysteresis Model - 2hymodel.m

```
function xdot=hymodel(t,x)

%     Function file used with 2hys.m
%     Used to simulate hysteresis for
%     "No Bristle Damping" model
%
%     State variables
%          |v
%     x = |x
%          |z

global Fc Fs vs alpha_0 alpha_1 alpha_2 flag  t1 t2 t3 t4 omega

% Define Input
      u=(1e-3)*omega*cos(omega*t);
```

```
% Computer g(v)
g=(Fc + (Fs-Fc)*exp(-(x(1)/vs)^2))/alpha_0;

% Differential Equations
xdot = [u;
      x(1);
      x(1)-(abs(x(1))/g)*x(3)];
```

Stickslip Simulation Scripts - 2stkslp.m

```
%     2stkslp.m
%     Script of simulation of stick-slip motion
%     for "No Bristle Damping Model" friction model
%

clear,clg,clf
global Fc Fs vs alpha_0 alpha_1 alpha_2 flag K

Fc = 1.0;                        % Model parameters
Fs = 1.5;
vs = .001;
alpha_0 = 1e5;
alpha_1 = 0;
alpha_2 = .4;
K=2;

t0 = 0;                                % Model parameters
tfinal = 20;
x0=[0 0 0 0]';
tol=1e-6;

[t,x] = ode45('ssmodel',t0,tfinal,x0,tol);      %ODE45


% Computing input
[count,width]=size(t);
for n = 1:count,
      g=(Fc+(Fs-Fc)*exp(-(x(n,1)/vs)^2))/alpha_0;
      zdot(n)=x(n,1)-(abs(x(n,1))/g)*x(n,3);

end

force=[alpha_2 alpha_1 alpha_0]*[x(:,1),zdot',x(:,3)]';
force=force';

% Plotting Data
whitebg('w'),figure(1),plot(t,x(:,1)),grid,title('Velocity')
whitebg('w'),figure(2),plot(t,x(:,2)),grid,title('Position')
whitebg('w'),figure(3),plot(t,x(:,4)),grid,title('Position')
whitebg('w'),figure(4),plot(t,force),grid,title('Force')
```

Stickslip Model - 2ssmodel.m

```
function xdot=ssmodel(t,x)

%     Function file used with 1stkslp.m
%     Used to simulate stick-slip motion for
%     "No Bristle Damping" model
%
%     State variables
%         |v
```

```
%      x = |x
%          |z
%          |y
%

global Fc Fs vs alpha_0 alpha_1 alpha_2 K

% Computer g(v)
g=(Fc+(Fs-Fc)*exp(-(x(1)/vs)^2))/alpha_0;

% Differential Equations
xdot = [K*(x(4)-x(2))-alpha_0*x(3)-alpha_1*(x(1)-(abs(x(1))/g)*x(3))-
alpha_2*x(1);
        x(1);
        x(1)-(abs(x(1))/g)*x(3);
       0.1];
```

C.4 "Modified Dynamics" Friction Simulations Scripts

The following are the simulation script files used to simulate the "No Bristle Damping" friction model.

Function	Filename
Presliding Simulation Script	3friction.m
Presliding Model	3fcmodel.m
Hysteresis Simulation Scripts	3hys.m
Hysteresis Model	3hymodel.m
Stickslip Simulation Scripts	3stkslp.m
Stickslip Model	3ssmodel.m

Presliding Simulation Script - 3friction.m

```
%      3friction.m
%      Script of simulation of Presliding
%      for Modified Dynamics friction model
%

clear,clg,clf
global Fc Fs vs alpha_0 alpha_1 alpha_2 flag t1 t2 t3 t4 omega

Fc = 1.0;                        % Model parameters
Fs = 1.5;
vs = .001;
alpha_0 = 1e5;
alpha_1 = sqrt(1e5);
alpha_2 = .4;
omega=1;

t0 = 0;                                % Simulation Parameters
tfinal =4;
tfinal =4;
x0=[0 0 0]';
tol=1e-6;
```

```
[t,x] = ode45('fcmodel',t0,tfinal,x0,tol);       %ODE45


% Computing input
[count,width]=size(t);
for n = 1:count,
      g=(Fc + ( Fs - Fc )*exp(-(x(n,1)/vs)^2))/alpha_0;
      zdot(n)=x(n,1)-
(abs(x(n,1))/g)*x(n,3)/(1+(alpha_1*abs(x(n,1)))/(alpha_0*g));

      t1=1;, t2=1;, t3=3;,t4=3;
            if (t(n)>=0 & t(n)<=t1),u(n)=1.425*t(n)/t1;,end;
            if (t(n)>t1 & t(n)<=t2),u(n)=1.425;,end;
            if (t(n)>t2 & t(n)<=t3),u(n)=-(2*1.425*(t(n)-t2)/(t3-
t2))+1.425;,end;
            if (t(n)>t3 & t(n)<=t4),u(n)=-1.425;,end;
            if (t(n)>t4),u(n)=1.425*(t(n)-t4)/t1 -1.425;,end;
end

force=[alpha_2 0 alpha_0]*[x(:,1),zdot',x(:,3)]';
force=force';


% Plotting Data
whitebg('w'),figure(1),plot(t,x(:,1))
grid,title('Modified Dynamics')
ylabel('Velocity [m/s]'), xlabel('Time [s]')

whitebg('w'),figure(2),plot(t,x(:,2),'-',t,x(:,3),'--')
grid,title('Modified Dynamics')
ylabel('Displacement [m]'), xlabel('Time [s]')
legend(' x','z')

whitebg('w'),figure(3),plot(x(:,2),force)
grid,title('Modified Dynamics')
ylabel('Force [N]'), xlabel('Displacement,x [m]')

whitebg('w'),figure(4),plot(t,force,t,u),grid,title('Force & u')
```

Presliding Model - 3fcmodel.m

```
function xdot=fcmodel(t,x)

%     Function file used with 3friction.m
%     Used to simulate Presliding for
%     Modified Dynamics model
%
%     State variables
%          |v
%     x = |x
%          |z
%


global Fc Fs vs alpha_0 alpha_1 alpha_2 flag  t1 t2 t3 t4 omega

% Define Input
      t1=1;, t2=1;, t3=3;,t4=3;
      if (t>=0 & t<=t1),u=1.425*t/t1;,end;
```

```
      if (t>t1 & t<=t2),u=1.425;,end;
      if (t>t2 & t<=t3),u=-2*1.425*(t-t2)/(t3-t2)+1.425;,end;
      if (t>t3 & t<=t4),u=-1.425;,end;
      if (t>t4),u=1.425*(t-t4)/t1-1.425;,end;

% Computer g(v)
g=(Fc + (Fs-Fc)*exp(-(x(1)/vs)^2))/alpha_0;
zdot = (x(1)-(abs(x(1))/g)*x(3))/ (1+(alpha_1*abs(x(1)))/(alpha_0*g));

% Differential Equations
xdot = [-alpha_0*x(3)-alpha_1*zdot-alpha_2*x(1)+u;
      x(1);
      zdot];
```

Hysteresis Simulation Scripts - 3hys.m

```
%     3hys.m
%     Script of simulation of hysteresis
%     for Modified Dynamics friction model
%

clear,clg,clf
global Fc Fs vs alpha_0 alpha_1 alpha_2 flag t1 t2 t3 t4 omega

Fc = 1.0;                        % Model parameters
Fs = 1.5;
vs = .001;
alpha_0 = 1e5;
alpha_1 = 0;
alpha_2 = .4;
omega=10;


t0 = 0;                                % Simulation Parameters
tfinal =1.26;
x0=[1.5e-3 0 0]';
tol=1e-9;


[t,x] = ode45('hymodel',t0,tfinal,x0,tol);      %ODE45


% Computing input
[count,width]=size(t);
for n = 1:count,
      g=(Fc + ( Fs - Fc )*exp(-(x(n,1)/vs)^2))/alpha_0;
zdot(n)=x(n,1)-(abs(x(n,1))/g)*x(n,3)/(1+(alpha_1*abs(x(n,1)))/(alpha_0*g));
      u(n)=(1.5e-1)+(1e-3)*sin(pi*omega*t(n));
end


force=[alpha_2 alpha_1 alpha_0]*[x(:,1),zdot',x(:,3)]';
force=force';


% Plotting Data
whitebg('w'),figure(1),plot(t,x(:,1))
grid,title('Modified Dynamics')
ylabel('Velocity [m/s]'), xlabel('Time [s]')

whitebg('w'),figure(2),plot(t,x(:,2),'-',t,x(:,3),'--')
```

```
grid,title('Modified Dynamics'),ylabel('Displacement [m]')
xlabel('Time [s]'),legend(' x','z')

whitebg('w'),figure(3),plot(x(:,1),force)
grid,title('Modified Dynamics')
ylabel('Force [N]'), xlabel('Velocity, [m/s]')
```

Hysteresis Model - 3hymodel.m

```
function xdot=hymodel(t,x)

%     Function file used with 3hys.m
%     Used to simulate hysteresis for
%     "Modified Dynamics" model
%
%     State variables
%          |v
%     x =  |x
%          |z


global Fc Fs vs alpha_0 alpha_1 alpha_2 flag  t1 t2 t3 t4 omega


      u=(1e-3)*omega*cos(omega*t);

% Computer g(v)
g=(Fc + (Fs-Fc)*exp(-(x(1)/vs)^2))/alpha_0;
zdot = (x(1)-(abs(x(1))/g)*x(3))/ (1+(alpha_1*abs(x(1)))/(alpha_0*g));


% Differential Equations
xdot = [u;
      x(1);
      zdot];
```

Stick-slip Simulation Scripts - 3stkslp.m

```
%     3stkslp.m
%     Script of simulation of stick-slip motion
%     for Modified Dynamics friction model
%

clear,clg,clf
global Fc Fs vs alpha_0 alpha_1 alpha_2 flag K

Fc = 1.0;                       % Model parameters
Fs = 1.5;
vs = .001;
alpha_0 = 1e5;
alpha_1 = 0;
alpha_2 = .4;
K=2;

t0 = 0;                                 % Simulation Parameters
tfinal = 20;
x0=[0 0 0 0]';
tol=1e-6;


[t,x] = ode45('ssmodel',t0,tfinal,x0,tol);      %ODE45
```

```
% Computing input
[count,width]=size(t);
for n = 1:count,
      g=(Fc+(Fs-Fc)*exp(-(x(n,1)/vs)^2))/alpha_0;
      zdot(n)=x(n,1)-
(abs(x(n,1))/g)*x(n,3)/(1+(alpha_1*abs(x(n,1)))/(alpha_0*g));

end

force=[alpha_2 alpha_1 alpha_0]*[x(:,1),zdot',x(:,3)]';
force=force';


% Plotting Data
whitebg('w'),figure(1),plot(t,x(:,1)),grid,title('Velocity')
whitebg('w'),figure(2),plot(t,x(:,2)),grid,title('Position')
whitebg('w'),figure(3),plot(t,x(:,4)),grid,title('Position')
whitebg('w'),figure(4),plot(t,force),grid,title('Force')
```

Stick-slip Model - 3ssmodel.m

```
function xdot=ssmodel(t,x)

%     Function file used with 3stkslp.m
%     Used to simulate stick-slip motion for
%     "Modified Dynamics" model
%
%     State variables
%          |v
%     x =  |x
%          |z
%          |y

global Fc Fs vs alpha_0 alpha_1 alpha_2 K

end

g=(Fc+(Fs-Fc)*exp(-(x(1)/vs)^2))/alpha_0;
zdot = (x(1)-(abs(x(1))/g)*x(3))/ (1+(alpha_1*abs(x(1)))/(alpha_0*g));

xdot = [K*(x(4)-x(2))-alpha_0*x(3)-alpha_1*zdot-alpha_2*x(1);
        x(1);
        zdot;
      0.1];
```

D. Engineering Drawings

This appendix contains the engineering drawings of the custom part of the precision stage. They are in the page that follows in the following order:

1. Actuator Tip
2. Piezo Holder
3. Stage
4. Bearing Way
5. Base (3 pages of drawings)
6. Pin 1
7. Pin 2

Components that are available off the shelves are:

- Piezoelectric Actuators (TOKIN Model ASB170C801NPO)
- 3/8" - 16 Coarse Thread Socket Cap Screws 1" length (McMaster Carr Part# 91251A624). For bearing way attachment to the base.
- 3/8" - 16 Coarse Thread Socket Cap Screws 6" length (McMaster Carr Part# 91251A648). For clamping actuator 1.

- 3/8" - 16 Coarse Thread Socket Cap Screws 4.5" length (McMaster Carr Part# 91251A642). For clamping actuator 2 & 3. (For 2D application only)
- 1" - 8 Coarse Thread Socket Set Screws 1" length (McMaster Carr Part#91375A904). The set screws for height adjustment mechanism.
- Compression Springs ¾" OD 2" length (McMaster Carr Part# 9657K26). Compression spring for height adjustment mechanism.

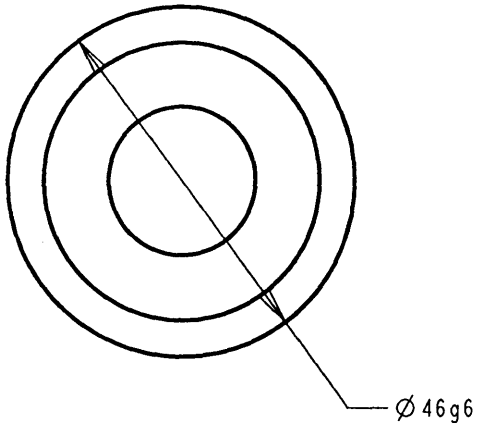

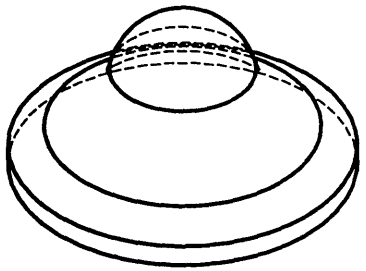

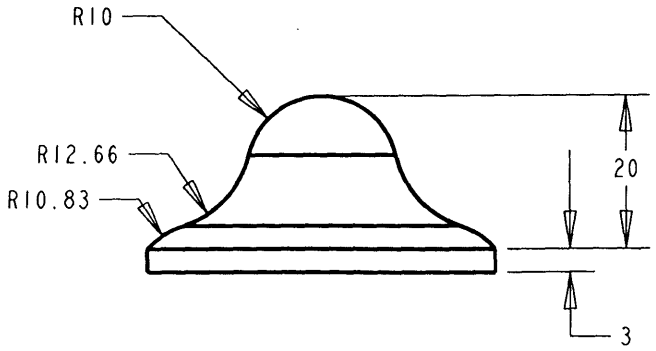

MASSACHUSETTS INSTITUTE OF TECHNOLOGY			
X. ±0.1 X.X ±0.1 X.XX ±0.01	Material: Al 6061-T651	Precision Stage ACTUATOR TIP	
	MM	1.000	THS_PZT_TIP
TOLERANCES	UNITS	SCALE	FILENAME

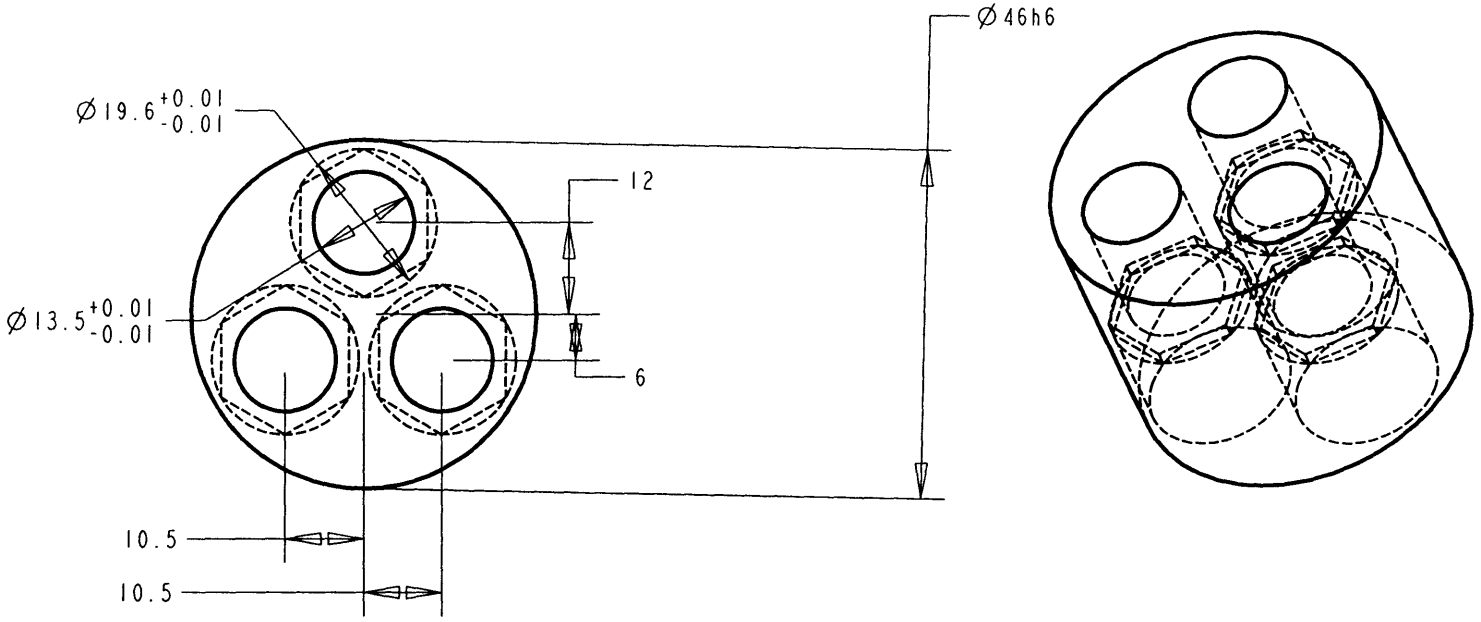

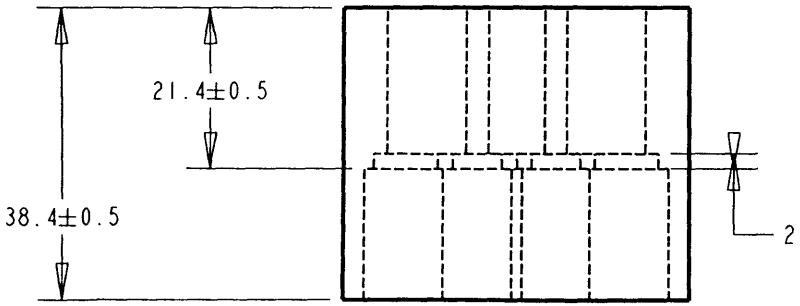

MASSACHUSETTS INSTITUTE OF TECHNOLOGY			
X. ±0.1 X.X ±0.1 X.XX ±0.01	Material: INVAR SUS416	Precision Stage PIEZE HOLDER	
	MM	1.000	THS_PZT_HOLDER
TOLERANCES	UNITS	SCALE	FILENAME

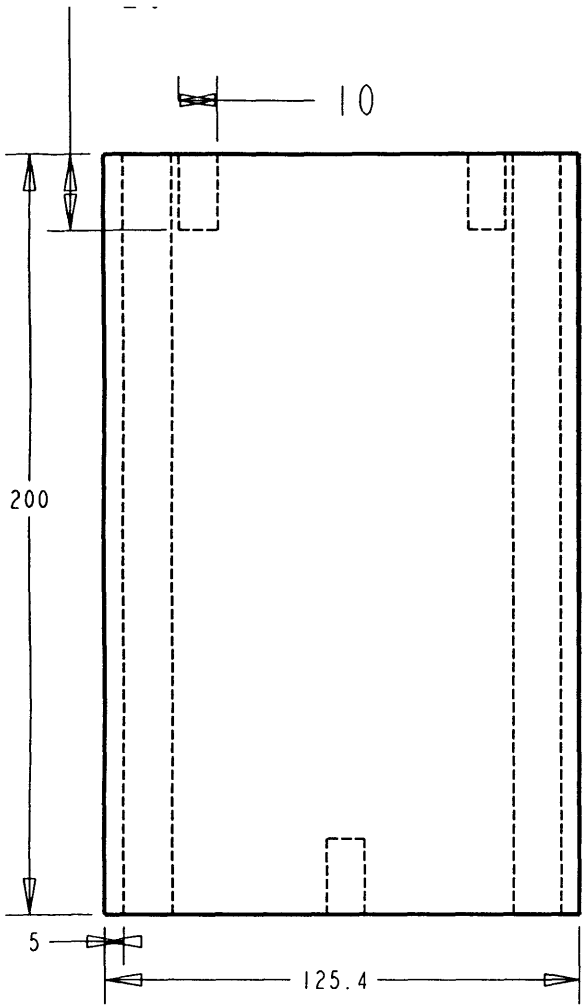

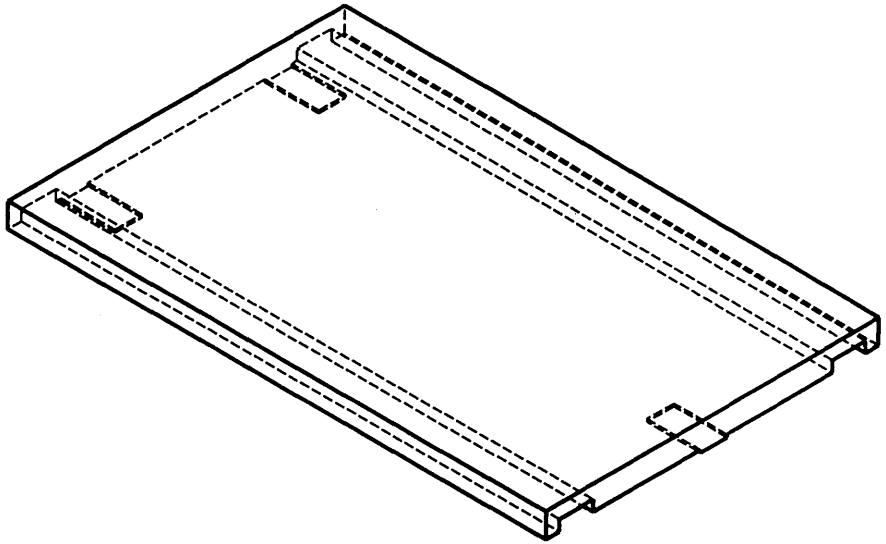

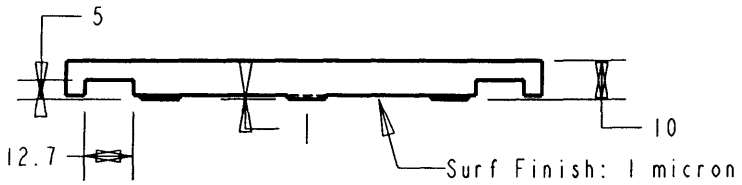

MASSACHUSETTS INSTITUTE OF TECHNOLOGY			
X. ±0.1 X.X ±0.1 X.XX ±0.01	Material: Al 6061-T651	Precision Stage STAGE	
	MM	0.500	THS_STG_CARR
TOLERANCES	UNITS	SCALE	FILENAME

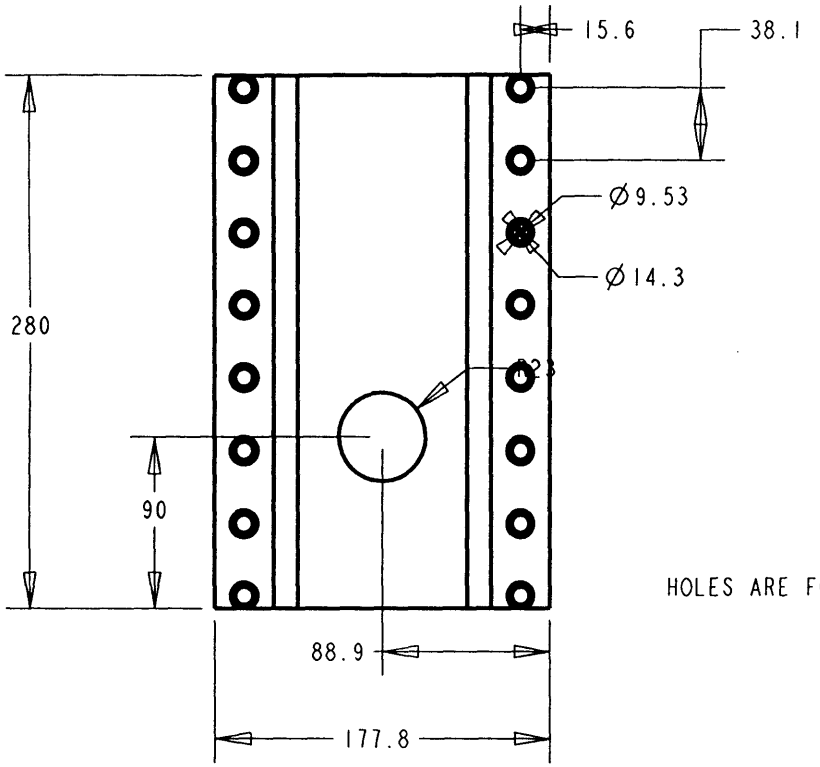

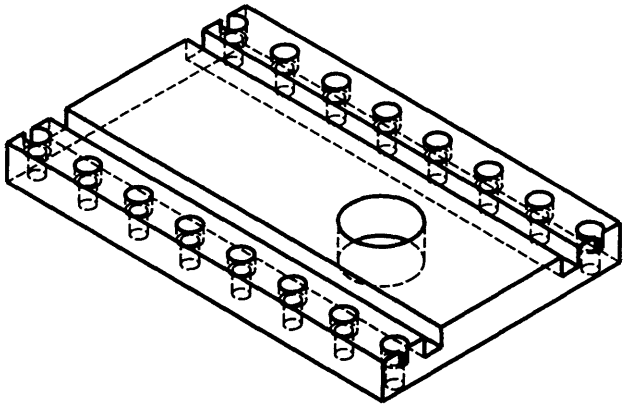

HOLES ARE FOR 3/8"-16UNC 1" LONG

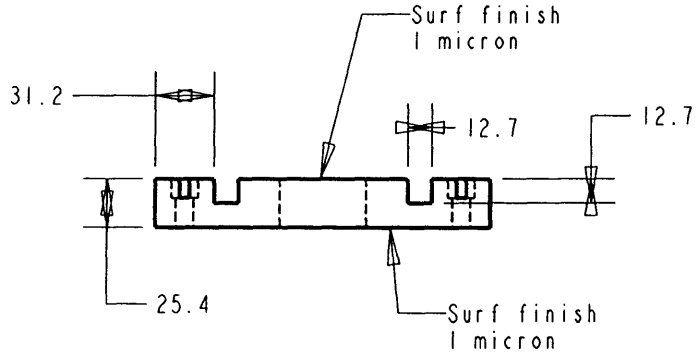

MASSACHUSETTS INSTITUTE OF TECHNOLOGY			
X. ±0.1 X.X ±0.1 X.XX ±0.01	Material: SiC	Precision Stage BEARING WAY	
	MM	0.250	THS_STG_PRS
TOLERANCES	UNITS	SCALE	FILENAME

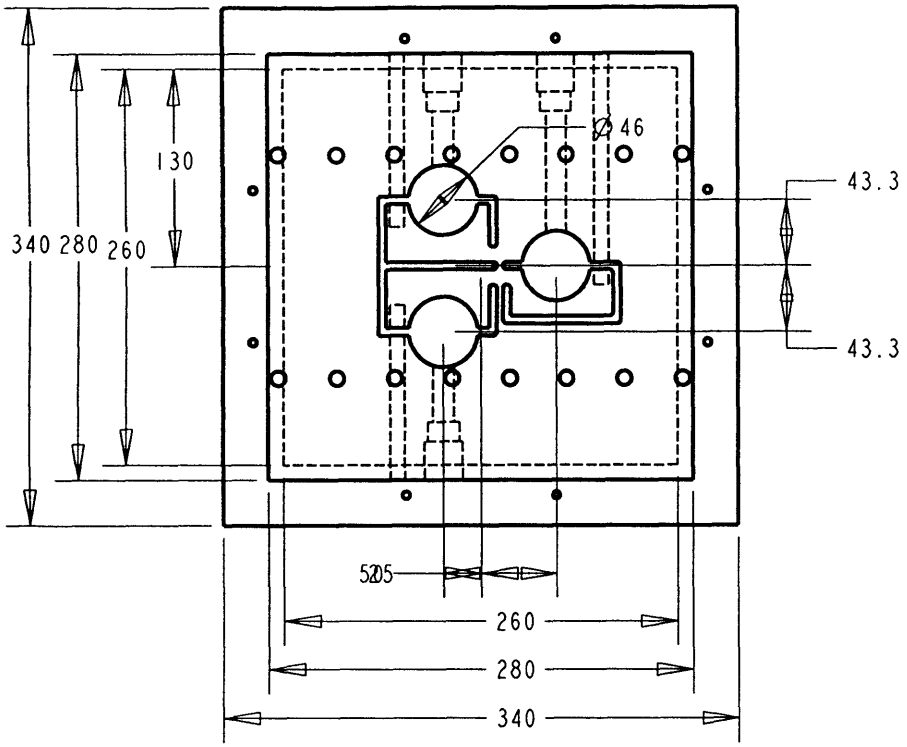

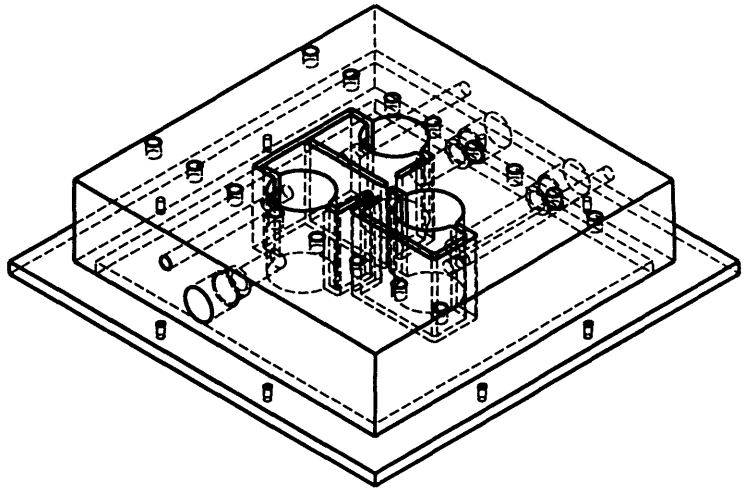

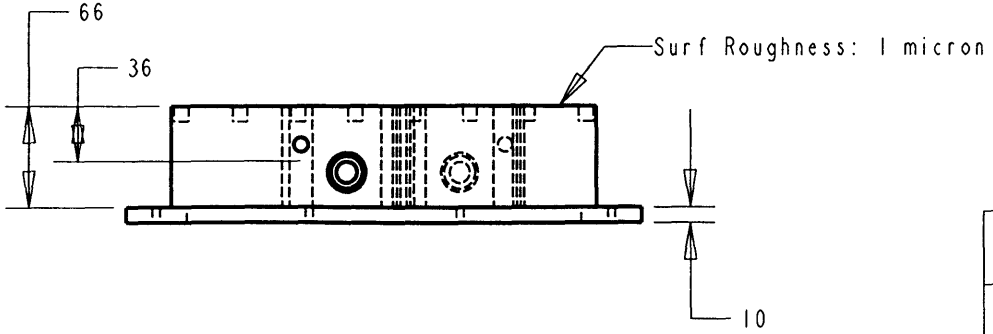

MASSACHUSETTS INSTITUTE OF TECHNOLOGY			
X. ±0.1 X.X ±0.1 X.XX ±0.01	Material INVAR SUS416	Precision Stage BASE 1/3	
	MM	0.200	THS_STG_BASE
TOLERANCES	UNITS	SCALE	FILENAME

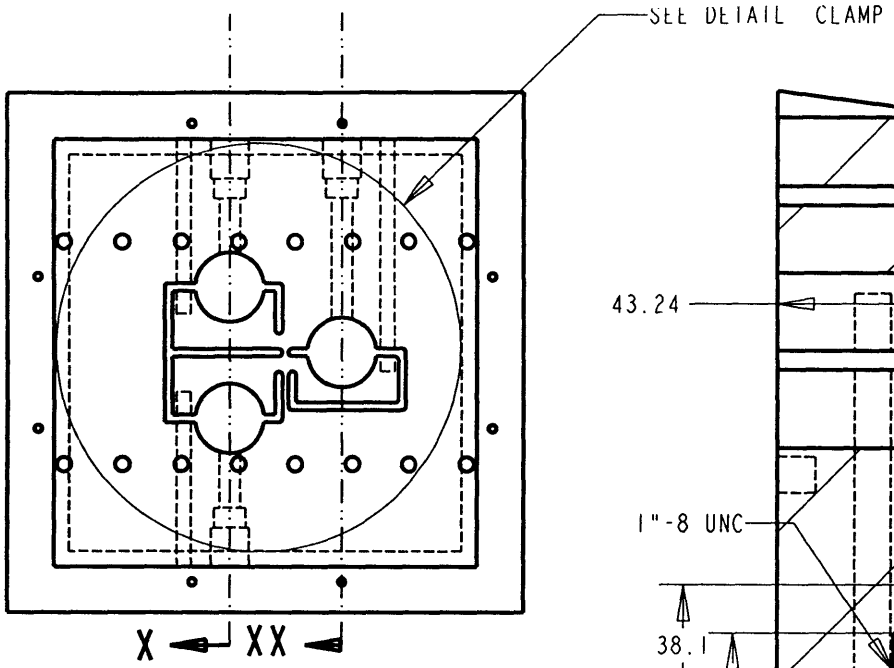

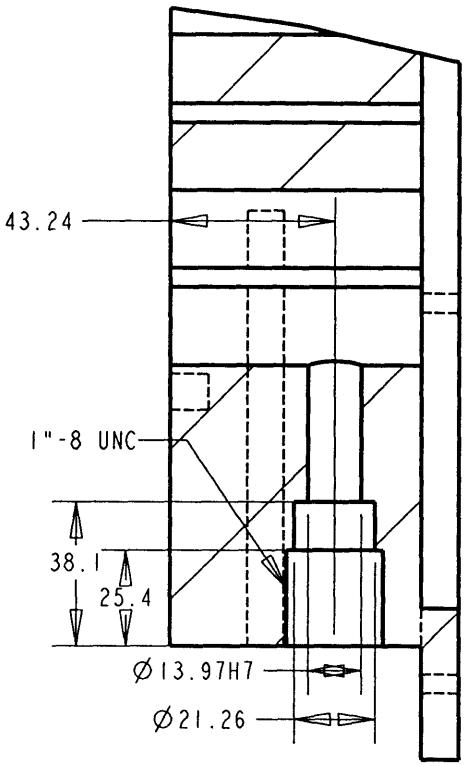

DETAIL X
SCALE 0.500

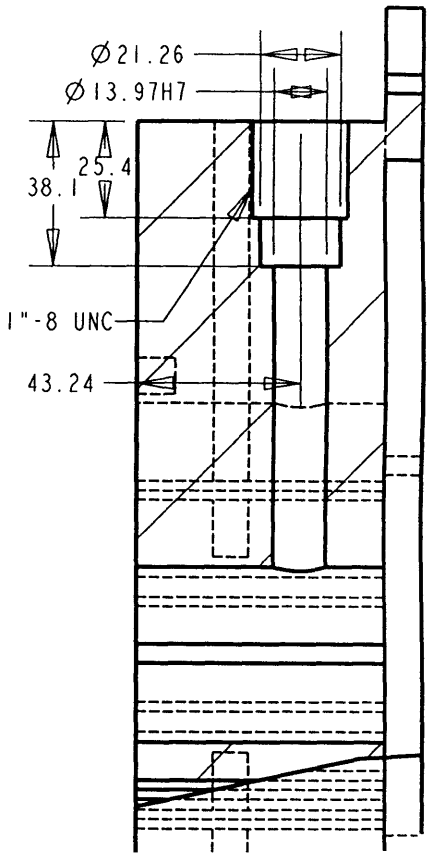

DETAIL XX
SCALE 0.500

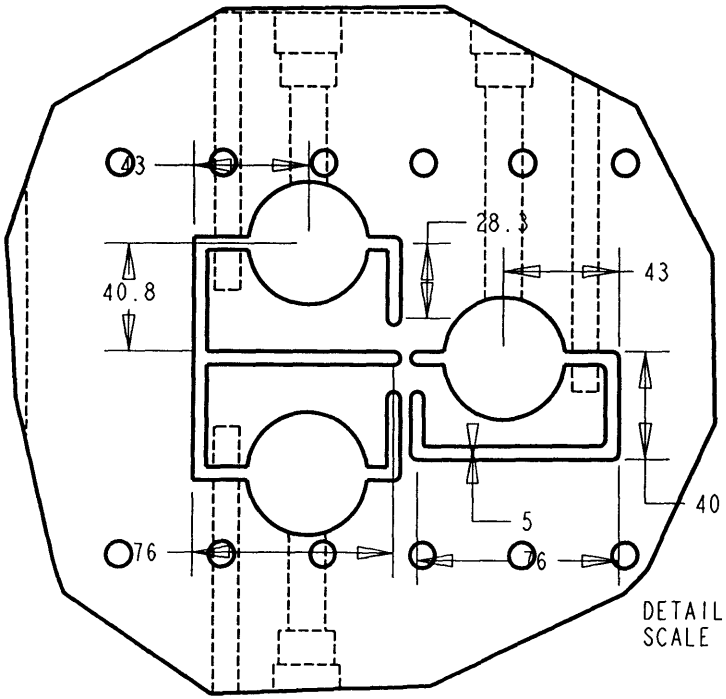

DETAIL CLAMP
SCALE 0.350

MASSACHUSETTS INSTITUTE OF TECHNOLOGY			
X. ±0.1 X.X ±0.1 X.XX ±0.01	Material: INVAR SUS416	Precision Stage BASE 2/3	
	MM	0.200	THS_STG_BASE
TOLERANCES	UNITS	SCALE	FILENAME

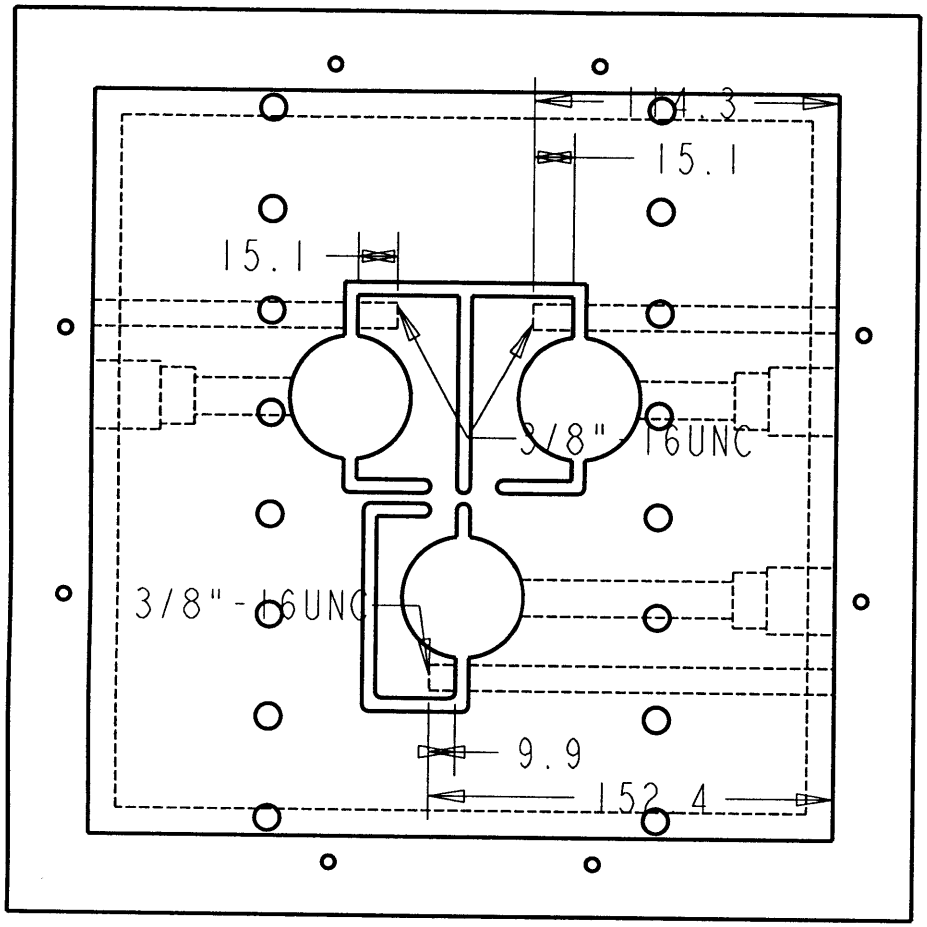

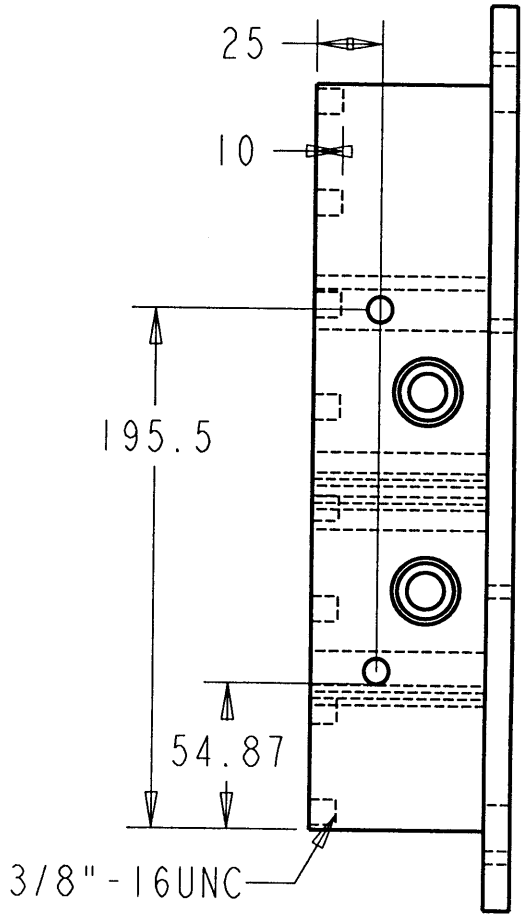

MASSACHUSETTS INSTITUTE OF TECHNOLOGY			
X. ±0.1 X.X ±0.1 X.XX ±0.01	Material: INVAR SUS416	Precision Stage BASE 3/3	
	MM	0.350	THS_STG_BASE
TOLERANCES	UNITS	SCALE	FILENAME

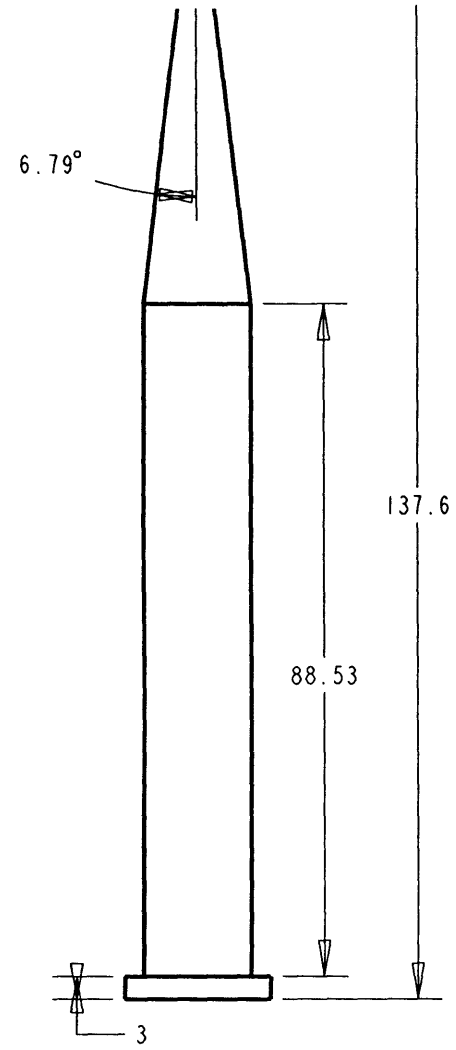

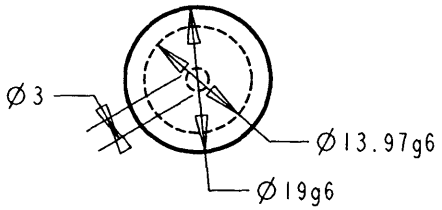

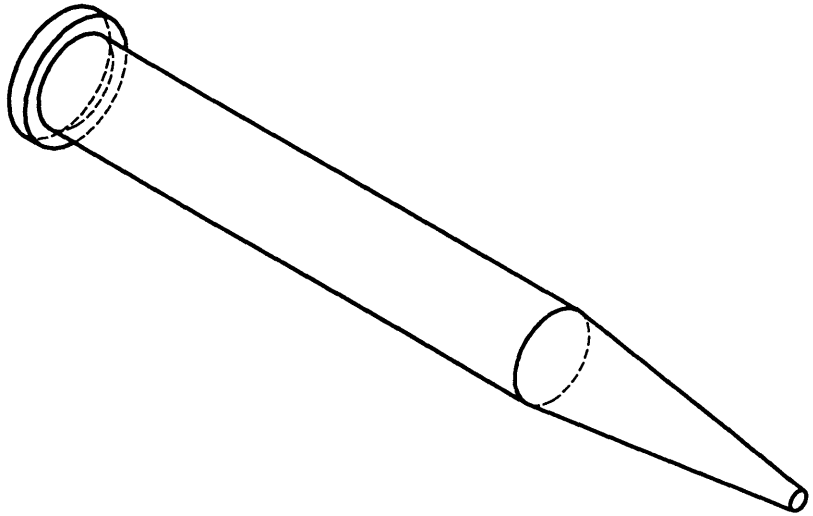

MASSACHUSETTS INSTITUTE OF TECHNOLOGY			
X. ±0.1 X.X ±0.1 X.XX ±0.01	Material: Al 6061-T651	Precision Stage HEIGHT PIN 1	
	MM	1.000	THS_STG_PIN1
TOLERANCES	UNITS	SCALE	FILENAME

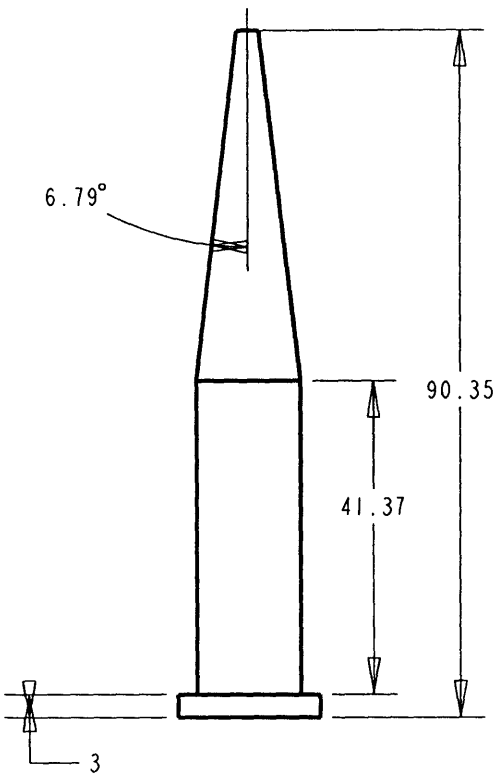

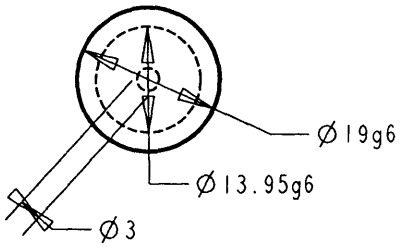

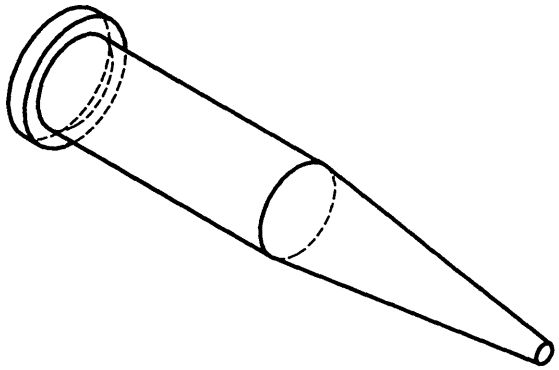

MASSACHUSETTS INSTITUTE OF TECHNOLOGY			
X. ±0.1 X.X ±0.1 X.XX ±0.01	Material: Al 6061-T651	Precision Stage HEIGHT PIN 2	
	MM	1.000	THS_STG_PIN2
TOLERANCES	UNITS	SCALE	FILENAME

References

[1] B. Armstrong-Helouvry, *Control of Machines with Friction.* Boston, MA: Kluwer, 1991.

[2] B. Armstrong-Helouvry, P.Dupont, and C. Canudas de Wit, "A Survey Of Models, Analysis Tools And Compensation Tools For The Control Of Machines With Friction," *Automatica,* vol. 30, no. 7, pp. 1083-1138, 1994.

[3] P. Beer, and E. R. Johnson, *Vector Mechanics for Engineers*, New York: NY, Mc Graw Hill, 1988

[4] I. J. Busch- Vishniac, "Applications Of Magnetic Levitation-Based-Micro-Automation In Semiconductor Manufacturing," *IEEE Trans. on Semiconductor Manufacturing,* vol. 3, no. 3, Aug 1990.

[5] C. Canudas de Wit, H. Olsson, K. J. Astrom, and P. Lischinsky, "Dynamic Friction Models And Control Design," *American Control Conf.,* vol. 16, no. 20, pp. 1920-1926, 1993.

[6] C. Canudas de Wit, H. Olsson, K. J. Astrom, and P. Lischinsky, "A New Model For Control Systems With Friction," *IEEE Trans. on Automatic Control,* vol. 40, no. 3, 1995.

[7] M. Chiu, *Low- Cost, Highly- Damped, Precision Linear Motion Using Porous Carbon Air Bearings and Epoxy Replication.* Masters Thesis, MIT, May 1994.

[8] H. Choi, *A Linear Ultrasonic Motor for Nanotechnology.* Masters Thesis, MIT, May 1996.

[9] J. Delamare, E. Rulliere, and J. P. Yonnet, "Classifications and Systhesis of Permanent Magnet Configurations," *IEEE Trans. on Magnetics,* no. 6, vol. 31, 1995.

[10] A. J. Devitt, "Development of Porous Air Bearing," *Motion Control,* May 1993.

[11] D. A. Haessig, and B. Friedland, "On Modelling And Simulation Of Friction," *Proc. 1990 American Contr. Conf.,* San Diego, CA, 1990 pp. 1256-1261.

[12] R. Hammer, R. L. Hollis, C. H. An, and F. Hendriks, "Design and Control of an Air-Bearing Supported Three Degree-of-Freedom Fine Positioner," *Proc. IEEE Int. Conf. on Robotics and Automation,* pp. 677-684, 1992.

[13] M. Holmes, and D. Trumper, "Magnetic/fluid-bearing Stage for Atomic Scale Motion Control (the Angstrom Stage)," *Precision Engineering,* no. 1, vol. 18, 1996.

[14] L. Horath, *Fundamentals of Material Science for Technologist,* Englewood Cliffs: NJ, Prentice Hall, 1995

[15] D. C. Karnopp, D. L. Margolis, and R.C. Rosenberg, *System Dynamics: A Unified Approach.* Davis: CA, John-Wiley, 1990.

[16] D. Karnopp, "Computer Models Of Hysteresis In Mechanical And Magnetic Components," *J. of the Franklin Institute,* vol. 316, no. 5, pp.405-415, 1983

[17] Lucascontrol Systems Products, 1000 Lucas Way, Hampton VA 23666. *Lucascontrol Systems Products DC-LVDT Manual.*

[18] V. J. Majd, and M.A. Simaan, "A Continuous Friction Model For Servo Systems With Stiction," *IEEE Conf. on Control Applications,* pp. 296-300, Aug 1995.

[19] Mechanical Technology Inc., 968 Albany- Shaker Road, Latham NY 12110, *MTI Instruments Division Instruction Manual.*

[20] New Way Machine Components, Inc., 4001-I Market Street, Aston PA 19014, *Air Bearings for Industry Product Catalog.*

[21] E. Oberg, F. D. Jones, H. L. Horton, and H. H. Ryffel, *Machinery's Handbook 24th Ed.,* New York: NY, Industrial Press Inc., 1992.

[22] T. Ohara, *A New High Precision Position Measurement System,* PhD Thesis, MIT, May 1995.

[23] Physik Intrumente (PI) GmbH & Co., Polytec-Platz 5-7, 76337 Waldbronn, Germany. *Products for Micropositioning Catalog Ed. E .*

[24] K. S. J. Pister, R. S. Fearing, and R. T. Howe, "A Planar Air Levitated Electrostatic Actuator System," *Proc. IEEE Micro Electro Mechanical Systems Investigations on Microstructures, Sensors, Actuators, Machines and Robots,* pp. 67-71, 1990.

[25] Queensgate Instruments Ltd., Waterside Park, Braknell, Berkshire RG12 1RB, United Kingdom, *NPS-XY100A 100micon range closed-loop X-Y stage Tech Note..*

[26] E. Rabinowics, "The Intrinsic Variables Affecting The Stick- Slip Process," *Proc. Physical Society of London,* vol. 71, no. 4, pp. 668-675, 1958.

[27] J. E. Shigley, and C. R. Mischke, *Mechanical Engineering Design,* New York: NY, McGraw-Hill, 1989.

[28] SKF, 149 Colebrook River Road, Winsted CT 06098. *General Catalog.*

[29] A. H. Slocum, *Precision Machine Design,* Englewood Cliffs:NJ, Prentice, 1992.

[30] K. Tanaka, Y. Uchiyam, and S. Toyooka, "The Mechanism of Wear of Polytetraflouroethylene," *Wear*, No. 23, pp. 153- 172, 1973.

[31] J. B. Taylor, and J. F. Tut, "Precision X-Y Microstage With Maneuvarable Kinematic Coupling Mechanism," *Precision Engineering,* No. 2/3, vol. 18, 1996.

[32] D. Trumper, W. J. Kim, and M. Williams, "Design and Analysis Framework for Linear Permanent-Magnet Machines," *IEEE Trans. on Industry Applications,* no. 2, vol. 32, 1996.

[33] I. A. Wang, and I. Busch-Vishniac, "A New Repulsive Magnetic Levitation Approach Using Permanent Magnets and Air-Core Electromagnets," *IEEE Trans. on Magnetics,* no. 4, vol. 30, 1994.

[34] R. Yang, M. Jouaneh, and R. Schweizer, " Design and Characterization of a Low-Profile Micropositioning Stage," *Precision Engineering,* no. 1, vol. 18, 1996.

[35] J. P. Yonnet, "Passive Magnetic Bearings with Permanent Magnets," *IEEE Trans. on Magnetics,* no. 5, vol. 14, 1978.

[36] J. P. Yonnet, "Passive Magnetic Bearings with Soft Magnetic Materials," *Journal of Magnetism and Magnetic Materials*, no. 26, pp. 329-332, 1982.

[37] J. P. Yonnet, G. Lemarquand, S. Hemmerlin, and E. Olivier-Rulliere, "Stacked Structures of Passive Magnetic Bearings," *J. of Applied Physics,* no. 10, vol. 70, 1991.

[38] K. Youcef- Toumi, Mechanical Engineering Department, MIT, 1995, *2.151 Advanced System Dynamics and Controls Class Notes*

[39] Zygo Corp., Laurel Brook Road PO Box 448, Middlefield CT 06445, *Zygo ZMI 1000 Three Axis Measurement Configuration Technical Note.*